Indian J. pure appl. Phys., Vol. 18 No. 1 pp. 1-66
January 1980
CODEN : IJOPAU ISSN : 0019-5596
18 (1) 1-66 (1980)

22
7.4.80.

INDIAN JOURNAL OF PURE & APPLIED PHYSICS

Published by
THE COUNCIL OF SCIENTIFIC & INDUSTRIAL RESEARCH, NEW DELHI
in association with
THE INDIAN NATIONAL SCIENCE ACADEMY, NEW DELHI

a quantum leap in recorder technology now available to the discriminating research scientist a range of reliable 'state of the art' recording instruments

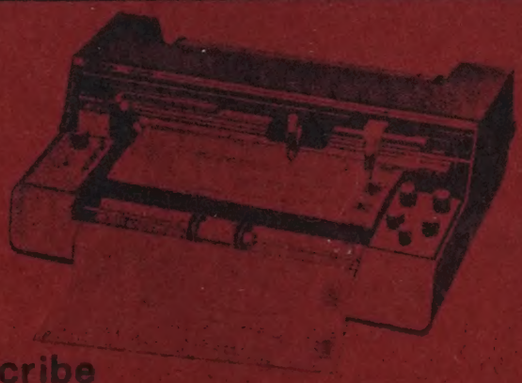

DigiScribe
Strip Chart Recorders One to Four Pens, 0.5 mV full scale and up, 0.5 sec response

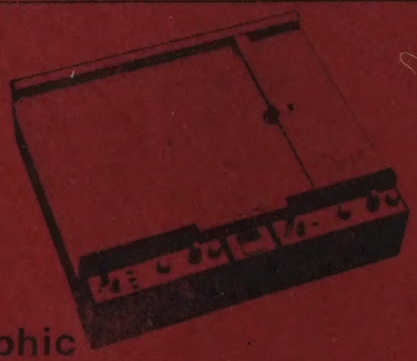

DigiGraphic
XY/t Recorders with plug-in modules to give wide ranges of sensitivity, time base facility and log recording.

HiScribe Oscillographic
Oscillographic Recorders DC to 80 Hz, One to eight channels. Heat or ink writing. Plug in modules to give wide range of sensitivities

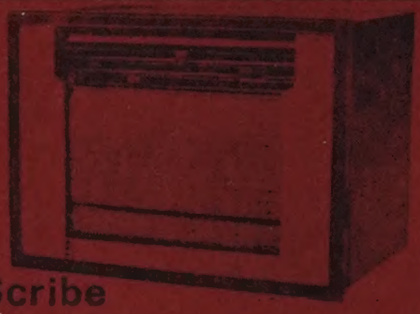

MultiScribe
One to Three Pen and 6, 12 and 24 point Recorders. Rack mounting with alarm contacts, cold junction compensation, and other features.

APPLICATIONS IN THE FIELDS OF

- METEOROLOGY • MATERIAL SCIENCES
- LIFE SCIENCES • PHYSICAL SCIENCES
- CHEMICAL AND ELECTROCHEMICAL SCIENCES
- BIOLOGICAL SCIENCES • PHYSIOLOGICAL AND BEHAVIOURAL SCIENCES • COMPUTER SCIENCES
- ENVIRONMENTAL AND POLLUTION STUDIES
- ENERGY STUDIES • PHARMACOLOGY
- MECHNICAL/ELECTRICAL ENEGINEERING
- METALLURY/METALLURGICAL ENGINEERING
- AERODYANAMICS/AERONAUTICAL ENGINEERING
- BIO-MEDICAL ENGINEERING
- QUALITY CONTROL APPLICATIONS

MANUFACTURED BY:

DIGITAL ELECTRONICS LIMITED

A Company in collaboration with

houston instrument | DIVN OF **BAUSCH & LOMB**

Office & Factory:

Digilog House, 74/II, C. Cross Road, Marol Industrial Area, MIDC, Andheri (East), Bombay-400 093. Phone: 577676. Gram: 'DIGILOG'

Indian Journal of Pure & Applied Physics

VOLUME 18 No. 1 JANUARY 1980

EDITORIAL BOARD

Dr B A Dasannacharya
Bhabha Atomic Research Centre
Bombay

Prof. B M Deb
Indian Institute of Technology
Bombay

Prof. P Krishna
Banaras Hindu University
Varanasi

Prof. Krishnaji
Allahabad University
Allahabad

Prof. K V Ramanathan
Tata Institute of Fundamental Research
Bombay

Prof. A K Saha
Saha Institute of Nuclear Physics
Calcutta

Prof. N C Sil
Indian Association for
Cultivation of Science
Calcutta

Prof. R Srinivasan
Indian Institute of Science
Bangalore

Prof. K Venkataramiah
Osmania University
Hyderabad

Nominees of the Indian National Science Academy

Dr S Chandrasekhar
Raman Research Institute
Bangalore

Dr K L Chopra
Indian Institute of Technology
New Delhi

Shri Y. R. Chadha, *Ex-officio* Secretary & Chief Editor

EDITORIAL STAFF

Editors : D S Sastry & K S Rangarajan

Assistant Editors : G N Sarma, J B Dhawan & Tarun Banerjee

Published by the Publications & Information Directorate, CSIR, Hillside Road, New Delhi-110 012

Chief Editor : Y R Chadha

The Indian Journal of Pure & Applied Physics is issued monthly. The Directorate assumes no responsibility for the statements and opinions advanced by contributors. The editorial staff in its work of examining papers received for publication is assisted, in an honorary capacity, by a large number of distinguished scientists, working in various parts of India.

Communications regarding contributions for publication in the journal should be addressed to the Editor, Indian Journal of Pure & Applied Physics, Publications & Information Directorate, Hillside Road, NewDelhi 110 012.

Correspondence regarding subscriptions and advertisements should be addressed to the Sales & Distribution Officer, Publications & Information Directorate, New Delhi-110 012.

Annual Subscription
Rs. 100.00 £ 16.50 $ 42.00
50% discount is admissible to research workers and students and 25 % discount to non-research individuals, on annual subscription.

Single Copy
Rs. 10.00 £ 1.80 $ 4.50
Payments in respect of subscriptions and advertisements may be sent by cheque, bank draft, money order or postal order marked payable *only* to **Publications & Information Directorate, New Delhi 110 012.**

Claims for missing numbers of the journal will be allowed only if received within 3 months of the date of issue of the journal plus the time normally required for postal delivery of the journal and the claim.

© 1980 The Council of Scientific & Industrial Research, New Delhi.

CSIR SCIENTIFIC PERIODICALS

JOURNAL OF SCIENTIFIC & INDUSTRIAL RESEARCH (monthly)

With a fine record of over 35 years' service to the scientific community, this Journal has grown into India's leading general science periodical. Intended to fulfil the responsibility of helping the research workers to keep themselves abreast of current developments in various fields of science and technology, the Journal carries editorial features highlighting important scientific events in India and abroad; articles on science policy and management of science; review articles on topics of current research interest; technical reports on international and national conferences; reviews of scientific and technical publications; and notes on major advances in various fields.

Annual subscription	**Rs 60.00**	**£ 10.00**	**$ 25.00**
Single copy	6.00	1.00	2.50

INDIAN JOURNAL OF CHEMISTRY (monthly)

This Journal which is running the 18th year of publication, was split up into two sections with effect from January 1976.

Section A : This section is devoted to papers in Inorganic, Physical, Theoretical and Analytical Chemistry.

Annual subscription	**Rs 70.00**	**£ 12.00**	**$ 30.00**
Single copy	**7.00**	**1.20**	**3.00**

Section B : This section is devoted to papers in Organic Chemistry including Medicinal Chemistry.

Annual subscription	**Rs 70.00**	**£ 12.00**	**$ 30.00**
Single copy	**7.00**	**1.20**	**3.00**

INDIAN JOURNAL OF PURE & APPLIED PHYSICS (monthly)

This Journal, which is running the 18th year of its publication, is devoted to original research communications (full papers and short communications) in all conventional branches of physics (except radio and space physics).

Annual subscription	**Rs 100.00**	**£ 16.50**	**$ 42.00**
Single copy	**10.00**	**1.80**	**4.50**

INDIAN JOURNAL OF RADIO & SPACE PHYSICS (bimonthly)

This Journal is intended to serve as a medium for the publication of the growing research output in various areas of radio and space physics.

Annual subscription	**Rs 60.00**	**£ 10.00**	**$ 25.00**
Single copy	**12.00**	**2.00**	**6.00**

INDIAN JOURNAL OF TECHNOLOGY (INCLUDING ENGINEERING) (monthly)

This Journal publishes papers reporting results of original research of applied nature pertaining to unit operations, heat and mass transfer, products, processes, instruments and appliances, etc. The Journal is of special interest to research workers in the departments of applied sciences in universities, institutes of higher technology, commodity research laboratories, industrial cooperative research institutes, and industrial research laboratories.

Annual subscription	**Rs 60.00**	**£ 10.00**	**$ 25.00**
Single copy	6.00	1.00	2.50

INDIAN JOURNAL OF EXPERIMENTAL BIOLOGY (monthly)

This Journal, devoted to the publication of research communications in the fields of experimental botany, zoology, microbiology, pharmacology, endocrinology, nutrition, etc., is the only one in India with such a wide coverage and scope.

Annual subscription	**Rs 120.00**	**£ 20.00**	**$ 50.00**
Single copy	12.00	2.00	5.00

INDIAN JOURNAL OF BIOCHEMISTRY & BIOPHYSICS (bimonthly)

This Journal, published in association with the Society of Biological Chemists (India), Bangalore, is the only research Journal in India devoted exclusively to original research communications in biochemistry and biophysics.

Annual subscription	**Rs 40.00**	**£ 7.00**	**$ 17.00**
Single copy	8.00	1.40	3.50

INDIAN JOURNAL OF MARINE SCIENCES (quarterly)

Commencing publication from June 1972, this Journal is devoted to research communications (full papers and short communications) pertaining to various facets of marine research, viz. biological, physical, geological and chemical oceanography.

Annual subscription	**Rs 40.00**	**£ 7.00**	**$ 17.00**
Single copy	12.00	2.00	5.00

RESEARCH & INDUSTRY (quarterly)

Intended to serve as a link between science and industry. This Journal is addressed primarily to technologists, engineers, executives and others in industry and trade. It publishes informative original articles containing practical details of processes and products developed in India which show promise of ready utilization, and technical digests on new processes, products, instruments and testing methods which are of interest to industry. Developments in Indian industry are regularly reported.

Annual subscription	**Rs 24.00**	**£ 4.00**	**$ 10.00**
Single copy	**7.25**	**1.30**	**3.50**

INDIAN JOURNAL OF TEXTILE RESEARCH (quarterly)

Commencing publication from March 1976, this Journal is devoted to the publication of papers reporting results of fundamental and applied researches in the field of textiles.

Annual subscription	**Rs 36.00**	**£ 6.00**	**$ 15.00**
Single copy	**12.00**	**2.00**	**5.00**

Please contact:

THE SALES & DISTRIBUTION OFFICER
PUBLICATIONS & INFORMATION DIRECTORATE, CSIR
HILLSIDE ROAD, NEW DELHI 110 012

Indian Journal of Pure & Applied Physics

VOLUME 18 No. 1 JANUARY 1980

CONTENTS

Solid State Physics

Layer Disorders in Cylindrical Crystallites & Their Effects on Diffraction Intensities 1

S BHATTACHERJEE, A K DE & B K RAY

X-ray Diffraction & Fluorescence Spectral Studies on (CaS,BaS) : Cu Phosphors ... 6

U K MISHRA, S L MOR & J D RANADE

Calculation of Current Gain of Planar Transistors 10

ASHOK SRIVASTAVA, O P WADHAWAN & B R MARATHE

Photoconducting Properties of CdS:Na Films 15

B B BARGALE & S H PAWAR

Thermal Currents in Magnetically Polarized Silastic Tubular Electrets 20

RUDRA KANT SRIVASTAVA, M L KHARE, M S QURESHI & C S BHATNAGAR

Charge Characteristics & Dielectric Behaviour of PVF2 Magnetoelectrets at Audio and Radio Frequency 24

J K QUAMARA, M L KHARE & C S BHATNAGAR

Nickel Oxide Electrode for Photolysis 28

V P SUNDER SINGH, (Mrs) P P WARNEKAR & G K BHAGAWAT

Chemical Physics

Ionization & Dissociation of Propylene by Electron Impact 31

EZZAT T M SELIM

Evaluation of Critical Constants from the Intermolecular Force Constants ... 36

V SHANMUGASUNDARAM & P THIYAGARAJAN

Dielectrics & Microwaves

Liquid Structure of *tert*-Butyl Alcohol in Nonpolar Solvents from Dielectric Studies ... 40

D C DWIVEDI & S L SRIVASTAVA

Spectroscopy

Application of a Wall-stabilized dc Arc for Spectral Analysis of Solutions ... 47

M A EID, K M EL BEHERY & F A EL ANANY

CONTENTS

COMMUNICATIONS

Excess Thermodynamic Properties & Interactions in Benzene + Tetrahydrofuran & Methyl Ethyl Ketone + Butanol Solutions 51

(Miss) V Tiwari & J D Pandey

NOTES

Flexibility of M—X Bond of Some Tetrahalides of Fourth Group Metals by Compliance Scheme 54

S L Gupta, R C Saxena, V K Rastogi & A N Pandey

Thermal Expansion of V_3Si at Elevated Temperatures 56

B K Rao & D B Sirdeshmukh

Evaluation of Grüneisen Constant of KCl-KBr Mixed System 57

Brinda Subramaniam

Prediction of Dipole Moments of Polar Molecules from the Relation between τ_{solute} & $\eta_{solvent}$ 58

Shekhar Kumar Datta

Diffraction Intensities from a Cluster of Curved Crystallites with Layer Shift ... 58

A K De, B K Ray & S Bhattacherjee

Crystal Growth from Binary Immiscible Liquid Systems 60

K Ravindran Nair

Preliminary Single Crystal X-ray Study of N-Methyl Crotananinium Iodide ... 62

K N Goswami, S D Sharma & O P Suri

A Heuristic Formula for the Dielectric Loading Factor of a Helix Supported by Dielectric Circular Rods 63

B N Basu & S N Joshi

Field Analysis of a Practical Helical Slow-wave Structure for TWTs 64

B N Basu

Indian Journal of Pure & Applied Physics
Vol. 18, January 1980, pp. 1-5

Layer Disorders in Cylindrical Crystallites & Their Effects on Diffraction Intensities

S Bhattacherjee, A K De & B K Ray
Department of Physics, Indian Institute of Technology, Kharagpur 721 302

Received 14 *February* 1979

Two different kinds of stacking disorder in the layer sequence, commonly observed in layer silicates, have been envisaged in the model of cylindrical crystallite due to G B Mitra and S Bhattacherjee [*Acta crystallogr.*, A27 (1971), 22]. Following these concepts, relevant expressions for the diffracted intensities from an agglomeration of such disordered cylindrical crystallites have been derived. To study the effects of the different defects and the various defect parameters, detailed numerical computations were carried out. Results of the calculations have been discussed and compared with those of ordered cylindrical crystallites. Some important conclusions have also been arrived at on the effect of varying the different defect parameters.

1. Introduction

It is well known that many silicate minerals and polymers possess curved lattices with cylindrical symmetry. In view of this fact, X-ray diffraction by curved lattices has become a very important field of study. Theoretical investigations of the problem on several models with varying approaches have been carried out by a large number of workers during the last few decades. However, most of these treatments deal with some specific models of curved crystallites having ordered cylindrical lattices as described by Whittaker[1] and Mitra and Bhattacherjee.[2]

All real crystals contain some imperfections and this is more true for naturally occurring minerals. In fact, it has been shown by many that silicate minerals like kaolinite,[3,4] chrysotile,[5] amphiboles[6] and zussamanite[7] do possess various types of stacking disorder. Therefore, it is quite natural to presume that the minerals (like chrysotile, halloysite) which are built of tubular layers will exhibit stacking disorders. Hence a more pragmatic approach is to consider the diffraction by a conglomeration of identical cylindrical crystallites with different probable layer disorders. Unfortunately very little work in this direction has so far been reported.

Mitra[8] and Mitra and Bhattacherjee[2] have developed a very simple and general expression for X-ray diffraction without any simplifying assumptions from a cluster of cylindrical crystallites. Accepting their model as ordered one, in this work two different types of layer disorders have been proposed and suitable intensity expressions from a cluster of such disordered cylindrical crystallites have been derived. A preliminary short report of the work has already been communicated and the present paper aims at giving a more detailed analysis of the effect of the different types of layer disorders on the diffraction intensities based on numerical computation.

2. Description of the Different Layer Disorders

Layered structures, especially layered silicate minerals are prone to develop various types of stacking faults. Mitra[8] and Mitra and Bhattacherjee[3,4] studied two specific types of layer disorder in kaolinite by X-ray method. The first one called layer shift of a layer parallel to itself by an amount $(1/3)\,b$ or $(2/3)\,b$ with respect to its adjacent layer and is of very common occurrence in this group of minerals. The second type is characterized as variability of interlayer spacing and consists of a random variation of the interlayer spacing by a constant fraction of the interlayer distance as discussed and studied by Wilson[9] and Mitra.[8]

Extending the above ideas, we have here defined two similar types of layer disorder in cylindrical crystallite with ordered cylindrical lattice due to Mitra and Bhattacherjee.[2] A crystallite is built up of M coaxial tubular layers of the type as shown in Fig. 1 (*b*) of Ref. 2 with radii R, $R + b$, $R + 2b$... $R + (M - 1)\,b$, R being the radius of the first one from the common axis. Each of the cylindrical layers consists of T identical arcs stacked at an interval c along the z-axis, each arc having N lattice

points placed equiangularly on it. Two neighbouring lattice points on the same arc subtend an angle ϕ at the common axis in their plane of curvature XY, other details being the same as defined by these authors. Referring to this model, the first kind of disorder characterizing layer shift is defined as the displacement of one coaxial cylindrical layer parallel to itself by an angular distance $\epsilon\phi$ with respect to its adjacent layer. In other words, the layer is rotated through $\epsilon\phi$ where ϵ is a small fraction. Here we have considered the case where $\epsilon = \frac{1}{2}$. This defect may be compared with the azimuthal misfit boundary in chrysotile.[10]

Similarly the second type of defect is defined as random variation of the interlayer spacing between the cylindrical layers by a constant fraction of the interlayer spacing. Here the interlayer distance between the cylindrical layers is obviously b, the radial repeat distance and the variation is gb where g is a small fraction. These two types of disorders are illustrated in Fig. 1 (a,b).

3. Derivation of the Intensity Expression

3.1 Layer Shift

All calculations that follow are based primarily on the model of the cylindrical crystallite described by Mitra and Bhattacherjee[2] where the position of any lattice point occupying rth site in the mth arc or layer in the tth stack is described by rmt. Following an approach similar to that of Wilson,[9] let us suppose that the first layer is in the right position and each added layer has a chance α_s of being displaced or twisted by $\phi/2$. If R_m and W_m be the probabilities of the mth layer being in the right and wrong position respectively, then the average angular position of the lattice point is given by $r\,\phi\,R_m + (r+\frac{1}{2})\,\phi\,W_m$. This reduces to $(r + 1/2\ W_m)\,\phi$ where $R_m + W_m = 1$ and $R_m = 1/2\,\{1 + (1 - 2\alpha_s)^m\}$

The position vector of the lattice point $\underset{\sim}{\tau}_{rmt}$ can now be written as

$$\underset{\sim}{\tau}_{rmt} = i_x\,(R + mb)\sin(r + 1/2\ W_m)\,\phi + i_y\,(R+mb) \times \cos(r + 1/2\ W_m)\,\phi + i_z\,tc \qquad \ldots(1)$$

where $\underset{\sim}{i}_x\ \underset{\sim}{i}_y, \underset{\sim}{i}_z$ are the unit vectors along the X, Y and and Z axes respectively. Using this value of $\underset{\sim}{\tau}_{rmt}$ and proceeding exactly in the same manner as that of Mitra and Bhattacherjee[2] the diffracted intensity $I(hkl_0)$ from a conglomeration of identical cylindrical crystallites with the above defects can be shown to be given by:

$$I(hkl_0) = T^2\,N \sum_{m=0}^{M-1}\sum_{n=0}^{M-1} J_0\{x_m^2 + y_n^2 - 2\,x_m y_n \cos(W_m - W_n)\,\phi/2\}^{1/2} + T^2 \sum_{m=0}^{M-1}\sum_{n=0}^{M-1}\sum_{q=1}^{N-1} (N-q) [J_0\{x_m^2 + y_n^2 - 2\,x_m\,y_n \cos(2q + W_m - W_n)\,\phi/2\}^{1/2} + J_0\{x_m^2 + y_n^2 - 2\,x_m\,y_n \cos(2q - W_m + W_n)\,\phi/2\}^{1/2}] \qquad \ldots(2)$$

with

$$x_m = QN(h + mk\,\phi)\{1 - (l_0/l)^2\}^{1/2}$$

$$y_n = QN(h + nk\,\phi)\{1 - (l_0/l)^2\}^{1/2}$$

and

$$Q = \frac{2\pi}{N\phi}\ ;\ h = \frac{2\,a\sin\theta}{\lambda}\ ;\ k = \frac{2\,b\sin\theta}{\lambda}$$

$$\frac{sc\cos\gamma}{\lambda} = l_0\ (\text{integer})\ ;\ l = \frac{sc}{\lambda}$$

γ is the angle between $\underset{\sim}{S}$ and the Z-axis [Fig. 2 (b) of Ref. 2] and $|\underset{\sim}{S}| = 2\sin\theta$

Introducing $r_1 = c/a$ and $r_2 = b/a$, Eq. (2) can be written as

$$I(hl_0) = T^2\,N \sum_{m=0}^{M-1}\sum_{n=0}^{M-1} J_0\left(B\{u_m^2 + v_n^2 - 2\,u_m\,v_n \cos(W_m - W_n).\,\phi/2\}^{1/2}\right)$$

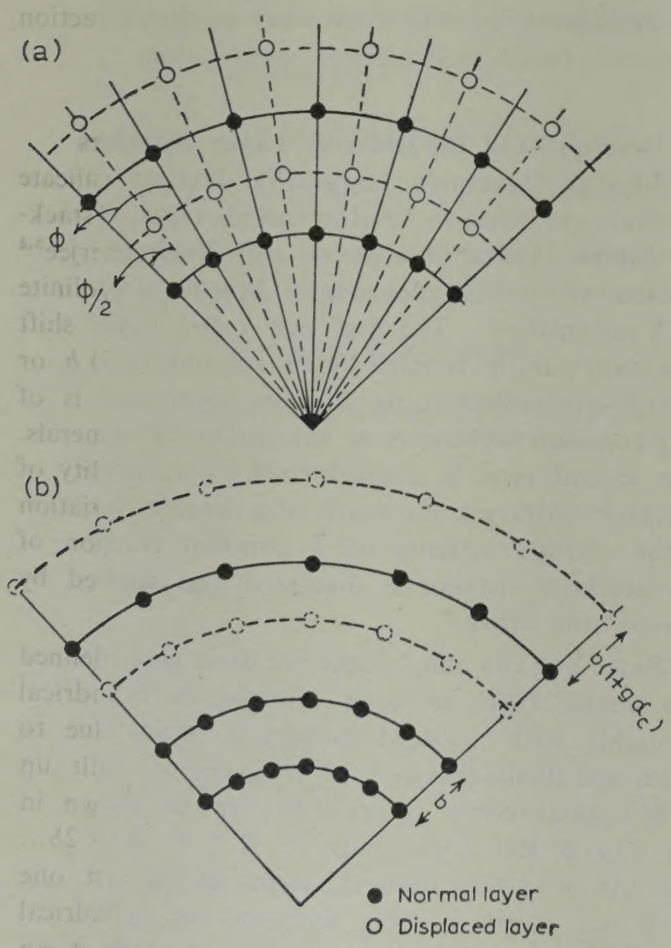

Fig. 1—Models of faulted cylindrical lattices (a) with layer shifts and (b) with variability of layer positions

$$+ T^2 \sum_{m=0}^{M-1} \sum_{n=0}^{M-1} \sum_{q=1}^{N-1} (N-q) \Big[J_0 \Big(B\{u_m^2 + v_n^2 - 2 u_m v_n \cos (2q + W_m - W_n)\, \phi/2\}^{1/2} \Big) + J_0 \big(B \{u_m^2 + v_n^2 - 2u_m v_n \times \cos (2q - W_m + W_n)\, \phi/2\}^{1/2} \big) \Big] \quad \ldots(3)$$

where

$$B = QNh \{1 - l_0^2/(r_1^2 h^2)\}^{1/2} ; \; u_m = 1 + mr_2\phi; \quad v_n = 1 + nr_2\phi$$

If there is no slip, then $W_m = W_n = 0$ and Eq. (3) reduces exactly to Eq. (16) of Mitra and Bhattacherjee,[2] as expected.

3.2 Variability of Interlayer Spacing

As discussed earlier, this type of stacking fault will consist of b being variable to the extent that b due to faulting is $b + gb$ where $|g|$ is a small fraction and is assumed to be constant. Hence the radial coordinate of the cylindrical layers will be affected and, as in the previous case, here also we need to find the average position of the mth layer in the faulted crystallite. To be more specific, we calculate the average value of $(R + mb)$ in the faulted crystallite. Following the arguments similar to that of Wilson,[9] the average radial position of the mth layer has been found to be $R + mb\,(1 + \alpha_c g)$ with $|g| < 1$ where α_c is the probability of a layer being so faulted. It is quite apparent from this result that mathematically the defective crystallite is equivalent to an ordered one with interlayer spacing $b\,(1 + \alpha_c g)$. So to derive the intensity expression we use this modified value of b in x_m and y_n and substitute these values in Eq. (2). The transformed values of x_m and y_m are given by

$$x'_m = QNh\, u'_m \{1 - (l_0/r_1 h)^2\}^{1/2}$$

$$y'_n = QNh\, v'_n \{1 - (l_0/r_1 h)^2\}^{1/2}$$

where $u'_m = 1 + mr_2\phi\,(1 + \alpha_c g)$;

and $v'_n = 1 + nr_2\phi\,(1 + \alpha_c g)$.

The intensity $I(hl_0)$ can be written as

$$I(hl_0) = T^2 N \sum_{m=0}^{M-1} \sum_{n=0}^{M-1} J_0 \Big(B \{u'^2_m + v'^2_m - 2\, u'_m\, v'_n \cos (W_m - W_n)\, \phi/2\}^{1/2} \Big) + T^2 \sum_{m=0}^{M-1} \sum_{n=0}^{M-1} \sum_{q=1}^{N-1} (N-q) \Big[J_0 \Big(B \{u'^2_m + v'^2_n - 2 u'_m\, v'_n \cos (2q + W_m - W_n)\, \phi/2\}^{1/2} \Big) + J_0 \Big(B \{u'^2_m + v'^2_n - 2u'_m\, v'_n \times \cos (2q - W_m + W_n)\, \phi/2\}^{1/2} \Big) \Big] \quad \ldots(4)$$

Eq. (4) is the general expression for the diffracted intensity from an aggregate of disordered cylindrical crystallites with the two stacking faults as discussed earlier. This expression will have all the characteristics of Eq. (16) of Mitra and Bhattacherjee[2] as discussed by these authors. For crystallites without any defects $W_m = W_n = 0$; $g = 0$ and Eq. (4) reduces to Eq. (16) as expected.

4. Numerical Computation and Discussion

In order to carry out numerical computations for studying the effect of the defect consisting of layer shift only on the diffraction intensity in the zeroth layer ($l_0 = 0$), Eq. (3) was simplified to

$$I(h) = T^2 N \sum_{m=0}^{M-1} \sum_{n=0}^{M-1} J_0 \Big(QNh \{u_m^2 + v_n^2 - 2u_m v_n \cos (W_m - W_n)\, \phi/2\}^{1/2} \Big) + 2T^2 \sum_{m=0}^{M-1} \sum_{n=0}^{M-1} \sum_{q=1}^{N-1} (N-q) \Big[J_0 \Big(QNh \{u_m^2 + v_n^2 - 2u_m v_n \cos (q\phi)\}^{1/2} \Big) \Big] \quad \ldots(5)$$

where $W_m - W_n$ has been neglected in comparison to $2q$. Under the same assumptions, the intensity distribution for variability defect only can be written from Eq. (4) as

$$I(h) = T^2 N \sum_{m=0}^{M-1} \sum_{n=0}^{M-1} J_0 (QNh \{m - n\}\, r_2 A \phi) + 2T^2 \sum_{m=0}^{M-1} \sum_{n=0}^{M-1} \sum_{q=1}^{N-1} (N-q) \Big[J_0 \Big(QNh \{(1 + mr_2 A\phi)^2 + (1 + nr_2 A\phi)^2 - 2\,(1 + mr_2 A\phi)(1 + nr_2 A\phi) \times \cos (q\phi)\}^{1/2} \Big) \Big] \quad \ldots(6)$$

where $A = 1 + g\alpha_c$

All numerical computations were carried out using Eqs. (5) and (6) for different values of α_c and A in Ryad (1030) computer. Results of the numerical calculations are shown graphically in Figs. 2 and 3. To facilitate direct comparison both the sets of graphs have been drawn for same values of N, M, ϕ and r_2, viz. 10, 6, 30° and 1 respectively. Fig. 2 represents the intensity distribution from an aggregate of axially

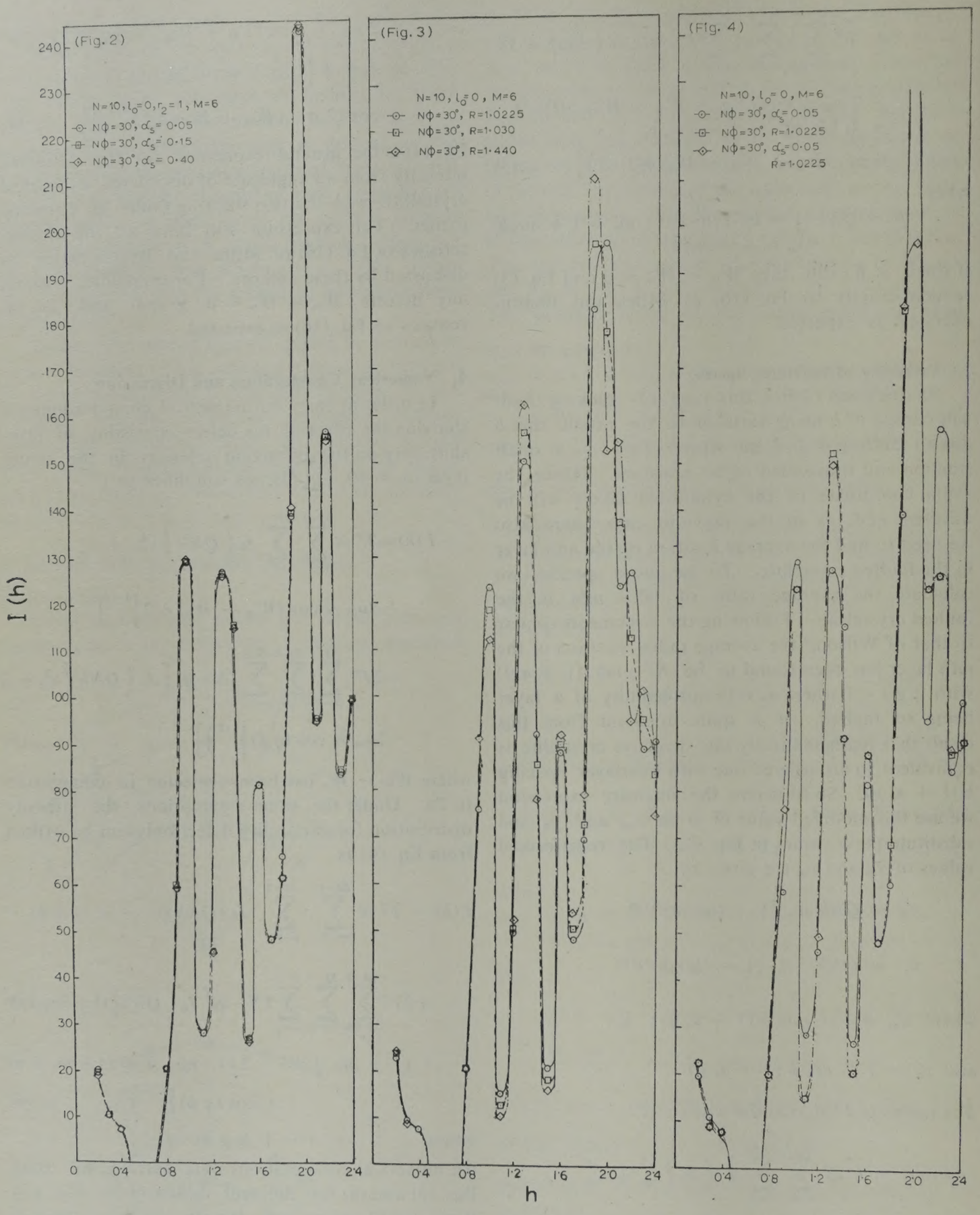

Fig. 2—Diffracted intensities from an axially parallel aggregate of cylindrical fragments with different values of α_s

Fig. 3—Diffracted intensities from an axially parallel aggregate of cylindrical fragment with different values of R

Fig. 4—Diffracted intensities from an axially parallel aggregate of cylindrical fragments with different faults

parallel ($l_0 = 0$) cylindrical crystallites with stacking fault characterizing layer shift corresponding to $\alpha_s = 0{\cdot}05, 0{\cdot}15$ and $0{\cdot}40$ respectively. It is seen that the three curves in Fig. 2 are almost identical showing thereby that increase in α_s practically has negligible or no effect on the intensity. Comparison of these curves with those of ordered cylindrical crystallites with similar parameters[11] reveals that the general features of the pattern remain more or less the same. Here also we get peaks around the same values of h. However, contrary to the case of ordered cylindrical crystallite, here the second primary maximum at $h=2{\cdot}0$ is much higher than the first one and unlike the ordered one is followed by a secondary peak of relatively large height at $h = 2{\cdot}2$. So it is seen that layer shift does not change the pattern radically in the lower angle range but in the high angle range some significant changes are observed.

Fig. 3 illustrates the effects of variability of interlayer distances for three different values of R. The distribution appears to be more or less the same for all the three values of R, viz. $1{\cdot}0225$, $1{\cdot}030$, $1{\cdot}040$ respectively. A close examination of the three curves reveals one interesting effect of increasing the values of R. While the heights of the first peak at $h = 1{\cdot}0$ progressively decrease, the heights of the following peaks increase with increase of R value. Further, it is observed that the peaks around $h = 2{\cdot}0$ shift slightly towards lower angle side as R increases. Also the primary peaks are followed by some small secondary peaks. Comparison of the curves in Figs 2 and 3 reveals that while the peaks in the case of variability are sharper in the region up to $h = 1{\cdot}6$, the peaks corresponding to layer shift become sharper in the higher angle region. The secondary peaks following the ones at $h = 1{\cdot}9$ are much more pronounced in the case of layer shift. Thus it appears that in both the cases the higher angle peaks are more distinctive in character and is likely to provide a basis for distinguishing the disordered crystallite from the ordered one and probably to identify the specific defect.

Fig. 4 shows the effect of combining both the defects. The positions and the nature remain practically same as that of curve (2) corresponding to variability $R = 1{\cdot}0225$. Thus it may be concluded that the effect of variability will be more discernible than the layer shift when both the defects co-exist.

Calculations were also carried out for different values of curvature up to 90°. The effects, in general, were found to be very much similar to those observed by Mitra and Bhattacherjee[2] in the case of radially thick crystallites. Hence these curves have not been reproduced here.

5. Conclusion

The intensity expression derived in this paper is actually the interference function which ought to be multiplied by the corresponding structure factor for quantitative comparison with experimental data. However, this expression can be used for a qualitative explanation of the experimental data at the initial stages and may be helpful in distinguishing between ordered and disordered crystallites from the observed intensity pattern particularly when the structure factor $F(S)$ is not completely known.

Acknowledgement

The authors wish to express their grateful thanks to Prof. G B Mitra for his kind interest and encouragement in the work.

References

1. Whittaker E J W, *Acta crystallogr.*, **8** (1955), 571.
2. Mitra G B & Bhattacherjee S, *Acta crystallogr.*, **A27** (1971), 22.
3. Mitra G B & Bhattacherjee S, *Amer. Min.*, **54** (1969), 1409.
4. Mitra G B & Bhattacherjee S, *Acta crystallogr.*, **B26** (1970), 2124.
5. Toman K & Frueh A J, *Acta crystallogr.*, **A24** (1968), 364.
6. Hutchison J L, Irusteta M C, Whittaker E J W, *Acta crystallogr.*, **A31** (1975), 794.
7. Jeffersen David A, *Amer. Min.*, **61** (1976), 470.
8. Mitra G B, *Z. Krist.*, **119** (1963), 161.
9. Wilson A J C, *X-ray optics* (Methüen, London), 1962, pp. 74, 77; 106.
10. Toman K & Frueh A J, *Acta crystallogr.*, **A24** (1968), 374.
11. Bhattacherjee S & Mathur B K, *Indian J. pure appl. Phys.*, **12** (1974), 230.

Indian Journal of Pure & Applied Physics
Vol. 18, January 1980, pp. 6-9

X-ray Diffraction & Fluorescence Spectral Studies on (CaS, BaS) : Cu Phosphors

U K Mishra & S L Mor
Department of Physics, Maharaja College, Chhatarpur
&
J D Ranade
Department of Physics, University of Saugar, Sagar

Received 2 *January* 1979

A series of (CaS, BaS):Cu phosphors with varying proportions of BaS in CaS have been prepared by firing a suitable mixture of sulphates, activator and flux at 920 ± 10°C with carbon as reducing agent. X-ray diffraction studies indicate the existence of a complete solid solution of BaS in CaS up to 12·00 mole % and that of CaS in BaS up to 12·6 mole %. Fluorescence studies show a single emission peak for such phosphors displaced towards the shorter wavelength side, as compared to single host lattice. This shift to shorter wavelength side is explained on the basis of a model prepared by J S Prener and F E Williams [*Phys. Rev.*, **101** (1956), 1427; *J. Phys. Radium*, **17** (1956), 667]. The luminescence may be considered due to a new solid formed by exchange of cations between the two host lattices mixed.

1. Introduction

Alkaline earth sulphide phosphors activated by specific impurities are of considerable importance. In the same host, different activators give emission in different spectral regions[1] and as such, the whole of the visible region from red to violet can be covered. It is of interest to determine how far a given activator emission is affected by changing the composition of the phosphor matrix by forming a solid solution of two host materials.

Literature is full of citings that ZnS and CdS form a solid solution with each other in all proportions.[2] The alkaline earth sulphides are known to form solid solution with each other resulting in a gradual alteration of the band gap. If the emission is on account of the modification of the host level by the activator there should be a shift in emission towards the longer wavelength side, if the band gap is reduced. This may provide a convenient test as to the nature of emission in relation to the activator. The intensity of emission depends on the efficiency with which the excitation energy is transferred to the luminescence centre. It would, therefore, be of interest to study a system in which the absorption levels are changed in a controlled manner by changing the composition of the mixed lattice containing a conventional activator.

2. Experimental Procedure

The activator copper is taken in the form of a solution of $CuSO_4{:}5H_2O$ and sodium sulphate as the flux. Purified gypsum and baryte were suitably powdered, meshed and mixed with carbon p rovided the charge, which was fired in graphite crucibles covered with lids at 920 ± 10°C for 4 hr using midway grinding of the phosphors. The characteristics of the phosphors investigated are given in Table 1.

X-ray powder patterns were recorded for all the samples using the X-ray (Cu K_α radiations) diffraction unit PW 1010 Philips India Ltd. The diffraction camera was of Burger type as improved by Cisney.[3] The samples were taken in Lindmann glass capillaries of 0·3 mm diameter. Powder patterns were recorded on high contrast double coated X-ray films (Ilford Industrial G). All diagrams were taken at 26 ± 1°C setting the X-ray unit at 30 kV and 12 mA.

The individual phase corresponding to each line in the pattern has been identified. The calculated lattice constant is plotted against mole % of BaS Fig. 1.

The emission characteristics of these phosphors were recorded on a Bellingham and Stanley direct reading wavelength spectrometer which uses an IP 21 photomultiplier coupled to a photonmeter (Cenco No. 86407). The photonmeter has a built-in power supply for IP 21 and a sensitive galvanometer.

3. Results

Fig. 1 shows the observed relation between lattice constant and mole % of BaS, which deviates from the dotted line representing the Vegard's law

Table 1—Characteristics of Different Samples of Phosphors Studied

Sample No.	Mole % of BaS in CaS	Band in blue-green region			Band in green-yellow region		
		Peak wave-length, Å	Max. inten-sity (arb. units)	Band width, Å	Peak wave-length, Å	Max. inten-sity (arb. units)	Band width, Å
1	00	5100	125	660	—	—	—
2	4·91	5050	71	770	—	—	—
3	10·13	5000	47	780	—	—	—
4	15·53	4950	45	560	5550	25	140
5	21·13	4900	31	330	5400	20	210
6	26·95	4850	25	190	5300	20	140
7	32·99	4800	20	260	5200	15	100
8	39·26	5000	60	350	5850	73	320
9	45·79	5050	25	230	5800	30	260
10	52·58	4800	15	230	5450	22	260
11	59·66	4900	18	140	5500	21	200
12	66·99	4900	23	170	5550	58	360
13	74·70	—	—	—	5600	70	360
14	82·76	—	—	—	5650	72	340
15	91·18	—	—	—	5700	88	310
16	100·00	—	—	—	5800	110	250

Each Sample contains :

a) flux.....Na_2SO_4 10% by weight and (b) activator-copper 0·1% by weight with respect to the base.

for this variation. The plot indicates that only on either end, data for the samples No. 1, 2, 3, 13, 14, 15 and 16, lie on the curve. The lattice constants of the other samples are scattered randomly about this curve.

The emission spectra of different samples are shown in Figs. 2 (a)-(c). The position of peak emission intensity, wavelength and band width are given in Table 1. The spectra of different samples reveal the following features.

Sample No. 1 which is CaS:Cu phosphor gives an emission band at 5100 Å. Samples No. 2 and 3 which have CaS as the major component show single-peaked emission bands at 5050 Å and 5000 Å respectively in the blue-green region. Similarly samples No. 16 to 13 (BaS:Cu phosphors) have a single emission band peaked at 5800, 5700, 5650 and 5600 Å respectively in the yellow-green region.

Samples No. 4 to 7 (where CaS is a major constituent) show two emission peaks in blue-green and green-yellow regions. The emission peak in the blue-green is more prominent as compared to the

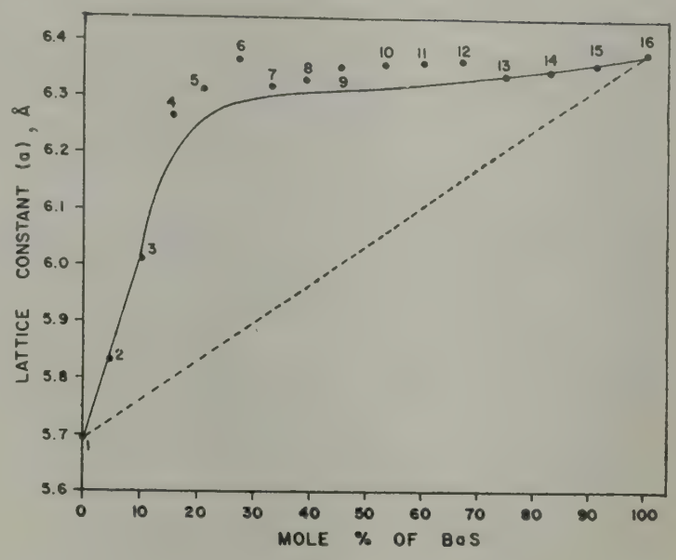

Fig. 1—Calculated lattice constant versus the mole % of BaS for different samples of the phosphors studied. The broken line represents variation according to Vegard's law

emission peak in the green-yellow region. For samples No. 12 and 11, two emission peaks in the blue-green and green-yellow regions are obtained, the prominent one being in the green-yellow region. For samples No. 8, 9 and 10, two well resolved peaks are observed at exactly the same positions as given separately by CaS:Cu and BaS:Cu phosphors.

4. Discussion

X-ray diffraction study is capable of revealing the order-disorder phenomenon in very small domains.[4] It also helps in finding the solubility limits and the nature of precipitation in the super-saturated solutions.[5] In the present case, the mole % versus lattice constant plot indicates that only samples No. 1 to 3 and 13 to 16 lie on the positive deviation from the Vegard's law. This indicates that solid solution of two sulphides exists only for samples No. 2, 3, 13, 14 and 15 and the solubility limit for BaS in CaS is up to 12 mole % of BaS, and for CaS in BaS up to 12·6 mole % of CaS. Further, one can also conclude that the solid solution of BaS in CaS as well as of CaS in BaS is of the interstitial type, (as the ionic radii of Ca^{2+} and Ba^{2+} are 0·99 and 1·34 Å respectively) and change in lattice constant is observed for mixed sulphides.[6-8]

Samples No. 1, 2 and 3 give only one emission peak in the blue-green region. Also for samples No. 16 to 13, only one emission peak in the yellow-green region is obtained. This can be taken as further indication that a complete solid solution is formed for these samples.

In samples No. 4 to 7, two emission peaks in the two regions are obtained. The emission peak in the

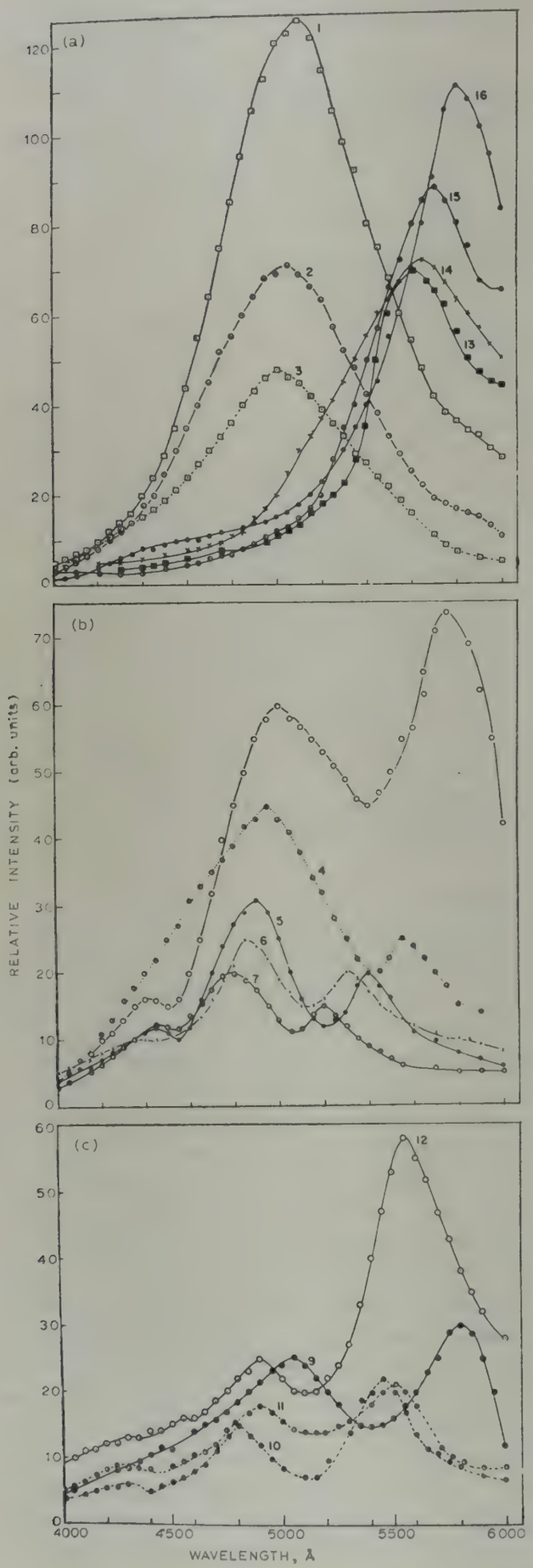

Fig. 2—Emission spectra of different samples of phosphors studied (a) samples 1-3 and 13-16 (b) samples 4-7 and (c) samples 9-12

blue-green region is more prominent as compared to the emission peak in the green-yellow region. This suggests the presence of both the phases of solid solution BaS in CaS and CaS in BaS, out of which BaS dissolved in CaS phase is predominant. For samples No. 12 and 11, two emission peaks with a prominent peak in the green-yellow region are obtained. This suggests that here also two phases are present, but the phase where CaS is dissolved in BaS is predominant as compared to the phase where BaS is dissolved in CaS.

The fact that samples No. 8 to 10 exhibit two well resolved peaks at exactly the same position, as given by CaS:Cu and BaS:Cu phosphors suggests that samples 8-10 are mere mixtures of the two phosphors and that no solid solution is formed.

X-ray and emission studies reveal that there exists a complete solid solution of CaS and BaS in each other only in samples No. 2 and 3 (up to 12 mole % of BaS) and 15 to 13 (up to 12·6 mole % of CaS). A single emission peak is obtained for these samples with some displacement of peak-emission to the shorter wavelength side as compared to individual peak in CaS:Cu and BaS:Cu phosphors respectively, as the concentration of the two sulphides is varied. Also a change in lattice constant is obtained. Thus one can say that the luminescence of mixed phosphors is modified by an exchange of calcium and barium cations during solid-solution formation.

As BaS is introduced in CaS, the band gap should decrease (The band gap of BaS being 4·00 eV and that of CaS 5·4 eV.). If the emission is explained by the Schon-Klasens or Lambe-Klick model, the shift should be towards the longer wavelength side as reported in the case of ZnS:CdS mixed phosphors.[9,10] The shift can be attributed partially to a change in band gap and partially to a change in crystal structure. In the present investigation there is a shift to the shorter wavelength side at either end of the series and is clearly not explainable in terms of a change in band gap or a change of structure. The Prener and Williams model is likely to be more applicable.

S^{2-} vacancies have been utilized to explain self-emission characteristics of CaS fired without activator by Ekbote.[11] Sharma[12] has observed emission of BaS:Cu phosphors in the infrared also at 3·7, 4·1 and 4·7 μ m. These are explained as transitions from the acceptor-like Cu^{+} level to the valence band and to a level little above the valence band.

Prener and Williams[13,14] have investigated the association of compensated impurities and the effect

of association on the energy-level structure. If the assumption is made that the donors and acceptors interact coulombically down to nearest neighbours, the degree of association (α_i) into pairs of ith type may be obtained from a statistical-mechanical analysis, as follows:[14]

$$\alpha_i = A \exp(e^2/\mu r_i K T) \exp(-C \sum_{i=1}^{i} Z_i) [\exp(CZ_i - 1)]$$

where A is a normalization constant, Z the number of available sites, μ the dielectric constant, r_i the inter impurity distance and C the concentration of donors and acceptors.

As we introduce BaS in CaS or CaS in BaS, the number of available sites are likely to decrease and hence the degree of association may increase. Williams[16] has pointed out that as the degree of association increases the donor and acceptor levels are perturbed towards their respective band edges and the transition energy is increased. For the case in question, we assume that Cu^+ gives rise to acceptor-like levels and S^{2-} vacancies to donor-like levels and that they are associated; the shift towards shorter wavelength is easily explained in either case in spite of the fact that the lattice constant in one case decreases and in the other increases and the band gap may decrease to some intermediate value.

References

1. Lehmaann W, *J. Lumin.*, 5 (1972), 87.
2. Pringsheim P, *Fluorescence and phosphorescence* (Interscience, New York), 1949, 597.
3. Parrish W & Cisney E, *Philips tech. Rev.*, **10** (1948), 157.
4. Lipson H, Order disorder phenomenon in alloys, in *Progress in metal physics*, edited by Bruce Chalmers, **2** (1950), 39.
5. Shizuo, Miyake & Kazuo Suzuki, *Acta crystallogr.*, **7** (1954), 514.
6. Tamman G, *Z. anorg. allgem Chem.*. **107** (1919), 1.
7. Marsh J S, *Principles of phase diagrams* (McGraw-Hill, New York), 1935.
8. Lumsden J, *Thermodynamics of alloys* (Institute of Metals, London), 1952.
9. Handerson S T. Ranby P W, Margaret B & Halstead, *J. electrochem. Soc.*, **16** (1959), 27.
10. Fehr F B, Studer F J & Fonda G R, *J. opt. Soc. Am.*, **42** (1952), 917.
11. Ekbote S N, Sivaraman S & Ranade J D, *Indian J. Phys.*, **45** (1971), 282.
12. Sharma B L, *Decay, thermoluminescence and emission studies of* BaS : Cu *phosphors*, PhD thesis, Bhopal University, Bhopal, 1977.
13. Prener J S & Williams F E, *Phys. Rev.*, **101** (1956), 1427.
14. Prener J S & Williams F E, *J. Phys. Radium*, **17** (1956), 667.
15. Prener J S, *J. chem. Phys.*, **25** (1956), 1924.
16. Williams F E, *Luminescence of organic and inorganic materials*, edited by H P Kallmann & G M Spruch (John Wiley, New York), 1962.

Indian Journal of Pure & Applied Physics
Vol. 18, January 1980, pp. 10-14

Calculation of Current Gain of Planar Transistors

ASHOK SRIVASTAVA, O P WADHAWAN & B R MARATHE
Solid State Devices Division, Central Electronics Engineering Research Institute, Pilani

Received 28 *July* 1978

An attempt has been made to explain the current gain of planar transistors from a unified approach. The analysis considers double-Gaussian model of the transistor and takes into account degeneracy in the emitter region and mobility variation in the emitter and base regions which so far have only been averaged. The closed-form analytical expression for the current gain has been obtained which has been tested for a few fabricated transistors and for transistors of known impurity profile obtained from the data of earlier workers. It is seen that the gain is very sensitive to the change in emitter profile distribution, and is maximum for an optimum emitter surface concentration.

1. Introduction

The current gain of planar transistors has been derived by several workers,[1-3] but the calculated values are always larger than the measured ones. Attempts have been made to explain this discrepancy by assuming low lifetime (in the nanosecond range) in the emitter region[4,5] and considering phosphorus atoms as very active recombination centres above $10^{19}/cm^3$ (Ref. 6). Both these assumptions lead to an increase in the base current component which, in effect, lowers the current gain. Recently it has been shown by several workers,[3,7,8] that the band-gap narrowing in the emitter region due to heavy doping explains closely the measured current gain.

However, in earlier work[3,7,8] for estimation of current gain, the mobility variation in the base and emitter regions has been assumed to have an average value which may lead to an error in the estimation of current gain. In the present paper, an attempt has been made to derive a closed-form analytical expression for the current gain, considering a double-diffused Gaussian profile which takes into account the retarding field in the base region. In calculating the base current component, narrowing of the band-gap has been considered using the expression of Volfson and Subashiev.[9] The mobility variation in the base region for the collector-current calculation has been taken into account by using an empirical relation.[10] For the emitter region, a suitable mobility variation function is developed which is close to the actual curve in the usable donor doping range for the emitter. In the present analysis, effects of varying donor concentration in the emitter region and varying junction depths on the gain have been studied. Theoretical results are compared with their corresponding measured values for several transistors made in this laboratory and close agreement has been obtained.

2. Theory

For the transistor structure (n^+-p-n-n^+) shown in Fig. 1, the current gain, limited by the injection efficiency,[1,11] is given by

$$\beta \simeq \beta_r = \frac{I_n}{I_p} \qquad \ldots(1)$$

where I_p is the minority carrier current in the emitter and I_n is the minority carrier current in the base reaching the collector junction. The corresponding double-diffused impurity profile (Fig. 2) is described by

$$N(x) = N_B \exp(-bx^2) - N_E \exp(-ax^2) + N_C \qquad \ldots(2)$$

where N_C, N_B and N_E are the collector doping, base and emitter surface concentrations respectively, x is the distance measured from the surface and is normalized with respect to X_{JE}, i.e. the emitter junction depth.

I_n has been obtained by solving the most general form of the continuity equation considering both the

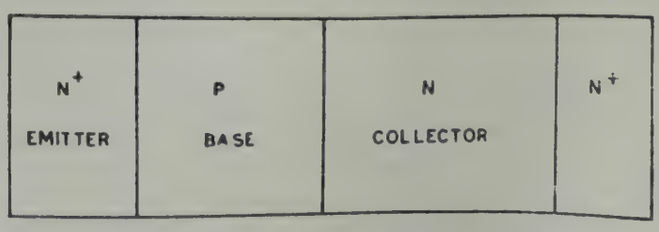

Fig. 1—Schematic of a transistor structure

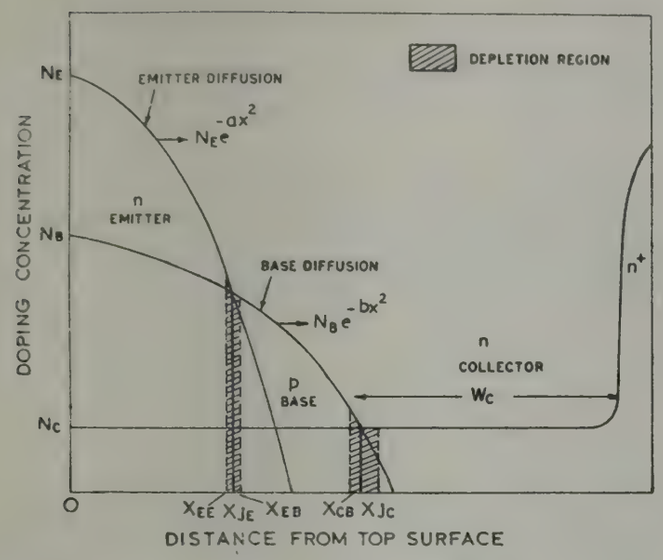

Fig. 2—Impurity profile of a double diffused epitaxial planar transistor

field and the mobility gradient which is given by

$$D_n \frac{d^2n}{dx^2} + \left(\frac{dD_n}{dx} + \mu_n E \right) \frac{dn}{dx} + \left(E \frac{d\mu_n}{dx} + \mu_n \frac{dE}{dx} - \frac{1}{\tau} \right) n = 0 \qquad ...(3)$$

where built-in field E is related to the impurity profile $N(x)$ by the expression

$$E = - \frac{kT}{q} \cdot \frac{1}{N(x)} \cdot \frac{dN(x)}{dx} \qquad ...(4)$$

The variation of mobility μ_n for silicon in the base may be suitably approximated by[10]

$$\mu_n(x) = \mu_{n_0} \cdot \left(\frac{N_B(x)}{N_\mu} \right)^{-\nu} \qquad ...(5)$$

where $N_B(x)$ is the base profile, $N_\mu = 6 \times 10^{15}/\text{cm}^3$, $\nu = 0{\cdot}25$ and μ_{n_0} can be expressed in terms of diffusion coefficient D_{n_0} using the Einstein relation which corresponds to the value of 13·5 cm²/sec.

Following the theory given by Moll and Ross,[12] one directly obtains[13]

$$I_n = \frac{A_E q n_i^2}{\Phi(x_{eb}, x_{cb})} \cdot \exp(q V_{BE}/kT) \qquad ...(6)$$

where

$$\Phi(x_{eb}, x_{cb}) = \int_{x_{eb}}^{x_{cb}} \frac{N(x)}{D_n(x)} dx = \left\{ \frac{\sqrt{(\pi)}\, N_B}{2 D_{n_0} \sqrt{[b(1+\nu)]}} \right\} \times \left(\frac{N_B}{N_\mu} \right)^{\nu} \left\{ \text{erfc} \sqrt{b(1+\nu)x} \Big|_{x_{cb}}^{x_{eb}} - \sqrt{\left(\frac{1+\nu}{\sigma+\nu} \right)} e^{a-b} \cdot \text{erfc} \sqrt{(a+\nu b)x} \Big|_{x_{cb}}^{x_{eb}} \right\} \qquad ...(7)$$

where $\sigma = a/b$ and x_{eb} and x_{cb} are the positions of depletion layer edges in the base region at emitter and collector respectively. A_E is the emitter area and V_{BE} the base-emitter junction voltage.

For deriving the expression for I_p, the continuity equation can be written as

$$D_p \frac{d^2p}{dx^2} + \left(\frac{dD_p}{dx} + \mu_p E \right) \frac{dp}{dx} + \left(E \frac{d\mu_p}{dx} + \mu_p \frac{dE}{dx} - \frac{1}{\tau} \right) p = 0 \qquad ...(8)$$

where

$$E = \frac{kT}{q} \cdot \frac{1}{N(x)} \cdot \frac{dN(x)}{dx} \qquad ...(9)$$

and

$$N(x) = N_E \exp(-ax^2) - N_B \exp(-bx^2) \qquad ...(10)$$

The effect of heavy doping in the emitter region has been considered by using the expression of Volfson and Subashiev[9] for the band-gap narrowing. The emitter profile described in Eq. (10) is thus transformed to[3]

$$N_E^{\text{eff}}(x) = N_E(x) \exp\left[- \frac{3{\cdot}4 \times 10^{-8}}{kT} q \times \left(N_E^{1/3}(x) - N_D^{1/3} \right) \right] \qquad ...(11)$$

for $x < x_D$ where x_D is the point on the emitter profile at which heavy doping starts. At $x = x_D$; $N_E^{\text{eff}}(x_D) = N_D = 1{\cdot}85 \times 10^{19}/\text{cm}^3$ (Ref. 3).

Following the theory given by Moll and Ross,[12] one gets

$$I_p = \frac{A_E q n_i^2}{x_{jE} \Phi(0, x_{ee})} \cdot \exp(qV_{BE}/kT) \qquad ...(12)$$

where

$$\Phi(0, x_{ee}) = \int_0^{x_{ee}} \frac{N(x)}{D_p(x)} dx \qquad ...(13)$$

x_{ee} is the position of the depletion layer width in the emitter region.

The integral in Eq. (13) can be broken into two parts, as

$$\int_0^{x_{ee}} \frac{N(x)}{D_p(x)} dx = \int_0^{x_D} \frac{N_E^{\text{eff}}(x)}{D_p(x)} dx + \int_{x_D}^{x_{ee}} \frac{N(x)}{D_p(x)} dx \qquad ...(14)$$

Letting

$$\int_0^{x_D} \frac{N_E^{\text{eff}}(x)}{D_p(x)} dx = \Phi(0, x_D) \qquad ...(15)$$

and

$$\int_{x_D}^{x_{ee}} \frac{N(x)}{D_p(x)}\, dx = \Phi(x_D, x_{ee}) \qquad ...(16)$$

we find

$$\Phi(0, x_{ee}) = \Phi(0, x_D) + \Phi(x_D, x_{ee}) \qquad ...(17)$$

For evaluating functions described by Eqs. (15) and (16), the following simplifications have been made.

The effective emitter profile $N_E^{\text{eff}}(x)$ which is part of the emitter profile has been approximated by the exponential function of the form:

$$N_E^{\text{eff}}(x) = Ae^{Bx} \qquad ...(18)$$

The actual effective profile and suitable approximated profile are shown in Fig. 3.

The constants A and B are obtained from the following conditions:

at $x = 0$, $N_E^{\text{eff}}(x) = A = N_E \exp\{-1{\cdot}36\times 10^{-6}(N_E^{1/3} - N_D^{1/3})\}$ and at $x = x_D$,

$$N_E^{\text{eff}}(x_D) = N_D = A.\exp(Bx_D) \qquad ...(19)$$

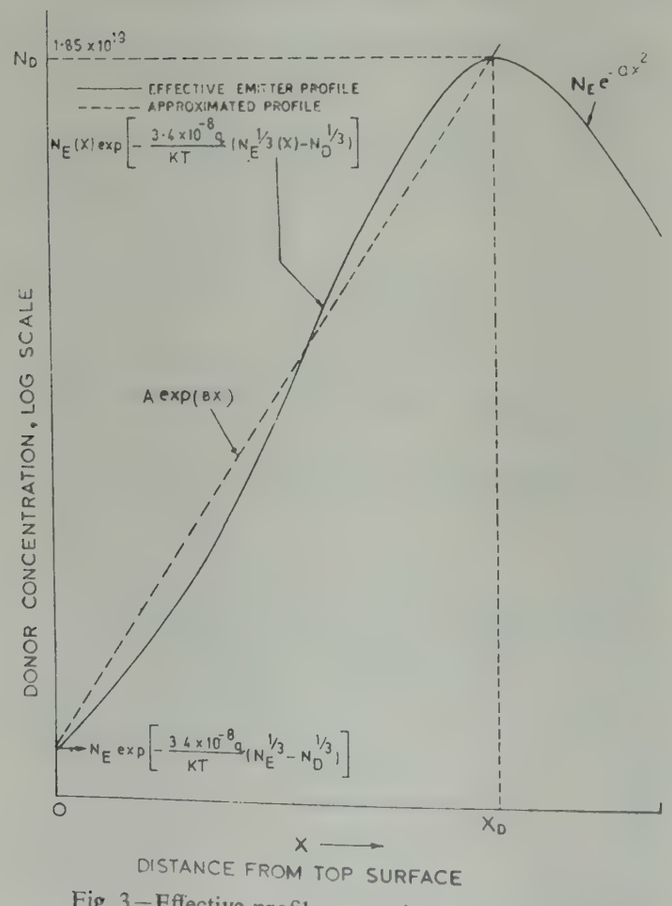

Fig 3—Effective profile approximation by exponential function for $0 \leqslant x \leqslant x_D$

or

$$B = \frac{1}{x_D} \ln\left[\frac{N_D}{N_E \exp[-1{\cdot}36\times 10^{-6}(N_E^{1/3} - N_D^{1/3})]}\right] \qquad ...(20)$$

For mobility variation in the emitter region, a suitable approximation has been developed. The approximated function is of the form

$$\mu_p = \mu_{p_0}\left(\frac{N_E(x)}{N_{r_0}}\right)^{-r} \cdot g \cdot \left(\frac{10^{19} + N_E(x)}{N_{\delta_0}}\right)^{\delta}$$

$$\text{for } 5\times 10^{16} \leqslant N_D \leqslant 10^{21}. \qquad ...(21)$$

Fig. 4 shows the variation of mobility of holes versus donor concentration together with the approximated function. The fitting parameters involved in Eq. (21) for the mobility variation shown in Fig. 4 are $\gamma = 0{\cdot}39$, $\delta = 0{\cdot}47$, $\mu_{p_0} = 400$ cm^2/V-sec. $N_{r_0} = 5\times 10^{16}$/cm^3, $g = 0{\cdot}72$ and $N_{\delta_0} = 10^{19}$/cm^3.

Expressing

$$10^{19} + N_E(x) = 10^{19} + (N_E)\exp(-ax^2) \equiv (N_1)\exp(-a_0x^2) \qquad ...(22)$$

where the constants N_1 and a_0 are obtained from the following conditions:

$$\text{at } x = 0;\ N_1 = 10^{19} + N_E$$

$$\text{and} \quad \text{at } x = 1;\ 10^{19} + N_E e^{-a} = N_1 e^{-a_0} \qquad ...(23)$$

$$\text{or } a_0 = \ln\left(\frac{N_1}{10^{19} + N_E e^{-a}}\right) = \ln\left(\frac{10^{19} + N_E}{10^{19} + N_E e^{-a}}\right) \qquad ...(24)$$

Substituting Eqs. (23) and (24) in Eq. (21), we obtain

$$\frac{1}{\mu_p} = \frac{1}{\mu_{p_0}\cdot g}\cdot\left(\frac{N_E}{N_{\gamma_0}}\right)^{\gamma}\cdot\left(\frac{N_1}{N_{\delta_0}}\right)^{-\delta} \times \exp\{-x^2(\gamma a - \delta a_0)\} \qquad ...(25)$$

or

$$\frac{1}{D_p} = \frac{1}{D_{p_0}}\left(\frac{N_E}{N_{\gamma_0}}\right)^{\gamma}\left(\frac{N_1}{N_{\delta_0}}\right)^{-\delta} \times \exp\{-x^2(\gamma a - \delta a_0)\} \qquad ...(26)$$

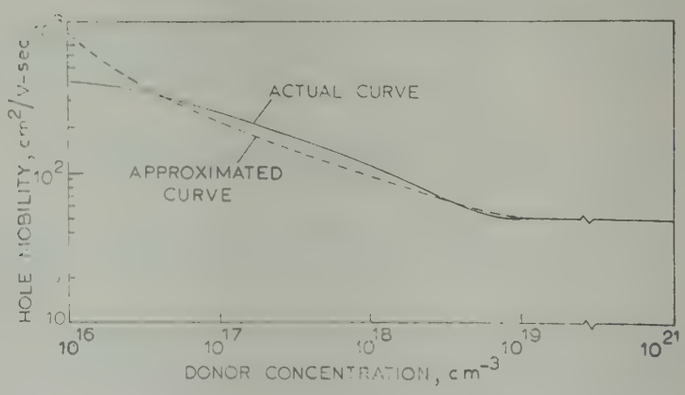

Fig. 4—Approximation to the mobility variation versus donor concentration

where $D_{P_0} = (kT/q) \cdot \mu_{P_0} \cdot g$

Substituting Eqs. (18) and (26) in Eq. (15), one gets

$$\Phi(0, x_D) = \frac{A \exp\{B^2/4(\gamma a - \delta a_0)\}}{D_{P_0}} \left(\frac{N_E}{N_{\gamma_0}}\right)^{\gamma} \cdot \left(\frac{N_1}{N_{\delta_0}}\right)^{-\delta} \frac{1}{\sqrt{(\gamma a - \delta a_0)}} \cdot \frac{\sqrt{\pi}}{2} \cdot \left[\operatorname{erfc}\left(\frac{B}{2\sqrt{(\gamma a - \delta a_0)}} - \sqrt{(\gamma a - \delta a_0)}\, x_D\right) - \operatorname{erfc}\left(\frac{B}{2\sqrt{(\gamma a - \delta a_0)}}\right)\right] \quad \ldots(27)$$

It is to be mentioned here that in evaluating the above function, contribution due to the base profile in considering the net profile in the emitter region has not been considered, since it is negligible in comparison to the contribution due to emitter profile.

Substituting Eqs. (10) and (26) in Eq. (16), one gets

$$\Phi(x_D, x_{ee}) = \frac{1}{D_{P_0}} \cdot \left(\frac{N_E}{N_{\gamma_0}}\right)^{\gamma} \left(\frac{N_1}{N_{\delta_0}}\right)^{-\delta} \frac{\sqrt{\pi}}{2} \cdot \left[\frac{N_E}{\sqrt{[a + (\gamma a - \delta a_0)]}} \cdot \left(\operatorname{erfc} \sqrt{[a + (\gamma a - \delta a_0)]}\, x_D - \operatorname{erfc} \sqrt{[a + (\gamma a - \delta a_0)]}\, x_{ee}\right) - \frac{N_B}{\sqrt{[b + (\gamma a - \delta a_0)]}} \cdot \left(\operatorname{erfc} \sqrt{[b + (\gamma a - \delta a_0)]} - \operatorname{erfc} \sqrt{[b + (\gamma a - \delta a_0)]}\, x_{ee}\right)\right] \quad \ldots(28)$$

Putting expression (5) and combination of expressions (12), (17), (27) and (28) in relation (1) for current gain, finally one obtains

$$\beta = \frac{\Phi(0, x_{ee})}{\Phi(x_{eb}, x_{cb})} = \frac{\Phi(0, x_D) + \Phi(x_D, x_{ee})}{\Phi(x_{eb}, x_{cb})} \quad \ldots(29)$$

where $\Phi(0, x_D)$, $\Phi(x_D, x_{ee})$ and $\Phi(x_{eb}, x_{cb})$ are given by Eqs. (27), (28) and (17) respectively.

3. Illustrative Example

To illustrate the effects of heavy doping, mobility variation and impurity profile variation on the current gain of bipolar transistors, a typical double diffused planar transistor is considered. The profile parameters are:

$N_C = 10^{15}$ cm^{-3}, $N_B = 10^{18}$ cm^{-3}, $N_E = 10^{21}$ cm^{-3}, $X_{jE} = 2{\cdot}5$ μm, $X_{jC} = 4{\cdot}0$ μm, $a = 9{\cdot}2$ and $b = 2{\cdot}7$.

In Fig. 5, current gain (β) versus donor concentration N_D is shown, β being expressed in percentage with respect to its maximum value. Initially β increases, reaches to its maximum value and finally decreases. The decrease in the current gain is due to the heavy doping which reduces the emitter charge. Similar variation has been reported by other workers also.[3,7,8]

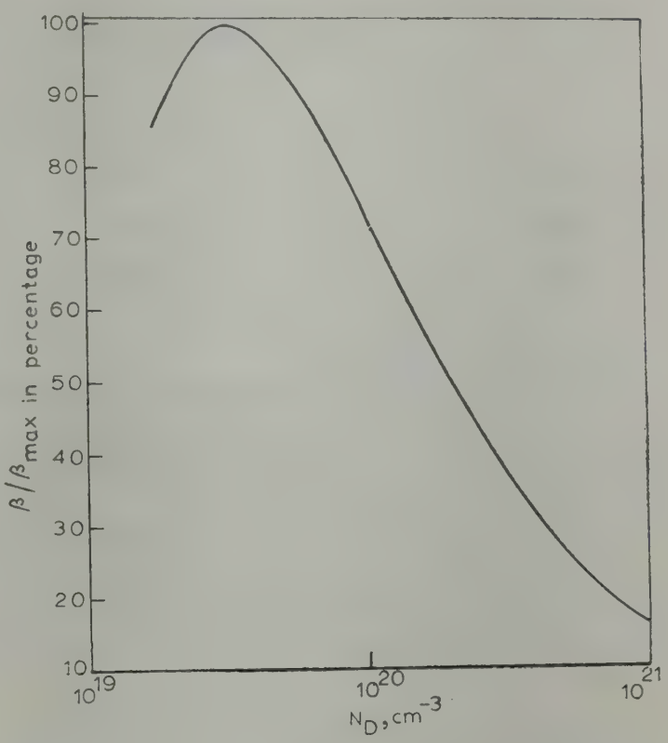

Fig. 5—Normalized common emitter current gain as a function of the donor surface concentration (N_D)

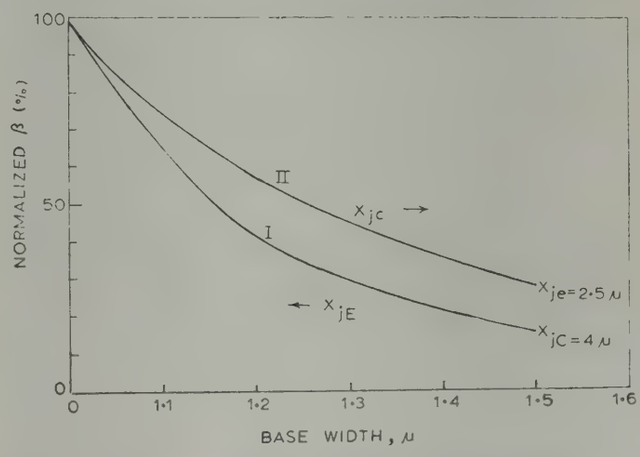

Fig. 6—Normalized current gain as a function of the base width for two emitter profiles

As noted from Fig. 5, maximum current gain for the profile taken is obtained at $N_D \simeq 3 \times 10^{19}$ cm^{-3}. To obtain maximum current gain, in the actual fabrication, the emitter surface concentration should be kept around this critical value.

In Fig. 6 the effect of changing emitter and base profile on the current gain is shown. Curve I shows the β variation with X_{jE}, keeping the other profile parameters to be the same. Curve II shows the variation with X_{jC} fixing the other profile parameters. It is seen from the figure that β is more sensitive to the emitter profile parameters rather than the base profile parameters.

Table 1 —Profile Parameters of the Self-fabricated Planar Transistors
(N's in cm^{-3} and X's in μm)

	N_C	N_B	N_E	X_{jE}	X_{jC}	β	
						Calculated	Measured
Wafer 1	5×10^{15}	10^{18}	10^{21}	2·8	4·4	750	700-800
Wafer 2	10^{15}	$6·5 \times 10^{17}$	10^{21}	2·1	3·7	1065	800-1100
Wafer 3	5×10^{15}	$1·5 \times 10^{18}$	10^{21}	1·9	4·3	76	35-50

4. Experimental Verification

In order to check the theoretical results and the validity of the approximations involved in the theory, three different types of double diffused transistors were fabricated on three silicon wafers, by changing the processing parameters. The collector background doping N_C was obtained from resistivity measurements. N_B was obtained from Irvin's curves[14] by the use of the measured B-C junction depth and the base sheet resistivity after drive-in. Both the B-C and E-B junction depths were measured by the angle lapping technique. Finally, N_E was determined from the solid solubility of phosphorus in silicon curve[15] at the diffusion temperature. The values of the various diffusion parameters are listed in Table 1.

The theoretical value of the current gain (β) of the transistors is calculated from Eq. (29) using profile parameters of Table 1. These values are also listed in this table along with their measured values. The measured current gain corresponds to the value of the gain for moderate collector current levels for which the gain is nearly independent of it. In Table 1, the range of the measured current gain is mentioned which represents the majority of the transistors probed on wafers 1, 2 and 3. The close agreement between the measured and theoretical current gain values reveals the significance of the heavy doping in the emitter and the mobility variation in the base and emitter regions and their effects on the gain.

Acknowledgement

The authors would like to thank Prof. A B Bhattacharyya (Indian Institute of Technology, New Delhi) and Dr S K Bhatnagar for their helpful discussions. They also wish to convey their sincerest thanks to Dr Amarjit Singh, Director, Central Electronics Engineering Research Institute, Pilani for critically going through the manuscript and interest taken.

References

1. Kennedy D P & Murley P C, *IRE Trans.*, ED-9 (1962), 136.
2. Tanneubaum M & Thomas D E, *Bell Syst. tech. J.*, 35 (1956), 1.
3. DeMan H J J, *IEEE Trans.*, ED-18 (1971), 833.
4. Ghosh H N, De La Mondea F H & Dono R N, *Solid St. Electron.*, 10 (1967), 705.
5. Hachtel G D, Joy R C & Cooley J W, *Proc. IEEE*, 60 (1972), 86.
6. Whittier R J & Downing J P, *Simple Physical Model for the Injection Efficiency of Diffused P-N Junctions*, Paper presented at the International Electron Devices Meeting, Washington DC, 1968, paper 12·4.
7. Mortens R P, DeMan H J & Van Overstraeten R J, *IEEE Trans.*, ED-20 (1973), 772.
8. Kannam P J, *IEEE Trans.*, ED-20 (1973), 845.
9. Volfson A A & Subashiev V K, *Soviet Phys., Semicond.*, 1 (1967), 327.
10. Thomas R E & Boothroyd A R, *Solid-St. Electron.*, 11 (1968), 365.
11. Whittier R J & Tremere D A, *IEEE Trans.*, ED-16 (1969), 39.
12. Moll J L & Ross I M, *Proc. IRE*, 44 (1956), 72.
13. Basavaraj T N & Bhattacharyya A B, *Solid St. Electron.*, 16 (1973), 921.
14. Irvin J C, *Bell Syst. tech. J.*, 41 (1962), 387.
15. *Fundamentals of silicon integrated devices technology*, edited by R M Burger and R P Donovan (Prentice-Hall, New York), 1968, 254.

Indian Journal of Pure & Applied Physics
Vol. 18, January 1980, pp. 15-19

Photoconducting Properties of CdS:Na Films

B B Bargale & S H Pawar
Department of Physics, Shivaji University, Kolhapur 416 004

Received 21 *August* 1978; *revised received* 19 *December* 1978

CdS thin films doped with varying concentrations of sodium have been prepared by the chemical bath deposition technique and their photoconducting rise and decay have been systematically studied at 260, 299 and 363 K. The rise and decay curves have been analyzed to yield the values of activation energies. The role of oxygen adsorption on the surface of the film is discussed at length. The time constants t_r and t_d have been evaluated and the effect of light intensity on them is discussed in the light of the pinning of quasi-Fermi level. The concept of pinning is supported further by the observations made on the variation of photocurrent with light intensity. A relatively simple approach has been developed to find the lifetime of electrons in the conduction band.

1. Introduction

Pavaskar *et al.*[1] have recently reported a new technique for the chemical bath deposition of CdS thin films. It has the advantages of simplicity, economy, large area and uniformity of film deposition of CdS. Further, the desired impurities can be doped during the preparation itself. A preliminary report has been made by them on the dopings of Cu, In, etc. No report is made on the dopants of IA impurities. In the recent years, an attempt has been made to prepare *p*-type CdS single crystals with Group IA impurities.[2-5] In the present investigation, CdS thin films have been prepared with various weight percentages of sodium as a dopant. Photoconducting rise and decay have been measured both for CdS and CdS:Na thin films at different intensities and temperatures. The time constants t_r and t_d respectively for rise and decay have been evaluated at various excitation light intensities. At a high intensity of excitation, the pinning of the quasi-Fermi levels has been observed. A relation has been set up between the photodesorption of oxygen molecules and the risetime of photocurrent. Further, a relatively simple approach has been followed to find the lifetime of an electron in the conduction band.

2. Experimental Details

2.1 Films Preparation

The CdS:Na thin films were prepared by the chemical bath deposition technique as reported by Pavaskar *et al.*[1] The compounds used in this method were cadmium sulphate, thiourea and ammonia solution. For each deposition, 20 cc of one mole cadmium sulphate solution was mixed with 100 cc of two mole ammonia solution in a 250 cc beaker, when a complex compound called cadmium tetra-ammonium sulphate was formed. To this solution 20 cc of one mole thiourea solution was added and the reaction vessel heated to about 90°C for 30 min after addition of appropriate sodium sulphate solution. In this solution four glass substrates were kept rotating with a constant speed of 100 rpm so that the substrates expose continuously to the fresh reacting solution. The films prepared were washed with distilled water, dried and were cut into small sizes of about 0·3 cm width and 1 cm length for experiments. Ohmic contacts were made by evaporation of indium in a vacuum of about 10^{-5} torr.

2.2 Photoconducting Rise and Decay Measurements

The sample was mounted in a cryostat under a vacuum of 10^{-3} torr. A tungsten filament lamp was used for excitation. To avoid heating, a water filter was interposed between source and the sample. The photoconducting rise and decay curves at different temperatures were recorded with Omniscribe recorder.

3. Results and Discussion

3.1 Concentration Quenching

Sodium dopant in CdS gave more photocurrent than with Li or K as dopant and hence this sample was studied in detail for its concentration effect. To dope sodium with various weight percentages in CdS, the appropriate solutions of Na_2SO_4 were added in the reaction vessel and the doping of sodium in the films was confirmed qualitatively by analyzing the deposited film material following the spec-

troscopic method. Dopant concentrations varying from about 0·005 to 3·0% by weight in CdS were prepared and the maximum photocurrents compared for an excitation light intensity of 44 mW/cm². The results are presented in Fig. 1. The photocurrent with different concentrations of Na, follows a specific pattern of increase in photocurrent with increase of concentration reaching a maximum at an optimum concentration level (about 1%) after which the photocurrent falls off for any further increase in dopant concentration. This is explainable in terms of the 'concentration quenching effect' and can be understood as follows.

For an *n*-type semiconductor, the photocurrent (I) is given by:[6]

$$I = \frac{e\,FV\,\mu_n\,\tau}{L^2} \qquad ...(1)$$

where e is the charge of an electron; F, the excitation rate; L, the length of the films (1 cm); V, the applied bias voltage (100 V); τ, the lifetime of an electron; and μ_n, the mobility of an electron.

The parameters F, V and L were kept constant for studying the sodium dopant effect on photocurrent. The increase in photocurrent with the increase in sodium concentration is, therefore, attributed to $\mu_n\,\tau_n$. However, recent observations[7] on photo-Hall effect of these films have revealed that μ_n decreases with sodium doping and hence the increase in photocurrent is mainly due to increase in τ_n. This is understood on the basis that Na^+ ions placed at the substitutional site at Cd^{2+} in CdS, act as the hole recombination centres. The increase in sodium concentration gives rise to increase in τ_n and hence photocurrent. This process continues only up to 1% wt of Na in CdS. Beyond that Na may go to the interstitial positions (due to lack of substitutional sites) which act as electron recombination centres. This gives rise to a decrease in photocurrent.

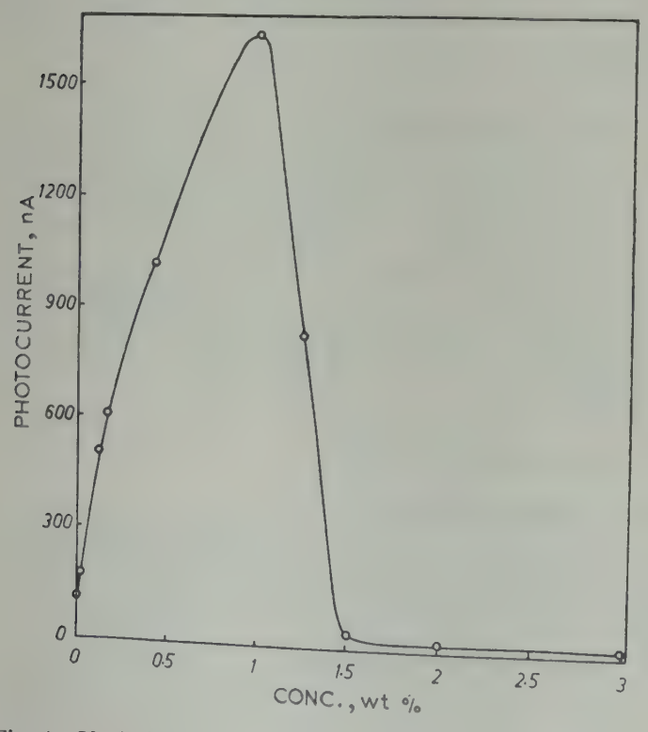

Fig. 1—Variation of the photocurrent with the weight percentage concentration of Na in CdS:Na films for an excitation light intensity of 44 mW/cm²

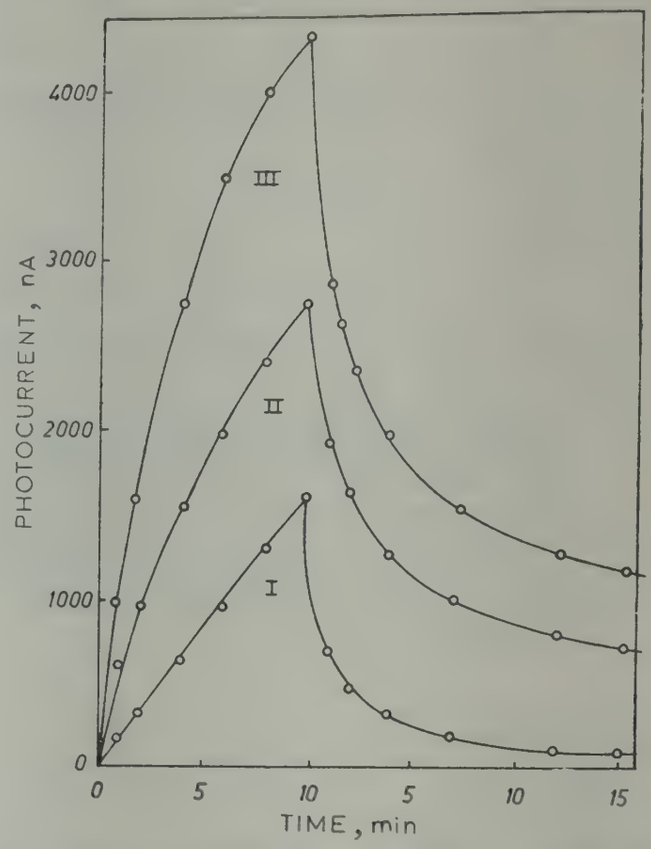

Fig. 2—Photoconducting rise and decay of CdS:Na films (Na = 1·0 wt %) for the first three cycles, each of 25 min (10 min rise and 15 min decay) at excitation light intensity of 44 mW/cm²

3.2 Effect of Oxygen Adsorption on Rise and Decay

Photoconducting rise and decay curves for CdS:Na (1% wt of Na) film of first three successive cycles each having a duration of 25 min, were recorded with an applied field of 100 V/cm across the film, and the plots are shown in Fig. 2. In the first cycle of excitation, the photoconducting rise curve is linear. But in the second and further successive cycles of excitation, the photocurrent gets increased and the rise curve has a bent towards the saturation value. The linear nature of the photoconducting rise curve in the first cycle of excitation is found for all the concentrations of sodium dopant. This type of nature, however, did not establish in case of undoped CdS thin films. The linear nature of photoconducting rise curve as

well as the low value of photocurrent in the first cycle of excitation are supposed to be due to the oxygen molecules adsorbed on the surface of the film. In this method of preparation, the films prepared with dopants were found to be less crystalline than those without dopant.[1] Comparatively the adsorption of oxygen on the surface of doped films is more than that for undoped films. The oxygen molecules adsorbed on the surface act as electron traps[8-11]. When the film is exposed first time to light under vacuum, there is photodesorption of oxygen, which in turn increases the photocurrent with time t after excitation. If N_1 is the number of oxygen molecules adsorbed on the surface at $t = 0$ and N the number of oxygen molecules adsorbed on the surface at time t, then

$$\frac{N_1 - N}{N_1} = \frac{\Delta I}{I} (= Se^{-E/kT})t \qquad ...(2)$$

where ΔI is the photocurrent at time t, I the saturation photocurrent, E the energy of photodesorption, T, the temperature, S, the escape frequency factor and k, the Boltzmann's constant. Eq. (2) explains the linear nature of photoconducting rise curve in Fig. 2. The slope of the curve is $I\ Se^{-E/kT}$. Assuming the value of $S = 10^{10}$ sec^{-1} (Ref. 12), the value of E has been evaluated and it comes to about 0·78 eV. This is in good agreement with the values reported earlier.[13,14]

The photodesorption of oxygen molecules during the first cycle of excitation will give rise to the higher photocurrent observed in the second cycle of excitation and so on.

Though the nature of the photoconducting rise curves in first and the next successive cycles of excitation is different, there is no difference in the nature of the photoconducting decay curves observed. The photocurrent values after 10 min of excitation are normalized to a value 100. The typical plot of log I versus time t is shown in Fig. 3, for the photoconducting decay curve of CdS:Na thin films. The nonlinear nature of the curve indicates that there is no exponential distribution of traps. The curve has been further analyzed by the 'peeling-off' method[14] and the values of trap depths E are evaluated. The value of E lies between 0·6 and 0·8 eV. This value is identical with that evaluated from the photoconducting rise curve. This reveals that both photoconducting rise and decay are attributable to electron traps due to the oxygen molecules adsorbed on the surface of the film.

3.3 Temperature Dependence of Rise and Decay

Photoconducting rise and decay curves were recorded at 260, 300 and 363 K for CdS:Na thin films. The linear nature of the photoconducting rise curve has been observed at 260 and 300 K but at higher temperatures the rise curve is exponential and this is due to lack of additional electron trapping centres of oxygen molecules. The photoconducting decay curves, though identical at all temperatures, have different values of decay constants. Fig. 4 shows log I versus log t plots for photoconducting decay at three different temperatures. For each temperature, there are two linear regions, obeying the relation

$$I_t = I_0\ t^{-b} \qquad ...(3)$$

where I_t is the photocurrent at time t after switching off the excitation, I_0 the initial photocurrent at $t = 0$ and b the decay constant. The decay constant is found to be a function of temperature. The values of decay constant for the regions I and II denoted respectively by b_1 and b_2 and are listed in Table 1. The region I is associated with the shallow traps while region II is due to deep traps. It is noted that

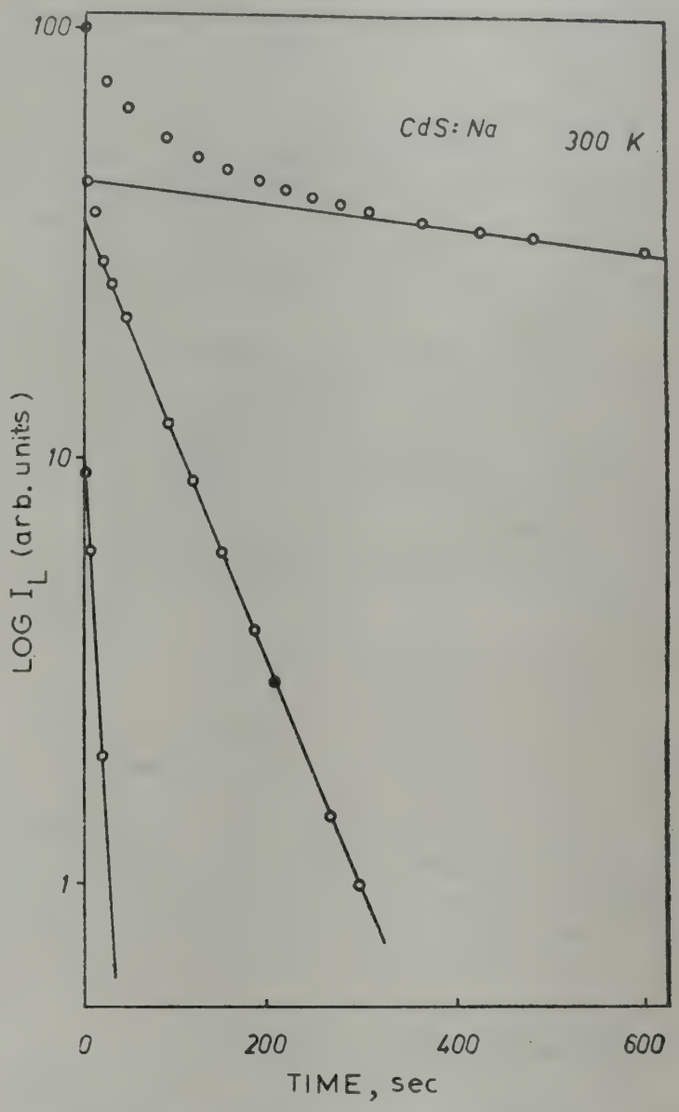

Fig. 3—Peeling-off of decay curve for CdS:Na film

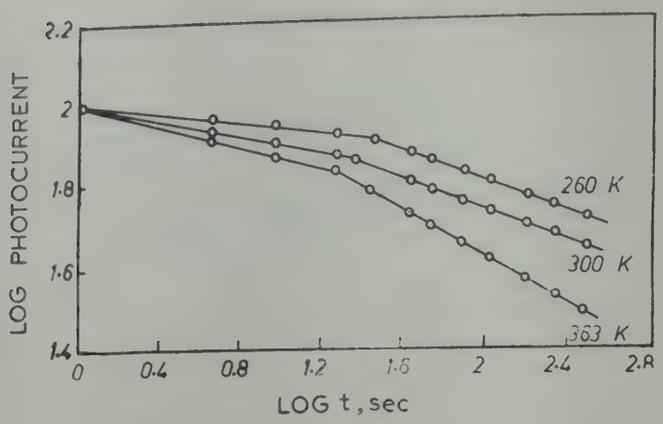

Fig. 4—Log photocurrent (in nA) versus log t for CdS:Na films at 260 K, 300 K and 363 K

Table 1—Values of Decay Constants for Region I and II

Temp. K	$-b_1$	$-b_2$	Demarcation time, sec
260	0·05	0·172	30·2
300	0·10	0·177	25·12
363	0·11	0·330	19·95

the decay is becoming faster as the temperature is increased. Further, the demarcation time between region I and region II is shifting towards the shorter value with increase of temperature. The values of demarcation times are listed in Table 1.

3.4 Rise and Decay Time-constants

The rise and decay time-constants, t_r and t_d defined as the time required for the photocurrent to rise to 63% of the stationary value or to decay to the same percentage of the preliminary value, are evaluated from the photoconducting rise and decay curves. The variation of time-constants t_r and t_d with light excitation density for CdS:Na films at 300 K is shown in Fig. 5. It is noted that t_r is larger than t_d. This decay in photocurrent has been attributed to the role of oxygen adsorbed on the surface of the film. The decay constants are found to decrease faster in the low excitation density region and to decrease slower at high excitations. This decrease in the value of decay constants can be understood by considering the spreading of the two quasi-Fermi levels with the excitation. The number of recombination centres M, will be increased due to the spreading of two quasi-Fermi levels.[15] The time-constant is given by the relation.[16]

$$\text{Time-constant} = \frac{1}{RM} \qquad \ldots(4)$$

where R is the recombination coefficient. The slow decrease of the time-constants is attributed to the pinning of the quasi-Fermi levels which will forbid the increase in M. The pinning of the Fermi levels might have originated due to the high density of trapping states near the quasi-Fermi levels. This is analogous to that reported by Pavaskar *et al.*[1] for CdS films.

The pinning of the quasi-Fermi level is further supported by the experimental results on variation of photocurrent with light intensity. The plot of log I versus log F_L is shown in Fig. 6. It is found that at the initial low intensities, the photocurrent rises linearly with a faster rate up to $F = 5 \times 10^{18}$ carriers/sec. Beyond this F, there occurs a slow linear decrease. From Fig. 5, it is noted that the slow decrease in t_r sets in for the same value of F.

3.5 Life-time of an Electron

The lifetime, τ_n of an electron in the conduction band is the key parameter for an understanding of

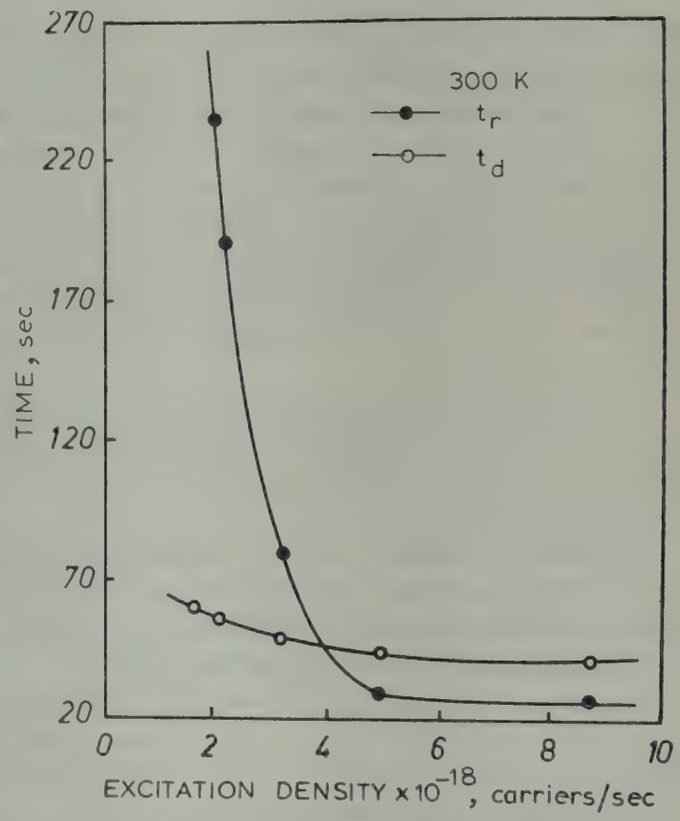

Fig. 5—Variation of time constant t_r and t_d with excitation density at room temperature for CdS:Na film

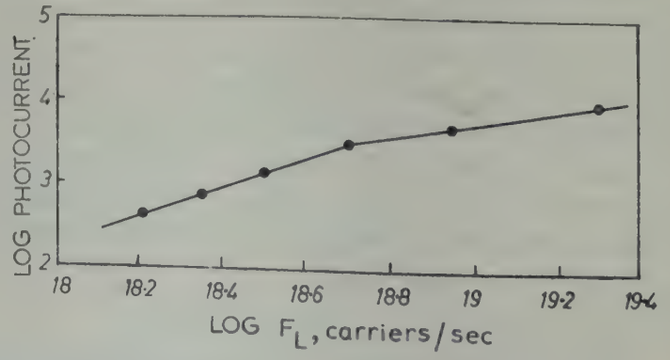

Fig. 6—Photocurrent (in nA) as a function of light intensity (F_L) forCdS:Na (log-log plot)

photoconductivity. An attempt has been made in the present investigation to evaluate τ_n from the study of photodesorption of oxygen molecules from the surface of the film. In this regard, the effect of excitation density on the desorption of oxygen molecules has been considered. The photocurrent ΔI is proportional to $N_1 - N$, i.e. the number of oxygen molecules desorbed. Due to desorption of oxygen molecules, the number n of electrons left behind in the conduction band, is given by

$$n = \frac{\Delta I}{e \mu_n V} \frac{l}{W \cdot x} \qquad ...(5)$$

where V is the voltage applied, l the length, W the width, x the thickness of the sample and μ_n the mobility of an electron which was determined from photo-Hall measurement and was found to be $2{\cdot}5 \times 10^{-3}$ cm^2/V-sec. For the value of $n = 6 \times 10^{15}$ carriers cm^{-3}, the plot of log F versus log t is found to be linear indicating that the excitation density (F) and time (t) follow the relation

$$F = c\, t^{-b} \qquad ...(6)$$

where the constant b depends on the rate of photodesorption, given by $\frac{n}{\tau_n} t^b$ and is the intercept on log F axis. The value of τ_n evaluated from this is of the order of 10^{-3} sec.

Acknowledgement

The authors wish to thank Dr A V Narlikar, Assistant Director, National Physical Laboratory, New Delhi, for his constant encouragement and comments. They are indebted to one of the CSIR Fellows, Mr A G Shikalgar for his help during experiments.

References

1. Pavaskar N R, Menezes C A & Sinha A P B, *J. electrochem. Soc.*, **124** (1977), 743.
2. Tell B, *J. appl. Phys.*, **42** (1971), 2919.
3. Anderson W W & Mitchell J T, *Appl. Phys. Lett.*, **12** (1968), 334.
4. Tell B & Gibson, *J. appl. Phys.*, **40** (1969), 5320.
5. Shikalgar A G, Bargale B B & Pawar S H, *Indian J. pure appl. Phys.*, **15** (1977), 747.
6. Rose A, *Concepts in photoconductivity and allied problems* (Interscience Publishers, New York), 1963, 6.
7. Bargale B B, Shikalgar A G & Pawar S H, *Indian J. Phys.*, **52A** (1978), 305.
8. Hughes D M & Carter G, *Phys. Status Solidi*, **25** (1968), 449.
9. Lerge J P & Martinuzzi S, *Phys. Status Solidi*, **A1** (1970), 689.
10. Thomas P A, Sebenne C & Balkanski M, *Rev. Phys. Appl.*, **5** (1970), 683.
11. Chen-Ho Wu$^+$ & Richard H Bube, *J. appl. Phys.*, **45** (1974), 2.
12. Bube R H, *Photoconductivity of solids* (John Wiley, New York), 1960.
13. Williams R, *J. Phys. Chem. Solids*, **23** (1962), 1957.
14. Mark P, *J. Phys. Chem. Solids*, **26** (1965), 959.
15. Rose A, *Concepts in photoconductivity and allied problems* (Interscience Publishers, New York), 1963.
16. Bhar Tarak N & Linder John S, *Thin Solid Films*, **21** (1974), 267.

Indian Journal of Pure & Applied Physics
Vol. 18, January 1980, pp. 20-23

Thermal Currents in Magnetically Polarized Silastic Tubular Electrets

Rudra Kant Srivastava, M L Khare, M S Qureshi & C S Bhatnagar
Department of Physics, M A College of Technology, Bhopal

Received 19 *September* 1978; *revised received* 26 *December* 1978

Thermal currents obtained from magnetically polarized silastic tubular electrets are interpreted in terms of dipole orientation, space charges due to ionic motion and electron and/or ion trapping. The trapping parameters are obtained using Bucci method [Bucci & Fieschi., *Phys. Rev.*, **148** (1966), 816] and the curve fitting technique due to Cowell and Woods [*Br. J. appl. Phys.*, **18** (1967), 1045]. The results are consistent with two traps in silastic at depths of 0·81 and 1·74 eV due to idiocharge and isocharge respectively. However, the nature of the second current maximum (1·74 eV) is ionic. The polarization in these tubular electrets is found to be uniform. The amount of charge (of both signs) released during depolarization (calculated from the area under the two peaks) has been evaluated and its variation with polarizing temperature (T_f) and polarizing field (H_f) has also been studied. The effect of different storage times (determined by the TSD technique) revealed that about 29% of the charge gets decayed during storage for 10 days. The outer surface of the electrets is found to have more charge than the inner surface. The depth of penetration of charge (for the second trap) comes out to be $4{\cdot}59 \times 10^{-3}$ cm which amounts to 2·3 % penetration.

1. Introduction

Murphy and Holly[1] and Gunter and Le Beau[2] have investigated the possibility of using tubular electrets of plexiglass as prostheses. But the high electric field used during their preparation, produces microscopic perforations, rendering them unsuitable for prosthetic work. As suggested by Gunter and Le Beau this problem can be eliminated by using magnetoelectrets[3] in which a magnetic field replaces the electric field during formation. Moreover, to prevent coagulation of blood, the tube should have negative charges[4] on inner and outer surfaces. This is possible in magnetoelectrets which under suitable conditions possess isocharge (charge of same sign).

The initial study of thermally stimulated discharge (TSD) in perspex (plexiglass) tubular magnetoelectrets[5] is quite encouraging. Therefore, the work has now been extended to a more useful substance for prosthetic work, namely silastic (silicone rubber) which has some specific advantages[6] over other plastic materials. Moreover, magnetoelectrets made with this material possess iso negative charge,[6] which is a desirable condition for prosthetic application. Hence, it is thought worthwhile to investigate magnetoelectrets made with this material following the TSD technique which gives a better understanding of the charging and discharging processes.

Perlman[7] and Perlman and Creswell[8] have reported an expression connecting the discharge current with temperature based on the release of charge carriers from traps. They have used this expression to analyze the TSD peaks obtained from near surface charged insulators, heated at a constant rate.

Perlman[7] has shown that both types of processes (dipole orientation and trapping of charges) must be used to explain the TSD of electrets. The same model has been adopted by us in the present investigation in the case of the magnetoelectret state in silastic. One may check whether a particular peak agrees with theory, either by the method due to Bucci and Fieschi[9] or that due to Cowell and Woods.[10]

2. Experimental Details

Silastic tubings of diameter 0·8 cm (including wall thickness of 0·2 cm) were used for the present study. The tubes were first cleaned with lukewarm water, to remove any surface impurity (as recommended by the manufacturer (Dow Corning, New York, USA). Pieces of 3·2 cm length were then cut to prepare magnetoelectret samples. The method of preparation was the same as that used earlier.[5] The constant forming temperature (T_f) was measured by a calibrated copper-constantan thermocouple. The forming magnetic field (H_f) was applied for 2 hr, one hour at the elevated forming temperature followed by one hour of cooling. Samples were prepared corresponding to T_f = 95, 120 and 140°C and at each T_f, forming magnetic fields of 3·11, 4·45, 5·04 and 5·96 kOe were used. Allowing an interval of 5 min after polarization, the discharge currents were obtained using a linear heating rate of 1·0 °C/min. The current was measured by a Keithley electrometer (model 610 C).

In order to study the effect of different storage times on these magnetoelectrets, some of the samples were kept in a desiccator for half, 1, 5 and

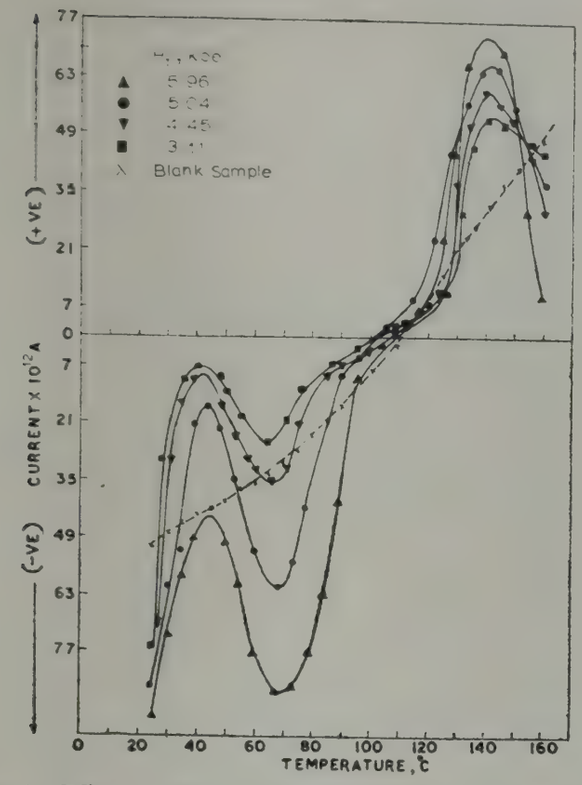

Fig. 1—Effect of different magnetic fields on the thermal current spectra of silastic tubular magnetoelectret (T_f=140°C)

10 days. The measurements were recorded by the TSD technique in the manner described above. The depth of penetration of charge was determined by following the method of Badian *et al.*[11]

3. Results and Discussion

All thermal current spectra show discharge currents in both negative and positive directions. Fig. 1 shows the TSD spectra for electrets corresponding to T_f = 140°C formed at different fields. The first maximum (termed as α-peak) is on negative region of current and occurs at 340 ± 2 K. The second maximum (called the ρ-peak) is on the +ve region of current and occurs at 413 K. There is evidence for the existence of another maximum in the −ve region of the current at a temperature lower than that of α-peak, because the high negative current shows a decrease with rise in temperature above this region. Thermal current from a blank sample prepared at 140°C with zero-field shows no peak. Values of I_{max} and E (charge trap depth) are given in Tables 1 and 2. The final average values of E for α- and ρ-peaks are 0·81 and 1·74 eV respectively.

The value of the released charge for different values of Hf is found from the areas of the two peaks in Fig. 1 and it is found to increase with magnetic field from $1·5 \times 10^{-7}$ to $3·11 \times 10^{-7}$ coul as the magnetic field increases from 3·11 kOe to 5·96 kOe for samples prepared at 140°C.

Table 1—Values of I_m, Q, E, and τ_{max} Calculated by Bucci and Fieschi Plot Method (T_f = 140°C)

H_f kOe	$Q\times10^{-7}$ coul	Peak	$I_m\times10^{-11}$ A	T_m K	E eV	τ_{max} sec
3·11	1·50	α	2·6	339	0·758	1·312
4·45	1·59	α	3·6	340	0·829	1·028
5·04	2·36	α	6·2	341	0·786	$8·09\times10^{-3}$
5·96	3·11	α	8·8	342	0·872	$5·057\times10^{-1}$
3·11	—	ρ	5·4	414	1·748	2836·43
4·45	—	ρ	6·0	413	1·785	2116·22
5·04	—	ρ	6·8	413	1·477	1727·21
5·96	—	ρ	7·4	413	1·928	947·12

Table 2—Values of E_a and τ_{max} Calculated by Cowell and Woods Curve Fitting Technique (T_f = 140°C)

H_f (kOe)	Peak	E (eV)	τ_{max} (sec)	δ, 10^{-3} cm
3·11	α	0·756	770·75	—
4·45	α	0·817	455·43	—
5·04	α	0·789	970·19	—
5·96	α	0·862	49933·83	—
3·11	ρ	1·754	3·237	4·552
4·45	ρ	1·485	6·616	0·527
5·04	ρ	1·820	1400·03	5·578
5·96	ρ	1·934	95137·73	5·762

Fig. 2 shows thermal current spectra for samples prepared at 5·4 kOe. Two maxima nearly at the same temperatures, as in Fig. 1, are obtained, the released charges being $3·17 \times 10^{-7}$, $2·40 \times 10^{-7}$ and $2·36\times10^{-7}$ coul (Fig. 2) respectively. This shows that the stored charge decreases with rise in T_f.

The effect of storage time is shown in Fig. 3. In general, it is seen that with the increase in storage time the height of current maxima decreases. The position of I_m for α-peak shifts to the low temperature side with increase in storage time. In the sample stored for 10 days, the charge is about one third the value obtained for a similar sample depolarized immediately after formation.

Fig. 4 shows the effect of interchanging the connecting terminals of the electrometer. The first peak (in Figs. 1-3) gets inverted (it also becomes positive). This is similar to the observation of Rojindar *et al.*,[12] in the case of carnauba wax, and shows that the α-peak is due to the release of idiocharge and the ρ-peak is due to isocharge.

Values of I_m and released charge (Q) are plotted against Hf in Fig. 5 which shows an increase in I_m and Q with the field. However, increase in I_m and Q is more for α-peak than for the ρ-peak.

The Bucci plot is observed to be linear and from the slope of this straight line the values of E and τ_0 are determined. Values of E are determined and

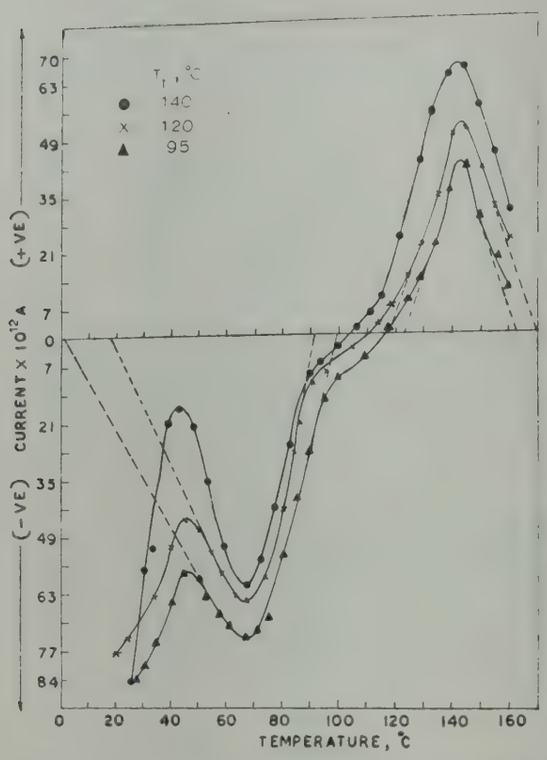

Fig. 2—Effect of forming temperature on the TSD of silastic tubular magnetoelectrets (forming field 5·04 kOe)

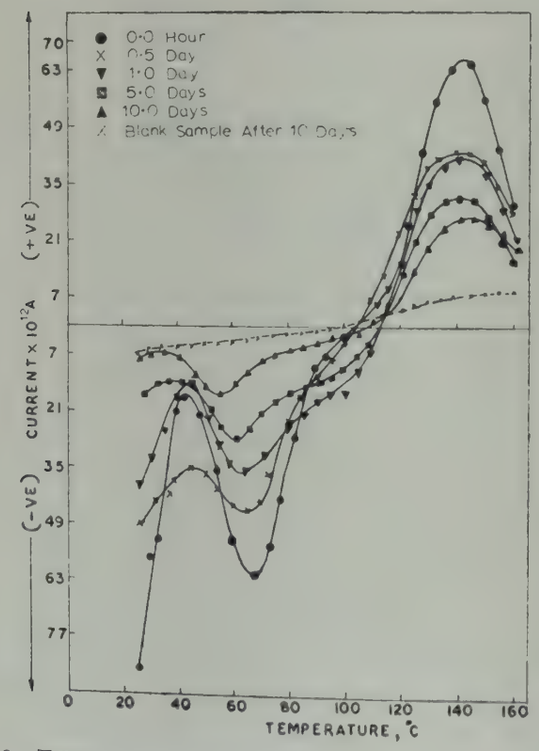

Fig. 3—Effect of various storage times on the silastic tubular magnetoelectret samples prepared at 140°C, 5·04 kOe

are reported in Table 1. Cowell and Woods' method is then applied to the TSD curve using the values of E from the Bucci plot. As seen from Fig. 6 for a representative sample (140°C, 3·11 kOe), an excellent fit is obtained of course with a slight deviation at higher temperatures. Values of E and τ_{max} calculated by this method are given in Table 2.

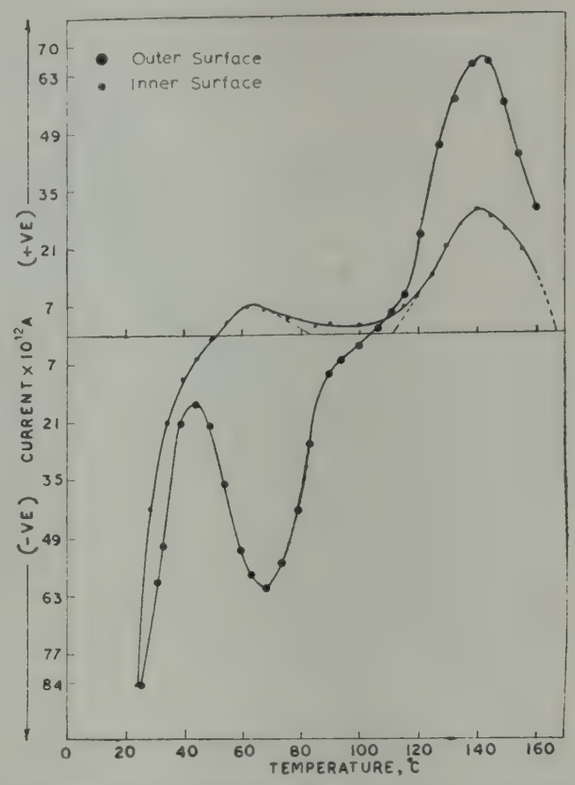

Fig. 4—Effect of interchanging the connecting electrodes to the electrometer for silastic tubular magnetoelectret prepared at 140°C, 5·04 kOe

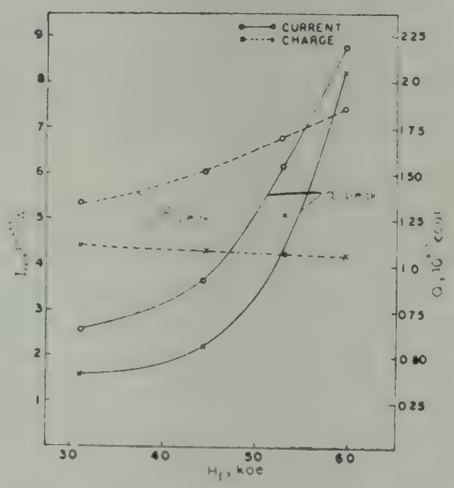

Fig. 5—Variation of I_m and released charge Q with the magnetic field for α- and ρ-peaks

Values of τ_0 obtained from Cowell and Woods method have been used to calculate δ, the depth of penetration of charge which comes out to be $4{\cdot}59 \times 10^{-3}$ cm amounting to 2·3% penetration.

Earlier study of surface charge density[6] shows that the electrets consist of a large isonegative charge over which a small idiocharge is superimposed. The electronegative methyl group in the structure of silastic imparts a dipole character to it. The idiocharge component may be due to dipole orientation and space charge polarization caused by ionic displacements. Isocharge may be due to trapping of ions and electrons. The trap sites exist

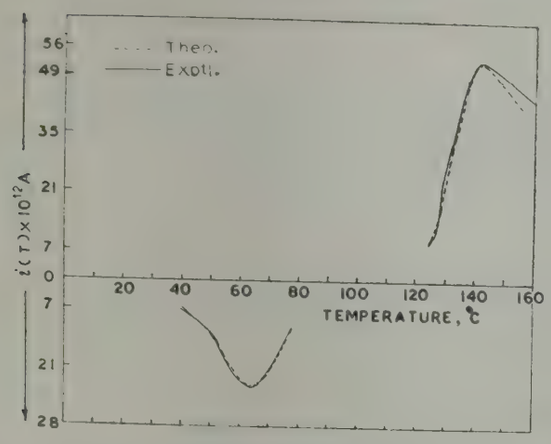

Fig. 6—Cowell and Woods curve fitting plot for the silastic tubular magnetoelectret sample [T_f=140°C, H_f=3·11 kOe]

because of impurities, structural defects and irregularities in the conformation of molecular chains (kinks, chain folding, chain ending, etc.).

As suggested by Turnhout,[14] the current maximum for dipole reorientation is expected to occur at a temperature lower than that due to excess charge motion. The first process requires only a rotational motion of molecular groups, whereas the second involves a motion of molecular groups (ions) over macroscopic distances. Hence the α-peak can be attributed to dipole reorientation or discharge of idiocharge. The ρ-peak is due to isocharge. The values of τ_{max} (Table 1) are higher for the ρ-peak as compared to α-peak. The idiocharge, decays first and gives rise to the low temperature α-peak. These ideas are further confirmed by the evidence of reversal of the α-peak when the electrodes to the electrometer are interchanged (Fig. 4).

From Fig. 2 it is seen that a decrease in forming temperature affects the ρ-peak height. Obviously, at a lower T_f, the conduction is low, and less charge carriers are available to cause polarization. This weakens the peak. Decrease in the released charge (calculated values) with increase in T_f can be explained on the basis of the helical structure of silastic macromolecule and the low forces of attraction between them, as given in surface charge study.[6]

A slight shift of peak position in Fig. 3 for samples stored for different periods may be due to dipole relaxation. A decrease in the α-peak height is caused by the reorientation of the faster reacting dipoles as discussed by Turnhout.[14] The ρ-peak, as a whole, becomes smaller. During the storage time of 10 days, total charge has decayed to 29%. This is nearly the same (31%) as found from charge decay measurements.[6] It seems that the charge decay during storage is mainly due to the reorientation of dipoles and not due to the neutralization of space charges which in our case are ions. An explanation for this may be that the number of ions in silastic in much larger than the number of dipoles.[15] Consequently, the reorientation of dipoles is more disastrous than the loss of (as many) ions.

Value of released charge calculated by the area under the peaks shown in Fig. 4, comes out to be $2{\cdot}36 \times 10^{-7}$ coul but reduces to $6{\cdot}74 \times 10^{-8}$ coul when the terminals are interchanged. This shows that the outer surface has more charge than the inner surface. This is in agreement with what has been observed in charge decay studies.[6] It is likely that the ρ-peak is ionic in nature because as believed by Jonscher[16] the activation energy as high as 1·74 eV is usually (but not always) associated with ionic traps. However, the distinction between the electronic and ionic traps is a difficult problem.

Acknowledgement

The authors are thankful to Dr B L Mehrotra, Principal, for his permission and to Dr Roy C Gunter for supplying the material and to Dr Jitendra Kumar Quamara, Kum Malini Variyar and V K Shrivastava for their help during this study. The authors are thankful to the National Science Foundation, USA, for providing financial help in carrying out this study.

References

1. Murphy P V, Holly F J & Bernhard W, Paper presented at the Electret Symposium at Chicago, 1967. Electrochemical Society, New York, 1968.
2. Gunter R C & Le Beau R J, paper presented at the 7th International Conference on Medical and Biological Engineering, Stockholm, 1967.
3. Bhatnagar C S, *Indian J. pure appl. Phys.*, **2** (1964), 331.
4. Sawyer P N & Pate J W, *Surgery*, 34 (1963), 791.
5. Shrivastava R K, Qureshi M S & Bhatnagar C S, *Japan J. appl. Phys.*, **17** (1978), 1537.
6. Shrivastava R K & Bhatnagar C S, *Indian J. pure appl. Phys.*, **15** (1977), 875.
7. Perlman M M, *J. electrochem. Soc.*, **119** (1972), 892.
8. Perlman M M & Creswell B A, *J. appl. Phys.*, **42** (1971), 537.
9. Bucci C & Fieschi R, *Phys. Rev.*, **148** (1966), 816.
10. Cowell T A T & Woods J, *Br. J. appl. Phys.*, **18** (1967), 1045.
11. Badian L, Ai B, Lacoste R & Mayour C, *C.r he'bd Sèanc. Acad. Sci. Paris*, **261** (1965), 2181.
12. Rojinder A P, Khare M L & Bhatnagar C S, *Indian J. pure appl. Phys.*, **13** (1975), 802.
13. Creswell R A, Perlman M M & Kabayama H A, *Dielectric properties of polymers*, edited by F E Karasz, (Plenum, New York) 1972, 295.
14. Turnhout J Van, *TSD of polymer electrets* (Elsevier Amsterdam), 1975, 9.
15. Stone F G A & Graham W A G, *Inorganic polymers* (Academic Press, New York) 1962, 261.
16. Jonscher A K, *Thin Solid Films*, 1 (1967), 213.

Indian Journal of Pure & Applied Physics
Vol. 18, January 1980, pp. 24-27

Charge Characteristics & Dielectric Behaviour of PVF2 Magnetoelectrets at Audio and Radio Frequency

J K Quamara, M L Khare & C S Bhatnagar
Department of Physics, M A College of Technology, Bhopal 462 007

Received 19 *September* 1978; *revised received* 22 *January* 1979

Magnetoelectret samples of thin PVF2 foil have been studied for their charge characteristics and dielectric behaviour. It is found that they develop negative isocharge. The intrinsic isocharge is always more than the intrinsic idiocharge. Both these charges are maximum at around 130°C. A decrease in the dielectric constant has been observed after magnetoelectret formation at 1 kHz, the decrease being maximum in samples formed at 130°C. At radio frequency (0·5 MHz) the dielectric constant is found to increase in samples formed at lower temperatures, but decrease in samples formed at higher temperatures. The behaviour is similar to the variation of refractive index in magnetoelectrets of other materials.

1. Introduction

Polyvinylidene fluoride (PVF2) has been added as a new member to the series of magnetoelectret-forming materials. It belongs to the family of vinyl polymer group having a very high dielectric constant (~11) at room temperature. For this reason it is widely used in electric capacitors. PVF2 thermoelectrets have been prepared and studied by Takamatsu and Fukada.[1]

The PVF2 foil used for the present study is manufactured by the Kureha Chemical Industry Co. Ltd, Tokyo, Japan. It is mechanically tough and has melting point around 180°C. It has low water absorption (<·03 g/m²/24 hr/mm at 90% relative humidity at 40°C) and hence its electrets are expected to have little adverse effect due to humidity. It is non-flammable and has good thermal stability. The additional advantage is that it contains no plasticizers or stabilizers.

2. Experimental Details

The samples have been prepared in the form of circular discs of 2·8 cm diameter and 0·2 mm thickness, at forming temperatures between 90 and 140°C, using magnetic field of strengths from 2·2 to 14·5 kgauss. The method of sample preparation and charge measurement are the same as adopted earlier.[2]

Measurement of dielectric constant at radio frequency (0·5 MHz) is done by using an admittance bridge (Russian 'SDELANO' Type E I0-2), while at audio frequency (1 kHz) a universal Marconi bridge (TF 2700) is used.

3. Results and Discussion

3.1 Charge Characteristics

The initial charge density measured just after electret formation is always negative on both the surfaces and its value for samples formed at different magnetic fields is higher than that on the blank samples. In magnetoelectret terminology the charge appearing on these samples is negative isocharge[3] (isocharge means a charge having same sign on both the surfaces). The charge density is of the order of 10^{-9} coul/cm² which is one magnitude higher than on magnetoelectrets of other materials,[4] and is comparable to the charge density on thermoelectrets. At lower magnetic fields up to 6·6 kgauss the charge on south pole facing surface (σ_S) is generally less than its value on north pole facing surface (σ_N) but at higher fields σ_N goes on decreasing in comparison with σ_S.

The separation of intrinsic isocharge and idiocharge according to the two-charge hypothesis[3] makes it possible to plot these charges against forming magnetic field and temperature. In Fig. 1 the initial intrinsic isocharge is shown against forming temperature for samples prepared at different magnetic field strengths. The charge has maximum value at 120 or 130°C. It seems that the peak actually lies at 125°C as shown by the dotted curve.

The intrinsic idiocharge is plotted against forming magnetic field in Fig. 2 for different forming temperatures ranging from 90-140°C. At lower fields the idiocharge is negative. This means that the negative part of polarization is towards the N-surface and positive towards the S-surface. But in samples

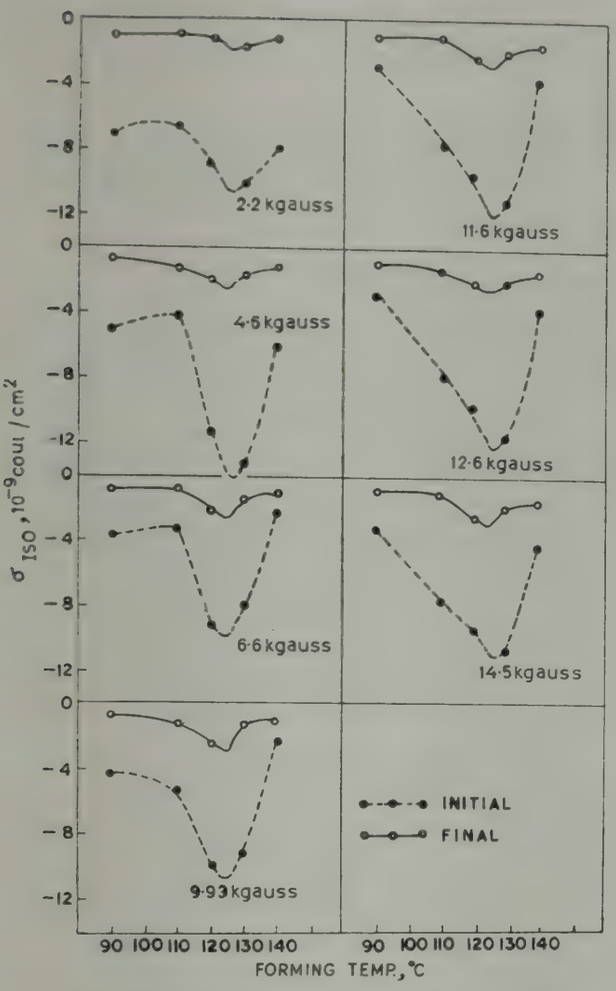

Fig. 1—Variation of initial and final isocharge with forming temperature for PVF2 samples prepared at different magnetic field strengths

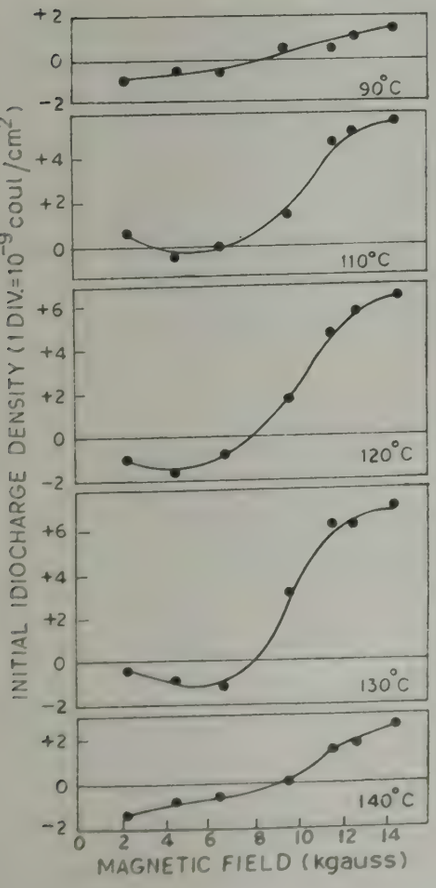

Fig. 2—Variation of initial intrinsic idiocharge in PVF2 with magnetic field at different forming temperatures

formed at higher magnetic fields, the idiocharge has the opposite sense. The inversion in the sense of polarization takes place near 6·6 kgauss (except in case of 140°C samples where this occurs at 9·3 kgauss). This behaviour is similar to what has been observed in perspex.[2]

The value of intrinsic idiocharge increases with the strength of forming magnetic field in a manner shown in Fig. 2. Its value also increases with forming temperature up to 130°C but decreases rapidly in samples formed at 140°C.

Figs. 1 and 2 show that intrinsic isocharge and idiocharge, both have maximum value near 130°C for PVF2 samples. The fact that overall charge on both the sides of the samples is always negative shows that in this material the intrinsic isocharge predominates over the idiocharge.

Charge decay and final charge—The charge decay patterns of samples prepared at different magnetic fields and temperatures are more or less similar. The representative curves corresponding to the forming temperature of 130°C are shown in Fig. 3. This temperature has been particularly chosen because the initial charges are maximum at this temperature. Moreover, the decay curves represented in Fig. 3

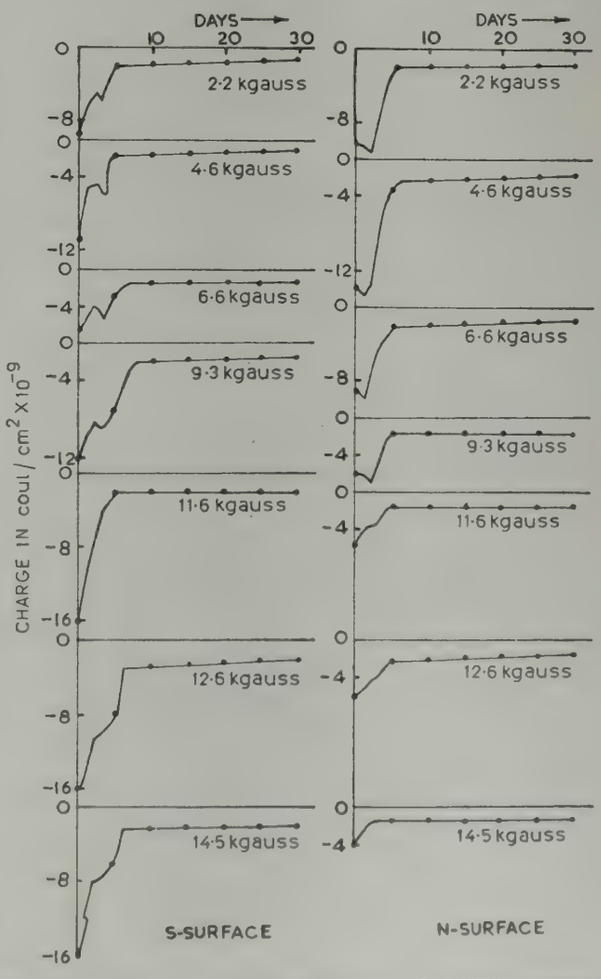

Fig. 3—Surface charge decay curves of PVF2 magnetoelectrets prepared at 130°C and different magnetic fields

show all the three varieties of curves obtained for samples formed at various temperatures and magnetic fields.

As is seen from Fig. 3 the charge undergoes rapid variation during the first 5-8 days following the sample preparation. Afterwards it gets stabilized to an almost constant value. The pre-stability period is more (~10 days) for samples formed at lower temperatures.

The decay curves are of three types. In the first type the charge decays rapidly for the first 2-3 days, but rises again, forms a peak on 4th or 5th day and then decreases. These curves correspond to the decay of charge on S-surface for sample formed at lower fields (2·2 to 9·3 kgauss) in Fig. 3. For samples prepared at lower temperature (90°C) all the decay curves corresponding to both the surfaces are of this type.

The second type of curves are as shown for N-surface in Fig. 3, for samples formed at lower fields. Here the charge increases from the beginning, forms a peak and then decays. Such patterns are also seen for N-surface curves in samples prepared at 120°C. The third type of curves correspond to samples formed at higher magnetic fields (>9·3 kgauss). In these curves the peak is absent and the charge continues to decay rapidly before getting stabilized to a constant value. All the decay curves for samples formed at 140°C are of this type only.

Despite the charge decay, there is no reversal in the sign of charge on any of the surfaces. This is in accordance with the charge behaviour of magnetoelectrets of other materials. The reversal in other materials is observed on one of the surfaces only when the initial charge is predominantly idiocharge.[2,4] When it happens to be isocharge, as in the present case, charge reversal is not to be expected.

The stable final charge is mainly isocharge which shows that idiocharge decays much more rapidly than isocharge. The peak formation in the decay curves is due to different decay rates of the two types of charges.

Variation of final intrinsic isocharge is shown in Fig. 1, and is similar to the initial intrinsic isocharge having maxima near 125°C.

3.2 Dielectric Behaviour

The dielectric constant at audio frequency (1 kHz) is found to decrease after magnetoelectret formation. This result is similar to what has been observed for other materials.[2,5] The decrease in dielectric constant ($\Delta\epsilon$) ranges from 0·5% to 6·5% (Table 1) and is maximum for samples formed at 130°C. Incidentally, at this temperature the intrinsic isocharge and idiocharge are also maximum. Variation of $\Delta\epsilon$ with magnetic field is however not regular. The magnitude of $\Delta\epsilon$ goes on increasing with magnetic field up to 12·6 kgauss but decreases a little at 14·5 kgauss.

At radio frequency (0·5 MHz) the dielectric behaviour is different. The dielectric constant is found to increase from its normal value in samples formed at lower temperatures. The increase is to the extent of 6·5%. But for samples formed at higher temperatures, the dielectric constant decreases below its normal value as in the case of audio-frequency. The magnitude of change in dielectric constant, irrespective of its sign, is minimum for samples prepared at 120-130°C.

The variation of $\Delta\epsilon$ with magnetic field at radio frequency is similar to the change in refractive index observed in the case of PVC, perspex, etc.[6,7] At lower forming temperature, $\Delta\epsilon$ is positive and goes on increasing with magnetic field. At somewhat higher temperatures, $\Delta\epsilon$ increases at lower forming field but then starts decreasing and may even become negative at higher fields and higher temperatures. At still higher temperatures, $\Delta\epsilon$ is negative even at lower

Table 1—Values of $\Delta\epsilon$ (in %) at af and rf for PVF2 Samples Observed After Magnetoelectret Formation at Various Fields and Temperatures

Forming mag. field (kgauss)	At audio frequency (1 kHz) Forming temp., °C					At radio frequency (0·5 MHz) Forming. temp. °C				
	90	110	120	130	140	90	110	120	130	140
2·2	−0·7	−1·7	−1·4	−4·8	−4·3	+1·8	+3·3	+0·4	−0·3	−2·6
4·6	−0·4	−1·0	−3·2	−5·2	−5·0	+3·2	+6·5	−1·3	−0·6	−3·2
9·3	−2·5	−1·7	−3·6	−6·0	−5·5	+3·0	+3·3	−1·7	−1·0	−3·5
12·6	−3·6	−2·1	−4·0	−6·4	−3·9	+2·2	+3·3	−1·9	−2·8	−4·2
14·5	−3·0	−2·5	−3·2	−4·8	−2·5	+2·2	+2·0	−1·5	−1·3	−2·8

+increase; −decrease

fields, goes on decreasing with the field but shows an upward trend at very high fields.

At radio frequency, dipolar polarizability does not contribute towards dielectric constant very much and only ionic and electronic polarizabilities are responsible for it. In optical refractive index, again there is no role of dipolar polarizability and only electronic polarizability contributes for it. Hence the similarity in the behaviour of variation of dielectric constant at radio frequency and refractive index at optical frequencies is quite understandable.

Dipolar and space charge contributions are important at audio frequency. The observed decrease in the dielectric constant at audio frequency is similar to what has been observed in other materials[2,5] in this range. The frozen dipoles are no longer free to rotate in response to the alternating audio frequency and hence a decrease in dielectric constant is to be expected.

Acknowledgement

The authors acknowledge their thanks to Dr B L Mehrotra, Principal, M A College of Technology, Bhopal, the National Science Foundation of U S A, for providing necessary facilities, funds and some of the equipments and to Shri R K Srivastava for help in the preparation of the paper, respectively.

References

1. Takamatsu T & Fukada E, *Phys. Chem. Res. Japan*, 45 (1969), 1.
2. Qureshi M S & Bhatnagar C S, *Indian J. pure appl. Phys.*, 10 (1972), 220.
3. Khare M L & Bhatnagar C S, *Indian J. pure appl. Phys.*, 7 (1969), 160.
4. Quamara J K, Khare M L & Bhatnagar C S, *Indian J. pure appl. Phys.*, 15 (1977), 617.
5. Deshpande (Mrs) Geeta & Khare M L, *Indian J. pure appl. Phys.*, 15 (1977), 692.
6. Quamara J K, Khare M L & Bhatnagar C S, *Indian J. pure appl. Phys.*, 14 (1976), 147.
7. Quamara J K, Khare M L & Bhatnagar C S, *Indian J. pure appl. Phys.*, 15 (1977), 138.

Indian Journal of Pure & Applied Physics
Vol. 18, January 1980, pp. 28-30

Nickel Oxide Electrode for Photolysis

V P Sunder Singh, (Mrs) P P Warnekar & G K Bhagawat

Department of Electrical Engineering, Indian Institute of Technology, Bombay 400 076

Received 14 *April* 1978; *revised received* 1 *July* 1978

I-V characteristics for nickel oxide in 2% acetic acid are reported with and without light irradiation on the oxide. Under illumination, lithiated nickel oxide shows a clear positive shift for hydrogen evolution potential, indicating enhanced catalytic properties of nickel oxide for electrochemical photolysis.

1. Introduction

Amorphous semiconductors if used as one of the electrodes for photolysis will be more economical if their efficiencies are comparable to that of a single crystal electrode. Amorphous metal oxides, viz. Fe_2O_3, V_2O_5, WO_3, CdO, Cr_2O_3, PbO, Bi_2O_3, CuO were investigated for such cells by many authors.[1-3] The present investigations deal with the photoelectrochemical properties of lithiated nickel oxide[4] and unlithiated nickel oxide in acetic acid.

2. Experimental Details

Nickel oxide electrode preparation—High purity nickel foil (99·9%) 100 μm thick was degreased, enclosed in a silica tube filled with commercial grade oxygen gas and oxidized by heating the tube in a diffusion furnace at 750°C for 1 hr. After this, the furnace was slowly cooled down to 100°C to avoid cracks on nickel oxide film. At one end of the sheet, the oxide layer was removed by grinding and a copper lead soldered. Except for an area of 1 cm^2, the surface was covered by apiezon wax. For lithiation, Li_2CO_3 was kept in a separate crucible inside the silica tube along with the nickel foil and oxidized as before. The thickness of the oxide measured by weight change method is found to be 0·38 μm.

These foils were fixed in an electrochemical cell to determine their photolysis properties as shown in Fig. 1. The potentiostat can control the working electrode potential with respect to saturated calomel electrode (SCE) from -2V to $+2$V with an accuracy of $\pm 0{\cdot}05$ mV.

Before deciding the light source, it was thought worthwhile to determine the absorption properties of nickel oxide. For this, nickel was sputtered on a transparent silica substrate in ultrahigh pure (UHP) argon atmosphere so as to form a thin film of nickel on the substrate. This film was heated in high purity oxygen atmosphere at 950°C and nickel oxide was formed. The optical absorption curve was then recorded in the range of 200 to 700 nm using Perkin-Elmer spectrometer. Fig. 2 shows the absorbance of the film versus the wavelength. It is clear that the absorption starts approximately at 400 nm. Hence Philips HPW 125 W lamp was used as the light source for determining the light effect. The *I-V* characteristics for lithiated and unlithiated nickel oxide are shown in Fig. 3.

3. Results and Discussion

Fig. 3 shows that in the anodic direction all the four curves A, A′, B, B′ (with and without light) show a break at 1·25 V (SCE) indicating the usual

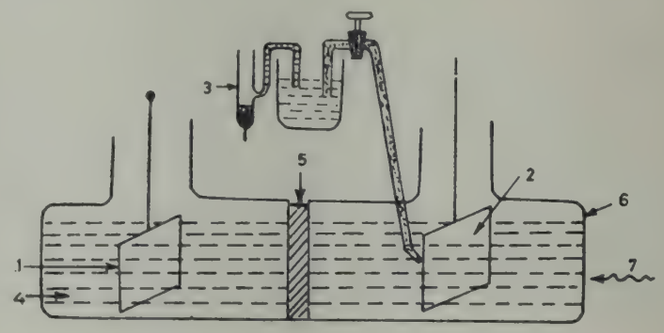

Fig. 1—Electrochemical cell [1. Pt electrode; 2. Nickel oxide electrode; 3. Saturated calomel electrode; 4. Acetic acid (2%) electrolyte; 5. Glass frit; 6. Quartz window; 7. Light source]

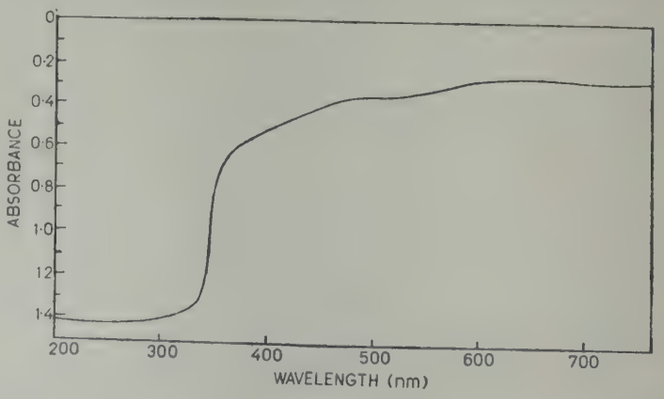

Fig. 2—Absorbance versus wavelength for nickel oxide film

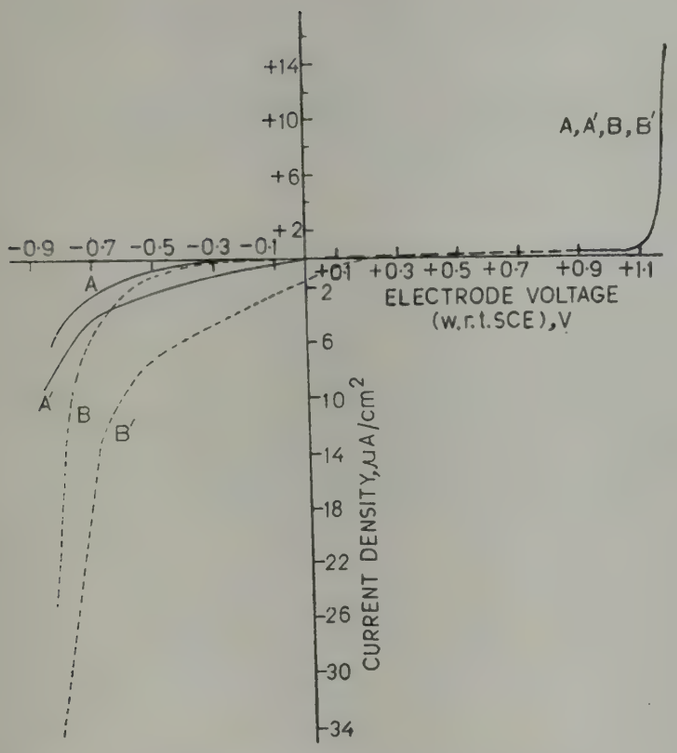

Fig. 3—*I-V* characteristics for nickel oxide and lithiated nickel oxide electrodes in 2% acetic acid [Curves: A without light, A′ with light for nickel oxide, and B without light and B′ with light for lithiated nickel oxide]

decomposition of water molecule and a *p*-type conductivity for the nickel oxide. At about + 0·3 V the curve B′ shows a current in the negative direction under light. Actual values of A′ also show a small current in the negative direction at this voltage. The direction of the current indicates that hydrogen evolution occurs at the nickel oxide semiconductor electrode under illumination.

In the cathodic direction, the dark current for unlithiated nickel oxide starts beyond −0·4 V, whereas for lithiated nickel oxide, it shifts to −0·25 V. This is explained as follows.

In the cathodic direction, beyond 0·25 V (SCE), the magnitude of the overvoltage depends on the nature of the electrode, the current density, the composition of the solution, etc. On the lithiated nickel oxide electrode, which is heavily *p*-type,[4] the fact that the dark current starts beyond −0·25 V shows that the overvoltage is mainly due to slow discharge of the ions. On the other hand, in the unlithiated nickel oxide for which the Fermi level is higher than the valence band [$\sigma = 10^{-6}$ ohm^{-1} cm^{-1} for sintered nickel oxide], the dark current starts only beyond −0·4 V. This means that an additional voltage corresponding to the activation energy is present.

The equation for overvoltage will then be

$$\eta = a + b \log J + (kT/\beta e) \ln J - (kT/\beta e) \ln J_0 \quad ...(1)$$

or $$\eta = A + b \log J + (kT/\beta e) \ln J \quad ...(2)$$

In Eq. (2) $A = a - (kT/\beta e) \ln J_0$

where a, b and A are constants, J_0 = exchange current density, J = current density, η = overvoltage, k = Boltzmann constant, T = absolute temperature, e = electronic charge and $\eta e\beta$ = reduction in the activation energy. In Eq. (1), the third and the fourth terms are due to activation energy.

When nickel oxide is lithiated, it becomes more *p*-type making the Fermi and H_3O^+ levels come closer to the valence band. Because of this, the direct transfer of electrons from the valence band to the H_3O^+ level is possible and the activation energy required for this becomes small. Hence, for heavily doped *p*-type nickel oxide, Eq. (2) reduces to

$$= A + b \log J \quad ...(3)$$

Since Fig. 4 shows a linear relationship between log J and the voltage V, one can use these equations to calculate the constant b.

For nickel oxide electrode using Fig. 3 and Eq. (2)

$$\eta = 0{\cdot}6 - V_{eq} = a + b \log 10^{-6} + (kT/\beta e) \ln 10^{-6} \quad ...(4)$$

$$\eta = 0{\cdot}8 - V_{eq} = a + b \log 3 \times 10^{-6} + (kT/\beta e) \ln 3 \times 10^{-6} \quad ...(5)$$

where V_{eq} = equilibrium voltage, and $\beta = 0{\cdot}5$

From Eqs. (4) and (5), $b = 0{\cdot}302$ at 300 K. Similar calculation for lithiated nickel oxide using Eq. (3) gives $b = 0{\cdot}3$ at 300 K. The closeness of these two values of b for lithiated and unlithiated nickel oxide is in agreement with the above explanation.

From the above experiment it is clear that nickel oxide shows photolysis properties and consequently under illumination the hydrogen evolution potential is shifted towards more positive potentials. Further, with lithiation, more hydrogen evolution is possible

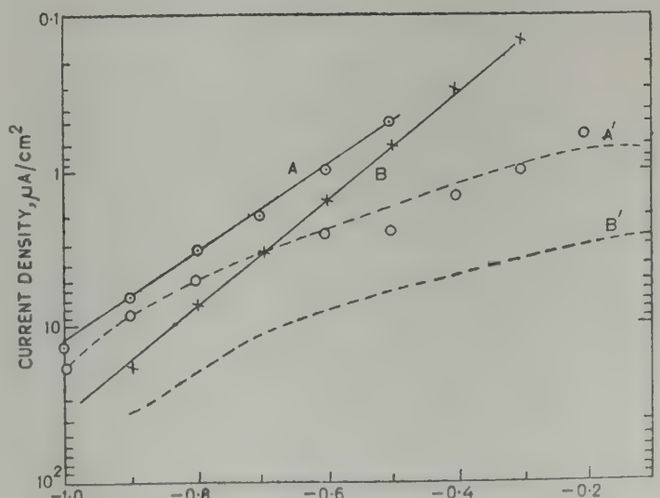

Fig. 4—*V* versus log *J* [A, A′, B, B′ same as in Fig. 3]

under illumination. However, even with lithiation, the magnitudes of currents are very small compared to those in Fe_2O_3, CuO, etc.

Experiments conducted with higher thickness of oxide (oxidized at higher temperature and/or for longer duration) show little light effect especially for undoped oxide films. This is due to the smaller diffusion lengths for minority carriers in nickel oxide films. It was further observed that the quality of the oxide plays an important role in limiting the dark current to theoretically explainable limits. The curves in Figs. 3 and 4 are the characteristics for the best possible oxide samples selected by surface observation for pin holes under microscope. The cracks on the oxide films make it difficult to optimize the film thickness for the best light effect. It is worthwhile growing these nickel oxide films either by controlled vapour deposition or anodization techniques to eliminate cracks and pin holes, so that higher photocurrents may be achieved.

References

1. Hardee K L & Bard A J, *J. electrochem. Soc.*, **124** (1977), 215.
2. Kung H H, Jarrett H S, Sleight A W & Ferritti A, *J. appl. Phys.*, **48** (1977), 2463.
3. Giniey D S & Butler M A, *J. appl. Phys.*, **48** (1977), 2014.
4. Van Houten S, *J. Phys. Chem. Solids*, **17** (1960), 7.

Indian Journal of Pure & Applied Physics
Vol. 18, January 1980, pp. 31-35

Ionization & Dissociation of Propylene by Electron Impact

Ezzat T M Selim
Nuclear Physics Department, Atomic Energy Establishment, Cairo, Egypt, ARE

Received 10 *February* 1979

Ionization efficiency curves for propylene parent ion and three fragment ions namely $C_3H_5^+$, $C_3H_3^+$ and $C_2H_3^+$ are reported for 10 eV above threshold. The energy distribution difference technique is used in this study. All the ionization efficiency curves reveal abundant structures. For the parent ion, the first ionization potential is detected at 9·69 eV (very probably adiabatic and due to π-electron) and the second ionization potential at 11·97 eV (due to σ-electron). Autoionization is assigned to step function levels occurring at 11·33, 13·84 and 14·19 eV in the parent ion curve. In the case of the fragment ions, appearance potentials are detected for $C_3H_5^+$ fragment at 11·90, 12·29, 12·57, 13·37, 13·89, 14·40, 17·00, 20·19 and 21·40 eV. On the other hand, the appearance potentials corresponding to $C_3H_3^+$ fragment occur at 14·21, 14·42, 15·09, 15·72, 16·33 eV and for $C_2H_3^+$ fragment at 13·78, 14·53, 15·27, 15·95 and 17·12 eV. The heats of reaction are calculated for the processes forming the fragment ions at threshold.

1. Introduction

The ionization efficiency (IE) curve for propylene had been studied early by Fox and Hickman[1] for 5 eV above threshold using an electron impact retarding potential difference (RPD) technique. Also, the propylene ion had been studied by other techniques[2-5] obtained rich structure which could not be explained. On the other hand, appearance potentials (APs) of fragment ions from propylene have been studied by many other authors[6-11] at threshold only.

The purpose of present paper is the careful investigation of IE curves of $C_3H_6^+$, $C_3H_5^+$, $C_3H_3^+$ and $C_2H_3^+$ ions from propylene for about 10 eV above threshold. The electron impact energy distribution difference (EDD) technique is used in the study. The structure present in these curves as well as the ionization potential (IP) and AP for the ions are determined. The EDD technique has proved to be useful for the present types of measurements.[12-17]

2. Apparatus and Experimental Technique

Ionization efficiency data have been obtained using an Atlas CH-4 mass spectrometer with a normal electron impact ion source (AN-3). The filament current is set at 4·5 A, while the emission current is stabilized at about 19 μA. Electron energy is varied with 10-turn helipot potentiometer. Experimental technique, calibration of energy scale and problems encountered in the study have been reported previously.[16]

The directly measured IE curves are smoothened by seven points smoothing technique with a least square quintic equation.[18] From the smoothened curves, the EDD, IE curves are calculated. A fortran computer program[15,16] is used for determining the exact position of the breaks in ΔI curves to avoid the subjective manual fitting technique.

3. Results and Discussion

The IE curves for the four ions studied are given in Figs. 1 and 2, while Fig. 3 shows the initial portions of all the curves plotted on a bigger scale. The results obtained from the study of the parent ion curves are given in Table 1 while the results of the fragment ions together with the calculated $\Delta H_{\text{reaction}}$ for the processes at threshold are given in Table 2.

3.1 $C_3H_6^+$ Parent Ion ($m = 42$)

The representative IE curve for the parent ion is given in Fig. 1, while the present result together with the previously reported results are shown in Table 1. The value 9·69 eV is obtained for the first IP. It is in close agreement with the previously reported experimental values (Table 1) except that given by Berry[2] (9·50 eV) using photoionization technique. The agreement (deviation from the mean of the previous values = 0·003 eV) indicates that the presently measured IP is the adiabatic one.

There are many evidences[22-24] which suggest that the first IP for propylene and higher mono-olefins corresponds to removal of one of the π-electrons in

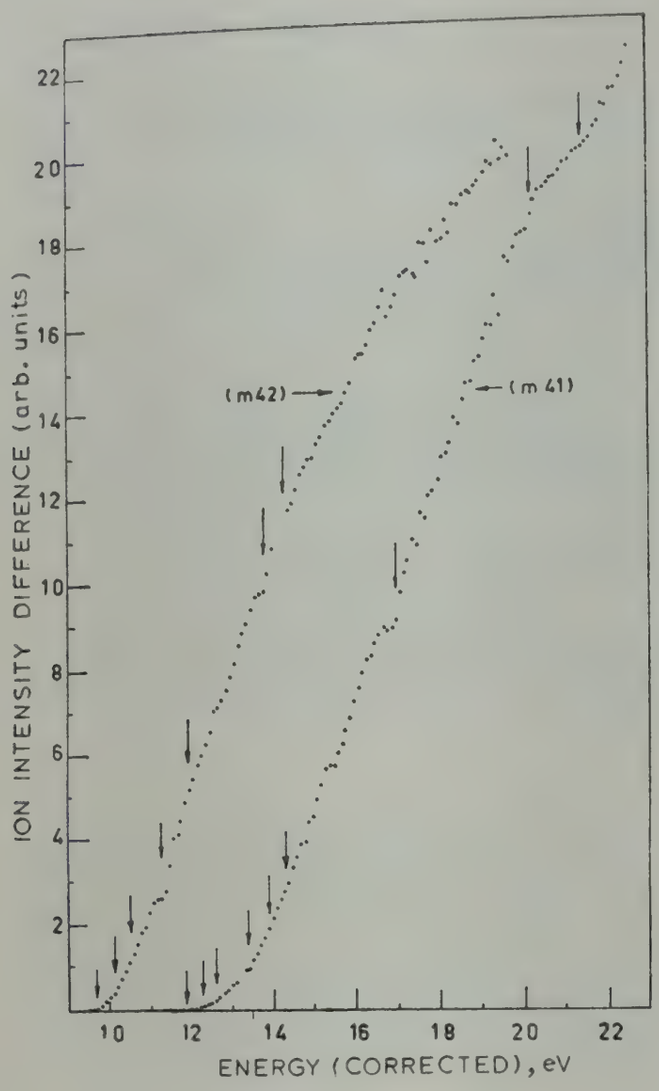

Fig. 1 – *I-E* curves for propylene parent ion ($m = 42$) and fragment ion ($m = 41$)

the double bond and not due to the removal of σ-electron from the alkyl group: (a) the π-electrons are held less tightly by the molecule; (b) the small decrease (almost negligible) in the IP of higher mono-olefins from 1-hexene to 1-decene indicates that ionization is not occurring in the saturated chains of these molecules;[25] (c) the decrease in IP for the substitution of the methyl group for hydrogen points directly to the double bond as the origin of the ionized electron.[23,26]

The resolution of the presently used EDD technique is not sufficient to detect the vibration state of the ion which is probably representing a twisting vibration about the C=C bond. This state has been detected previously by photoionization[3] and also by UV spectra[21] at 9·80 eV.

The two levels measured at 10·05 and 10·53 eV are in good agreement with those obtained early by Fox and Hickam[1] (10·13 and 10·53 eV) using RPD technique. These two levels may be explained as due to excitation of the electrons of the C—H bond

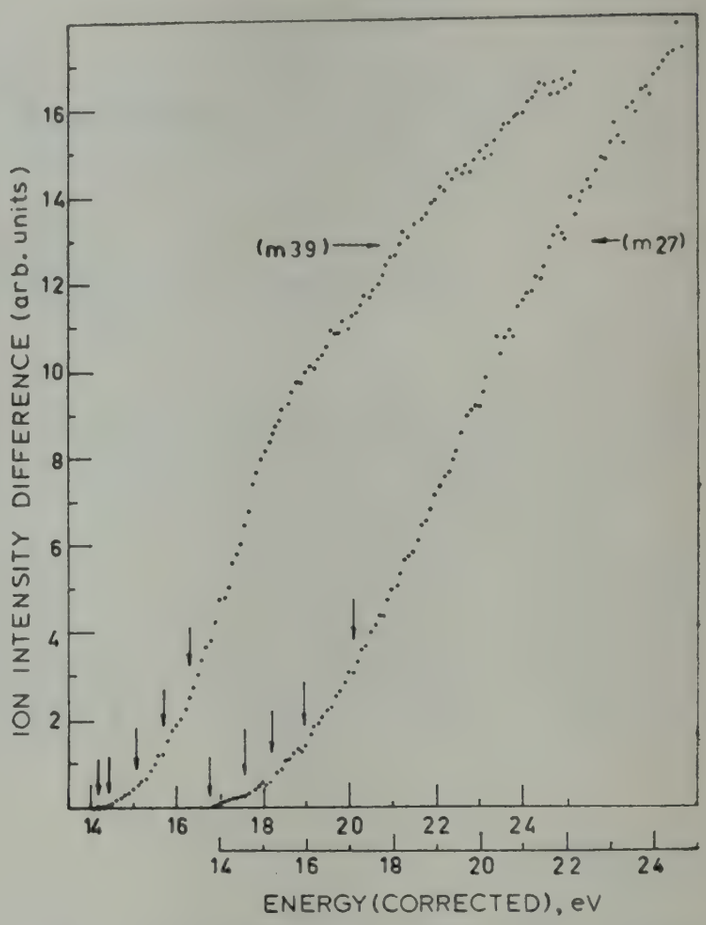

Fig. 2 – *I-E* curves for fragment ion ($m = 39$) and fragment ion ($m = 27$)

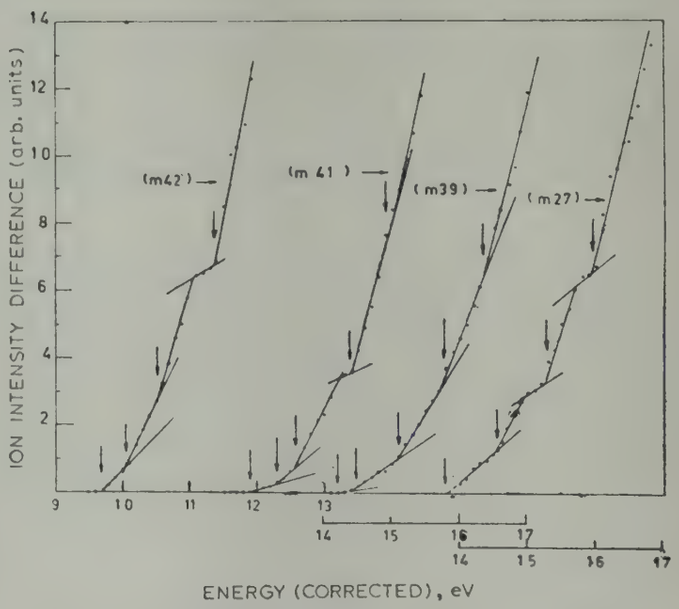

Fig. 3—The low energy portions of the IE curves for propylene parent ion ($m = 42$), fragment ion ($m = 41$), fragment ion ($m = 39$) and fragment ion ($m = 27$) plotted on larger scale.

(σ-electrons). As photoionization,[2,3] photoelectron spectroscopy[4] and UV[21] studies for $C_3H_6^+$ ion do not show any marked evidence for similar levels, the reported two levels at 10·05 and 10·53 eV must be either optically forbidden or have very low cross-section for photon impact.

Table 1—Energy Levels (in eV) of Propylene Parent Ion

No of det.	Present work	Other investigations						
		Electron impact		Photoionization		Photo-electron spectrosc.	Penning ionization	UV spectrosc.
		Lossing[6]	Fox and Hickman[1]	Berry[2]	Steiner *et al.*[3]	Dewar and Worley[4]	Cermak[5]	Samson *et al.*[21]
	9·69±0·09*	9·72	9·78±0·04	9·50±0·02	9·73±0·02	9·69	9·76	9·70
	—	—	—	—	9·80	—	—	9·80
	10·05±0·03	—	10·13±0·04	—	—	—	—	—
	10·53±0·08	—	10·54±0·04	—	—	—	—	—
	11·33±0·03	—	—	—	—	—	—	—
	—	—	—	—	—	11·76	11·80	—
14	11·97±0·03	—	12·10	—	—	—	—	—
	—	—	13·23±0·04	—	—	13·01	13·15	—
	13·84±0·20	—	—	—	—	—	—	—
	14·19±0·10	—	—	—	—	14·14	14·18	—
	—	—	—	—	—	15·78	15·70	—
	—	—	—	—	—	(18·03)	—	—

*A non-reproducible level is detected at 12·89 eV.

Table 2—Appearance Potentials of $C_3H_5^+$, $C_3H_3^+$ and $C_2H_3^+$ Fragment Ions from Propylene

Mass	Ion	Appearance potentials			Mass	Ion	Appearance potentials		
		Present work	Other determinations	$\Delta H_{reaction}$			Present work	Other determinations	$\Delta H_{reaction}$
41	$C_3H_5^+$	11·90±0·05*	11·88[6], 11·40[7],	11·85†	39	$C_3H_3^+$	14·21±0·09	14·21[3], 14·20[29]	13·15
			12·11[8], 12 06[10]				14·42±0·06		
		12·29±0·08					15·09±0·08		
		12·57±0·10		12·50			15·72±0·05		
		13·37±0 07					16·33±0·10		
		13·89±0·12			27	$C_2H_3^+$	13·78±0·03	13·80[8], 13·70[29]	13·54
		14·39±0·08					14·53±0·06		
		17·00±0·06					15·25±0·06	15·20[11]	
		20·19±0·10					15·95±0·12		
		21·40±0·11					17·12±0·16		

*Non-reproducible levels have been detected at 17·00 eV in $C_3H_5^+$ IE curve, at 17·05 eV in $C_3H_3^+$ curve, and at 14·09, 19·95 and 21·60 in $C_2H_3^+$ curve.

†Heat of formation of $C_3H_5^+$ is taken from Ref. 6, that of $C_3H_3^+$ (cyclopropenyl) from Ref. 6 and Ref. 30 and that of $C_2H_3^+$ from Ref. 31. Heats of formation of C_3H_6, CH_3 and H neutrals are from Ref. 30.

The level 11·33 eV has been detected in the form of step function. An equivalent value has been obtained only by Dewar and Worley[4] using the MINDO calculation technique at 11·45 eV. The level may be explained as due to autoionization of super-excited state of propylene molecule, though the nature of this state is not known.

A higher level has been detected at 11·97 eV. Equivalent values have been detected by different techniques in the range 11·76-12·10 eV. Walsh[27] estimated a higher IP in propylene at about 12·00 eV due to the removal of σ (C—C) electron. Many authors[23,26] predict that in case of simple olefins, the alkyl substitution for hydrogen at the double bond would lower the IP. Turner *et al.*[28] obtained the value 12·38 eV as the second IP of ethylene. This latter value justifies the present author's opinion that the level reported at 11·97 eV is probably corresponding to the second IP of propylene (due to σ-electron).

Two higher levels have been detected at 13·84 (in the form of step function) and 14·19 eV. The second has a value close to those obtained by photoelectron spectroscopy[4] (14·14 eV), Penning ionization (14·18 eV)[5] and by MINDO calculation technique[4] (14·22 eV). These two levels at 13·84 and 14·19 eV agree very well with the APs of $C_2H_3^+$ (13·78 eV) and $C_3H_3^+$ (14·21 eV) fragments obtained in the present work. This agreement suggests that the two levels are probably pre-dissociated to form the respective two fragment ions.

3.2 $C_3H_5^+$ Fragment Ion ($m = 41$)

Fig. 1 gives a representative IE curve for the fragment ion. This curve shows considerable tail at threshold. The value 11·90 eV is measured for the AP at threshold. It is in close agreement with the value reported by Lossing[6] (11·88 eV) but higher by 0·50 eV than the value obtained by Dorman[7] using second derivative electron impact IE data. It appears that the value of Dorman[7] is badly in error since it differs largely from all the other published values.

No evidence has been found for low energy ion-pair process at threshold. This process is characteristic for (P−1) fragment ions obtained from ethane, propane and *n*-butane.

The calculated $\Delta H_{reaction}$ values for the process at threshold differ according to the value of ΔH_f for $C_3H_5^+$ (allyl) used in the calculation. Using ΔH_f value for $C_3H_5^+$ reported by Lossing[6] (9·80 eV) the value of 11·85 eV is obtained for $\Delta H_{reaction}$ but when one uses the lower value given by Franklin *et al.*[30] (9·37 eV), the value 11·41 eV is obtained. The first $\Delta H_{reaction}$ value suggests negligible excess energy while the second one gives a value for excess energy equal to 0·49 eV. Since the process forming the ion is a simple bond-breaking one which requires no excess energy,[32,33] one may conclude that the ΔH_f value for $C_3H_5^+$ given by Franklin *et al.*[30] is probably low and inaccurate.

It had been suggested that $C_3H_5^+$ fragment is produced from propylene through both or either of the following processes:

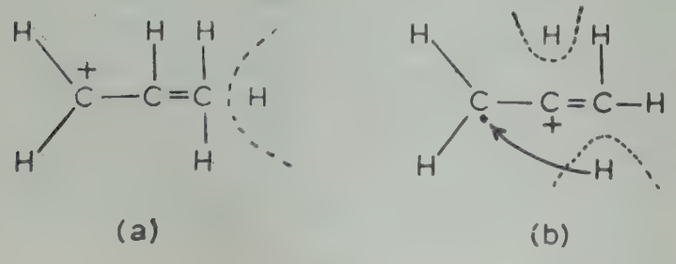

(a)

(b)

Process (a) needs no excess energy but process (b) probably requires excess activation energy. However, Lossing[6] had concluded that allyl ion formation from different compounds including propylene requires little or no excess energy, even when extensive skeletal rearrangements are necessary.

A break is obtained in IE curve of $C_3H_5^+$ fragment at 12·57 eV and is probably corresponding to the formation of cyclopropyl ion. Using ΔH_f value of $C_3H_5^+$ corresponding to cyclopropyl ion which is reported by Lossing[6] (10·45 eV) the value 12·50 eV is obtained for $\Delta H_{reaction}$ for the formation of cyclopropyl ion.

3.3 $C_3H_3^+$ Fragment Ion ($m = 39$)

The IE curve for this fragment shows considerable tail which is typical for a process which competes with another one at lower energy ($C_2H_3^+$ at 11·78 eV). The value 14·21 eV is measured for the AP at threshold. It is the same value as that reported by Omura[8] and is in excellent agreement with the earlier value of Field and Franklin[29] (14·20 eV).

The process of formation of the $C_3H_3^+$ fragment involves the elimination of H_2 molecule together with H atom. Excess activation energy is known to be required in processes involving H_2 elimination.[32,33] Using ΔH_f values for $C_3H_3^+$ as for cyclopropenyl ion reported by Lossing[6] (11·10 eV) and that identical value reported by Franklin *et al.*[30] (11·06 eV) for the calculation of $\Delta H_{reaction}$ for the process of formation of $C_3H_3^+$ at threshold, approximately the same value is obtained as ~ 13·15 eV. This value suggests excess energy equal to 1·06 eV which is attributed to excess activation energy and probably also to kinetic shift. The latter value although relatively high for excess energy, appears reasonable since the formation of cyclopropenyl ion from propylene involves skeletal rearrangement and hence needs large excess activation energy. Also the process forming $C_3H_3^+$ requires kinetic shift (though $C_3H_6^+$ has relatively few degrees of freedom) since the fragmentation very likely occurs via rigid complex and also the process competes with another one forming $C_2H_3^+$ fragment with a threshold 0·43 eV lower in energy.

Using ΔH_f value for $C_3H_3^+$ as propargyl ion ($^+CH_2—C \equiv CH$) reported by Lossing[6] (12·18 eV) for the calculation of $\Delta H_{reaction}$, the value 14·23 eV is obtained. This value suggests zero excess energy which is unreasonable for the present process. This conclusion suggests that propargyl ion is not obtained at threshold.

3.4 $C_2H_3^+$ Fragment Ion ($m = 27$)

The first measured AP for this ion is 13·78 eV which is in close agreement with the value given by

Omura[8] (13·80 eV) and that reported by Field and Franklin[29] (13·70 eV). The present value is lower by 1·42 eV than the old value given by Delfosse and Bleakney[11] (15·20 eV). The latter value may be in serious error or corresponds to higher AP. However, the presently reported IE curve reveals a break at 15·17 eV which may correspond to that high value for the AP reported by Delfosse and Bleakney.

The process of formation of $C_2H_3^+$ fragment from propylene is a simple bond-breaking process which requires no excess activation energy.[32,33] However, using the value of Field *et al.*[30] (11·66 eV) for ΔH_f for the vinyl ion to calculate $\Delta H_{\text{reaction}}$ for the process at threshold, the value 12·92 eV is obtained. This value suggests excess energy equal to 0·86 eV. The situation is much improved if one uses the value of ΔH_f reported by Bernecker[31] (13·28 eV), since in this case $\Delta H_{\text{reaction}}$ is found to be 13·54 eV which suggests the presence of excess energy equal to 0·24 eV. This excess energy is outside the quoted error for AP and may be attributed to kinetic shift necessary for the process either to occur in the time of residence in the ion source or to compete with other processes.

The break obtained in $C_2H_3^+$ IE curve at 19·95 eV is tentatively explained as due to the following process with calculated $\Delta H_{\text{reaction}}$ equal to 19·80 eV.

$$C_3H_6 \longrightarrow (C_2H_3^+)^\circ + (CH_3)^*$$

The excitation energy for CH_3 radical which is used in the calculation is given by Prophet[34] to be equal to 6·3 eV.

References

1. Fox R E & Hickman W H, *J. chem. Phys.*, **22** (1954), 2059.
2. Berry R S, *J. chem. Phys.*, **38** (1963), 1934; private communication from Schoen to the author.
3. Steiner B, Gieze C F & Inghram M G, *J. chem. Phys.*, **34** (1961), 189.
4. Dewar M J S & Worley, S D, *J. chem. Phys.*, 50 (1969), 654.
5. Cermak V, *Proc. int. Conf. Mass Spectrometry, Berlin*, 1967, 697.
6. Lossing F P, *Can. J. Chem.*, **50** (1972), 3973.
7. Dorman F H, *J. chem. Phys.*, **43** (1965), 3507.
8. Omura I, *Bull. chem. Soc. Japan*, 35 (1962), 1845.
9. Omura I, *Bull. chem. Soc. Japan*, **34** (1961), 1227.
10. Pottie R F, Harrison A G & Lossing F P, *J. Am. chem. Soc.*, **83** (1961), 3204.
11. Delfosse J & Bleakney W, *Phys. Rev.*, 56 (1939), 256.
12. Collins J H, Winters R E & Engerholm G G, *J. chem. Phys.*, **49** (1968), 2469.
13. Winters R E & Collins J H, *J. Am. chem. Soc.*, **90** (1968), 1235.
14. Allinson I I O, Sedgwick R D, *Proc. int. Conf. Mass Spectrometry, Berlin*, 1967, 20.
15. Selim E T M & El-Kholy S B, *Indian J. pure appl. Phys.*, **13** (1975), 233.
16. Selim E T M, *Indian J. pure appl. Phys.*, 14 (1976), 547.
17. Selim E T M & Zahran N F, Fine Structure in the First Differential Ionization Curves of Formic Acid, *Arab. J. Nucl. Sci. App.*, 1979 (Accepted for publication),
18. Savitzky A & Golay M J E, *Anal. Chem.*, **36** (1964), 1627.
19. Lifshitz C S & Long F A, *J. chem. Phys.*, **41** (1964), 2468.
20. Chupka W A & Berkowitz J, *J. chem. Phys.*, **47** (1967), 2921.
21. Samson J A R, Marma F F & Watanabe K, *J. chem. Phys.*, 36 (1962), 783.
22. Price W C & Tute W T, *Proc. R. Soc. Lond.*, **A174** (1940), 207.
23. Price W C, Bralsford R, Harris P V & Ridley R G, *Spectrochim. Acta*, **4** (1959), 45.
24. Streitwiesser A (Jr), *Prog. phys. org. Chem.*, **1** (1963), 1.
25. Demeo D A & El-Sayed M A, *J. chem. Phys.*, **52** (1970), 2622.
26. Mulliken R S, *Rev. mod. Phys.*, **14** (1942), 265.
27. Walsh A D, *Trans. Faraday Soc.*, **42** (1946), 779.
28. Turner D W, Baker C, Baker A D & Brundle C R, *Molecular photoelectron spectroscopy* (Wiley Interscience, London, New York, Toronto), 1970, 166.
29. Field F H & Franklin J L, *Electron impact phenomena and the properties of gaseous ions* (Academic Press, New York), 1957, 242.
30. Frahklin J L, Dullard J G, Rosenstock H M, Herron J T, Draxyl K, & Field F H, *Ionization potential and heats of formation of gaseous positive ions*, NSRDS-NBS Document No. 26 (U S Government Printing Office, Washington D C) 1969.
31. Bernecker R R & Long F A, *J. phys. Chem.*, 65 (4961), 1565.
32. Ref. 29, p. 91.
33. Rosenstock H M, Wallenstein M B, Wahrhaftig A L & Eyring A L, *Proc. Natn. Acad. Sci. Wash.*, **38** (1952), 667.
34. Prophet A, *J. chem. Phys.*, **38** (1963), 2345.

Indian Journal of Pure & Applied Physics
Vol. 18, January 1980, pp. 36-39

Evaluation of Critical Constants from the Intermolecular Force Constants

V Shanmugasundaram & P Thiyagarajan

Department of Physics, Annamalai University, Annamalainagar 608 101

Received 13 *November* 1978; *revised received* 5 *February* 1979

The intermolecular force constants σ and ϵ of the Lennard-Jones (12-6) potentials are evaluated from the polarizability (α) of the polyatomic molecules, calculated by the δ-function potential model of chemical binding. From the value of α, the van der Waals constants and the critical constants are computed.

1. Introduction

The intermolecular forces which act between the molecules have been expressed in terms of two-parameter Lennard-Jones (12-6) potentials

$$\phi(r) = 4\epsilon\left[\left(\frac{\sigma}{r}\right)^{12} - \left(\frac{\sigma}{r}\right)^{6}\right] \qquad ...(1)$$

where $\phi(r)$ is the potential energy of interaction of a pair of non-polar spherically symmetric molecular force centres at a mutual distance r; ϵ is the depth of the potential at an equilibrium distance $r^* = 2^{1/6}\sigma$, where σ denotes the distance of approach when $\phi(r)=0$, called collision diameter. The attraction or repulsion term of L-J potential

$$\phi_{L-J}\, r^6 = -4\epsilon\sigma^6 \qquad ...(2)$$

describes the induced dipole-dipole interaction neglecting contributions from the dipole-quadrupole interactions and higher terms. The r^{-12} dependence of the repulsion term is chosen for mathematical convenience and approximates the experimental law required by quantum mechanics.

The intermolecular force constants σ and ϵ are determined by the statistical interpretation of the non-ideal behaviour of real gases and solid state properties in terms of Eq. (1). Only in a few cases all experimental observations can be related quantitatively to one set of force constants, indicating the insufficient representation of the real interaction between molecules by two-parameter potentials.[1] It appears, therefore, impossible to deduce uniquely the force constants of Eq. (1) from the electronic structure of real molecules. To evaluate σ and ϵ, Werner Brandt[2] proposed two relations based on Slater-Kirkwood (hereafter referred to simply as S-K) theory of intermolecular forces.

2. Theory

2.1 Dispersion Energies

The S-K theory relates the dispersion energy between two identical spherically symmetric molecules to their polarizabilities and the number of electrons in their valence shell. At distance r larger than the sum of their gas kinetic diameters, the dispersion energy ϕ is given by[3]

$$\phi_{S-K}\, r^6 = -\frac{3}{4}\, a_0^{1/2}\, e^2\, (N\alpha^3)^{1/2} \qquad ...(3)$$

where a_0 is the Bohr radius, e the electronic charge, N, the number of electrons in the molecular valence shell and α is the average molecular polarizability. If α is expressed in relative units (A^3/A^3) and r in cm, the S-K dispersion term may be written as

$$\phi_{S-K}\, r^6 = -12{\cdot}58\times10^{-60}\,(N\alpha^3)^{1/2}\ \text{erg-cm}^6 \qquad ...(4)$$

And the two-parameter equation of S-K for predicting L-J dispersion energies of spherically symmetric or nearly spherically symmetric molecules, will be of the form

$$\phi r^6 = B[N\alpha^3]^{\beta} \qquad ...(5)$$

where B and β are adjustable parameters. Expressing α in relative units (A^3/A^3) and r in cm, they can be calculated by the method of least squares and the values will be

$$B = 11{\cdot}1\times10^{-60}\ \text{erg-cm}^6,\ \beta = 0{\cdot}62.$$

2.2 Collision Diameter

Kirkwood derived by the variational method a relation between the polarizability of an atom with n electrons and the distance of the electronic orbitals from the nucleus, as

$$\alpha_F = \frac{4}{a_0 n}\,[k^2\theta_x + l^2\theta_y + m^2\theta_z]^2 \qquad ...(6)$$

where α_F is the polarizability in the direction of the field F; k, l and m are the directional cosines of the field with respect to a suitable x, y, z coordinate system in the atom such that

$$\theta_x = \sum_{i=1}^{n}\left\langle x_i^2\right\rangle;\ \theta_y = \sum_{i=1}^{n}\left\langle y_i^2\right\rangle$$

$$\text{and } \theta_z = \sum_{i=1}^{n} \left\langle z_i^2 \right\rangle$$

When $\theta_x = \theta_y = \theta_z$, Eq. (6) reduces to

$$\alpha = \frac{4}{9a_0} \left| \sum \left\langle r^2 \right\rangle \right|^2 \qquad \ldots(7)$$

$$\text{where } \frac{1}{3} \left\langle r^2 \right\rangle = \left\langle x^2 \right\rangle + \left\langle y^2 \right\rangle + \left\langle z^2 \right\rangle$$

For nearly spherically symmetric molecules one can apply the general Eq. (7) to the problem only when the valence shells contribute substantially to α. If the equilibrium distance between two molecules is taken to be proportional to the average radius of their valence shell, i.e.

$$r^* = 2c\bar{r} \qquad \ldots(8)$$

where c is a constant, n is replaced by N and

$$\sum \left\langle r^2 \right\rangle \text{ by } N\bar{r}^2 = N\left(\frac{r^*}{2c}\right)^2$$

Eq. (7) becomes

$$\alpha = (4/9)a_0 (2c)^{4\gamma} [N r^{*4}]^{\gamma} \qquad \ldots(9)$$

In addition to c, Eq. (9) contains an adjustable parameter γ which should be of the order of unity. Because of the conventional form $\phi(r) = 4\epsilon[(\sigma/r)^{12} - (\sigma/r)^6]$ it is convenient to introduce the L-J collision diameter σ, as

$$\sigma = 2^{-1/6} r^* \qquad \ldots(10)$$

Then by substituting $r^* = \sigma 2^{1/6}$ in Eq. (9) we have

$$\alpha = (4/9)a_0 (2c)^{4\gamma} [N\sigma^4 . 2^{4/6}]^{\gamma}$$

or

$$\alpha = C [N\sigma^4]^{\gamma} \qquad (11)$$

where

$$C = (4/9)\, a_0 [2^{5/6} c]^{-4\gamma}$$

Eq. (11) yields a straight line for each of the N values on a log α versus log $N\sigma^4$ plot. These isoelectronic lines are empirically found to fall on a straight line if Eq. (11) is modified so as to depend on the deviation of N from $N_0 = 8$, the number of valence electrons in the noble gas configuration. Then one finds

$$\alpha = C [N\sigma^4]^{\gamma k} \exp [(4{\cdot}57)\, \gamma\, (1-k)] \qquad \ldots(12)$$

where

$$k = \frac{\log N_0}{\log N} \qquad \ldots(13)$$

By the method of least squares, the parameters in Eq. (12) are found to be $C = 2{\cdot}65 \times 10^{-29}$ and $\gamma = 1{\cdot}56$. The intermolecular force constant σ can be calculated from the modified S-K formula as

$$\sigma = \left[\frac{1}{N}\left(\frac{\alpha}{C} \exp\{-(4{\cdot}57)\, \gamma\, (1-k)\}\right)^{1/\gamma k}\right]^{1/4} \qquad \ldots(14)$$

And ϵ can be evaluated from the relation

$$\epsilon = \frac{B\, k\, [N\alpha^3]^{\beta}}{4\sigma^6} \qquad \ldots(15)$$

2.3 Van der Waals Constants

Let it be supposed that a fluid is made up of interacting molecules and that each molecule sets up a potential around it. Let the molecules be randomly distributed. In such a case, each molecule can be considered to move freely in a uniform field produced by the other molecule. The potential energy between any two molecules is

$$U(r) = -\alpha;\ r < r^*$$

$$= -\left(\frac{r^*}{r}\right)^6;\ r \geqslant r^*$$

with minimum occurring at $U = -\epsilon$, $r = r^*$. Since the molecules are randomly distributed, in the vicinity of a molecule, the density of other molecules would become zero between $r = 0$ and $r = r^*$ and constant (N/V) from $r = r^*$ to $r = \alpha$. The number of molecules between r and $r + dr$ would be $(N/V)\ 4\pi r^2\, dr$ for $r \geqslant r^*$. The potential energy between any one of these molecules and the molecule at $r = 0$ is given by the above equation. Therefore the potential energy of the molecule at $r = 0$ due to the molecules at $r \geqslant r^*$ is given by

$$\phi = -\int_{r^*}^{\infty} \left(\frac{r^*}{r}\right)^6 (N/V)\, 4\pi r^2\, dr$$

$$= -\frac{4\pi\, \epsilon\, r^{*3}\, N}{3V} = -2\, a\, (N/V)$$

where

$$a = \frac{2\pi\, \epsilon\, r^{*3}}{3}$$

When a molecule moves randomly through a volume V, every other molecule in the system apportions a volume $4/3\pi r^{*3}$ to the molecule under consideration. Since the intermolecular attraction between pairs of molecules gives rise to this effect, only half of the effect can be assigned to each molecule. Therefore, the free volume

$$V_f = V - N\, \frac{2\pi\, r^{*3}}{3}$$

$$= V - Nb$$

$$\text{where } b = \frac{2\pi\, r^{*3}}{3}$$

The van der Waals constants a and b are calculated from the intermolecular force constants ϵ and r^* and hence the critical constants P_c, V_c and T_c can be computed.

Table 1—Values of α, σ, ϵ, a, b and Critical Constants of Hydrocarbons, Cycloalkenes, Alcohols and Alkyl Halides

Molecule	α 10^{24}cm^3	σ Å	ϵ 10^{16}erg/deg	a 10^5atm-cm^6	b 10^2cm^3	V_c 10^5cm^3	T_c K	P_c atm
CH_4	2·5650	3·743 (3·79)	211·284 (198·8)	237·0447	417·251	1251·753	45·95	5·043
C_2H_6	4·5890	4·419 (4·42)	325·296 (317·5)	600·934	687·042	2061·126	70·72	4·715
C_3H_8	6·6039	5·035 (5·06)	365·284 (350·7)	997·752	1015·845	3047·537	79·45	3·581
C_4H_{10}	8·6149	5·611 (4·99)	368·090 (566·0)	1391·204	1405·634	4216·901	80·06	2·608
C_5H_{12}	10·6246	6·158 (5·77)	353·693 (476·3)	1767·545	1858·571	5575·714	76·93	1·895
C_6H_{14}	12·6334	6·685	331·912	2121·514	2377·159	7131·476	72·19	1·390
C_7H_{16}	14·6418	7·195	307·630	2451·808	2964·100	8892·301	66·91	1·033
C_8H_{18}	16·6498	7·6923 (7·45)	283·234 (441·8)	2758·370	3621·949	10865·849	61·60	0·778
C_3H_6	6·0208	4·851	360·317	880·121	905·744	2717·233	78·60	3·973
C_4H_8	8·0278	5·436	371·289	1248·275	1278·525	3835·575	78·97	2·828
C_5H_{10}	10·0347	5·991	360·474	1658·569	1711·175	5133·524	78·40	2·098
C_6H_{12}	12·0417	6·523	340·065	2019·592	2208 703	6626·109	73·96	1·533
C_7H_{14}	14·0486	7·039	315·760	2355·990	2774·925	8324·775	68·68	1·133
C_8H_{16}	16·0556	7·538	291·519	2671·409	3408·069	10224·207	63·40	0·852
CH_3OH	3·2032	4·108 (3·58)	258·460	383·426	551·736	1655·207	56·21	4·665
C_2H_5OH	5·2505	4·775 (4·45)	327·619	764·469	866·679	2600·039	71·25	3·764
C_3H_7OH	7·2944	5·381	347·063	1157·200	1240·044	3720·131	75 48	2·787
C_4H_9OH	9·3368	5·949	342·111	1541·507	1675·774	5027·322	74·41	2·033
$C_5H_{11}OH$	11·3785	6·492	325·781	1906·959	2176·972	6530·916	70·85	1·490
$C_6H_{13}OH$	13·4196	7·015	304·639	2249·853	2746·661	8239·984	66·26	1·104
$C_7H_{15}OH$	15·4605	7·522	282·159	2569·809	3387·227	10161·683	61·37	0·829
$C_8H_{17}OH$	17·5012	8·018	259·985	2867·145	4101·464	12304·392	56·54	0·631
$C_9H_{19}OH$	19·5417	8·504	238·866	3142·694	4893·093	14679·279	51·95	0·489
CH_3Cl	4·4836	4·399 (3·37)	320·481	583·677	677·339	2032·018	69 70	4·712
C_2H_5Cl	6·5136	5·019	362·926	981·881	1006·179	3018·538	78·94	3·592
C_3H_7Cl	8·5636	5·603	367·309	1382·031	1399·330	4197·991	81·82	2·614
C_4H_9Cl	10·6168	6·157	353·614	1766·116	1857·484	5572·451	76·91	1·896
$C_5H_{11}Cl$	12·6728	7·691	332·087	2128·155	2383·339	7150·019	72·23	1·387
$C_6H_{13}Cl$	14·7303	7·208	307·849	2466·427	2979·649	8938·949	66·95	1·029
$C_7H_{15}Cl$	16·7887	7·712	283·349	2780·315	3649·285	10947·854	61·63	0·773
CH_3Br	5·3826	4·565	360·262	733·589	757·300	2271·900	78·36	4·737
C_2H_5Br	7·3503	5·161	384·352	1130·631	1094·024	3282·071	83·59	3·498
C_3H_7Br	9·3106	5·721	378·317	1516·088	1490·321	4470·964	82·29	2·528
C_4H_9Br	11·3015	6·261	359·368	1887·079	1952·925	5858·776	78·16	1·832
$C_5H_{11}Br$	13·2978	6·782	334·948	2235·295	2481·949	7445·848	72·85	1·344
$C_6H_{13}Br$	15·2974	7·289	309·075	2559·621	3079·971	9239·914	67·22	0·999
$C_7H_{15}Br$	17·2989	7·782	283·555	2861·093	3749·428	11248·283	61·72	0·754
CH_3I	6·6381	4·765	411·908	953·223	860·656	2581·968	89·59	4·766
C_2H_5I	8·5638	5·347	413·279	1351·504	1216·212	3648·636	89·88	3·384
C_3H_7I	10·5525	5·904	395·501	1741·514	1637·627	4912·881	86·02	2·405
C_4H_9I	12·5632	6·440	369·276	2110·705	2125·748	6377·244	80·31	1·729
$C_5H_{11}I$	14·5842	6·959	340·495	2455·738	2643·885	7931·657	75·13	1·301
$C_6H_{13}I$	16·6106	7·465	311·948	2776·259	3309·882	9929·646	67·85	0·938
$C_7H_{15}I$	18·6408	7·959	284·866	3072·732	4011·614	12034·841	61·95	0·707

3. Results and Discussion

The polarizability of the molecules calculated by using the δ-function model of chemical binding[4] and hence the intermolecular force constants σ and ϵ are given in Table 1. It has been observed that α and σ increase with the size of the molecules. The value of σ varies as $\sigma_{CH_4} < \sigma_{CH_3OH} < \sigma_{CH_3Cl} < \sigma_{CH_3Br} < \sigma_{CH_3I}$. And the evaluated values of σ and ϵ are found to be fairly agreeing with the literature values (given in brackets) calculated from the viscosity and virial coefficient measurements.[5] The potential depth ϵ of the molecules increases up to propyl or butyl group in all cases and decreases afterwards. This may be partially explained as due to the inductive effect. The addition of methylene group after the propyl or butyl group is found to decrease the depth of the potentials and keep more or less constant in the bigger molecules in all cases of our investigation. The calculated values of van der Waals constants and the critical constants are also given in Table 1. The value of the ratio RT_c/P_cV_c is found to be 2·6 in all the cases, justifying the critical constants.

Acknowledgement

One of the authors (PT) is thankful to the University Grants Commission, New Delhi for the award of a Junior Research Fellowship.

References

1. Werner *Discuss. Faraday Soc.*, **15** (1953), 108 ff.
2. Brandt Werner, *J. chem. Phys.*, **24** (1956), 501.
3. Slater J C & Kirkwood K G, *Phys. Rev.*, 37 (1931), 682.
4. Lippincott E R & Stutman J M, *J. phys. Chem.*, **68** (1964), 2926.
5. Hirschfelder J O, Curtiss C F & Bird R B, *Molecular theory of gases and liquids* (John Wiley, New York), 1954.

Indian Journal of Pure & Applied Physics
Vol. 18, January 1980, pp. 40-46

Liquid Structure of *tert*-Butyl Alcohol in Nonpolar Solvents from Dielectric Studies

D C Dwivedi & S L Srivastava

Physics Department, University of Allahabad, Allahabad 211 002

Received 3 *October* 1978; *revised received* 9 *April* 1979

Significant structure theory has been used to obtain the solute-solute interaction parameter (G) and the solute-solvent interaction parameter (G^*) from the measured static dielectric constants and the refractive indices in the liquid state for the systems *tert*-butyl alcohol (TBA) in benzene and TBA in cyclohexane in the concentration range 0-1 mole fraction of TBA at 31°C. Dipole moment (μ) of TBA has been determined from Guggenheim equation, modified Guggenheim equation and the Onsager's equation. Values of μ are solvent dependent, 1·67 D in benzene and 1·21 D in cyclohexane. Assuming μ of TBA to be 1·67 D, the G value comes out to be 0·727 ± 0·003 and G^* depends on the concentrations of the solvents. Excess volumes of these binary systems have been explained on the basis of the significant structure theory. Mixing of TBA with cyclohexane has been found to be ideal, whereas the system TBA-benzene shows non-ideal mixing behaviour. The non-ideality parameter in TBA-benzene system is found to be −0·024.

1. Introduction

A number of investigations on dispersion in optical region and X-ray studies have shown that a liquid has elements of crystalline structure. Eyring and his coworkers[1-3] using the lattice picture postulated the presence of vacant lattice sites (holes). Extending the hole concept as a significant structure approach, Eyring *et al.* concluded that a liquid has an excess volume ($V-V_s$), where V and V_s are the molar volumes of the liquid and the solid respectively. Based on this approach Eyring *et al.* explained many thermodynamical, transport and the dielectric properties of different systems.[2]

In the present communication we present the data on low and high limiting electric permittivities of the binary systems TBA-benzene and TBA-cyclohexane in the concentration range 0-1 mole fraction and have obtained the solute-solute and solute-solvent interaction parameters from these dielectric measurements, using the significant structure theory. The dipole moment of TBA has been evaluated using different equations based on Debye theory and Onsager's reaction field model.

2. Experimental Details

Tert-butyl alcohol (TBA) procured from M/s BDH Chemicals has been used as such. Benzene, AnalaR grade and cyclohexane (LR grade) also procured from M/s BDH Chemicals, have been used after double distillation.

Measurements of the static dielectric constant (ϵ_0) of the two systems have been carried out at 31°C using a Muirhead Heterodyne bridge at 100 kHz. The refractive index, n_D, at sodium D-line frequency by Abbe's refractometer and the density using a pyknometer, have also been measured. The experimental arrangements and the procedure for all the measurements have already been described earlier.[4] The estimated accuracies of the various measurements are: ϵ_0 within ± 0·002, n_D, within ±0·002, $\epsilon_\infty = n_D^2$ within ±0·004, density within ± 0·0002 g/ml and the temperature within ±0·5°C. The measured values of ϵ_0, n_D (ϵ_∞) and d_{12} are listed in Table 1 as a function of concentration of TBA. The values of (ϵ_0) and ($\epsilon_0-\epsilon_\infty$) versus mole fraction of TBA are plotted in Figs. 1 and 2 for the solvent benzene and cyclohexane respectively.

3. Analysis of the Data

The data analysis has been carried out in two parts (i) evaluation of the molecular dipole moment, and (ii) application of significant structure theory to explain the observed dielectric properties and density of the solutions.

3.1 Evaluation of the Dipole Moment

The dipole moment of TBA from the solution data has been evaluated by the use of Guggenheim equation, modified Guggenheim equation and the Onsager equation as detailed below:

3.1.1 *Guggenheim equation*—According to Guggenheim, the electric dipole moment of the polar solute from the solution data is given by[5]

$$\frac{4\pi N}{3kT}\cdot\frac{\mu^2}{3} = \frac{3}{(\epsilon_{01}+2)(\epsilon_{\infty 1}+2)}\left.\frac{(d\Delta)}{dc}\right|_{c\to 0} \quad ...(1)$$

Table 1—Experimental Values of ϵ_0, ϵ_∞ $(= n_D^2)$ & d_{12} for the Binary Systems TBA-Benzene and TBA-Cyclohexane at 31°C for the Different Mole-fraction Concentrations of TBA

	TBA-Benzene system				TBA-Cyclohexane system		
Conc. in MF	ϵ_0	ϵ_∞	d_{12} (g/ml)	Conc. in MF	ϵ_0	ϵ_∞	d_{12} (g/ml)
Pure benzene	2·262	2·223	0·8657	Pure cyclo.	2·005	2·019	0·7679
0·0886	2·575	2·199	0·8547	0·0778	2·109	2·009	0·7663
0·2164	3·034	2·148	0·8404	0·1636	2·241	1·997	0·7657
0·2948	3·360	2·119	0·8329	0·2470	2·398	1·985	0·7654
0·3883	3·790	2·091	0·8241	0·3412	2·620	1·977	0·7653
0·4736	4·202	2·059	0·8159	0·4328	2·947	1·966	0·7652
0·5976	5·210	2·016	0·8051	0·5369	3·522	1·954	0·7658
0·7104	6·267	1·984	0·7959	0·6907	4·953	1·936	0·7673
0·8104	7·341	1·960	0·7879	0·7606	5·991	1·929	0·7687
0·8920	8·660	1·938	0·7827	0·8831	8·464	1·920	0·7716
1·0000	10·832	1·909	0·7756	1·0000	10·832	1·909	0·7759

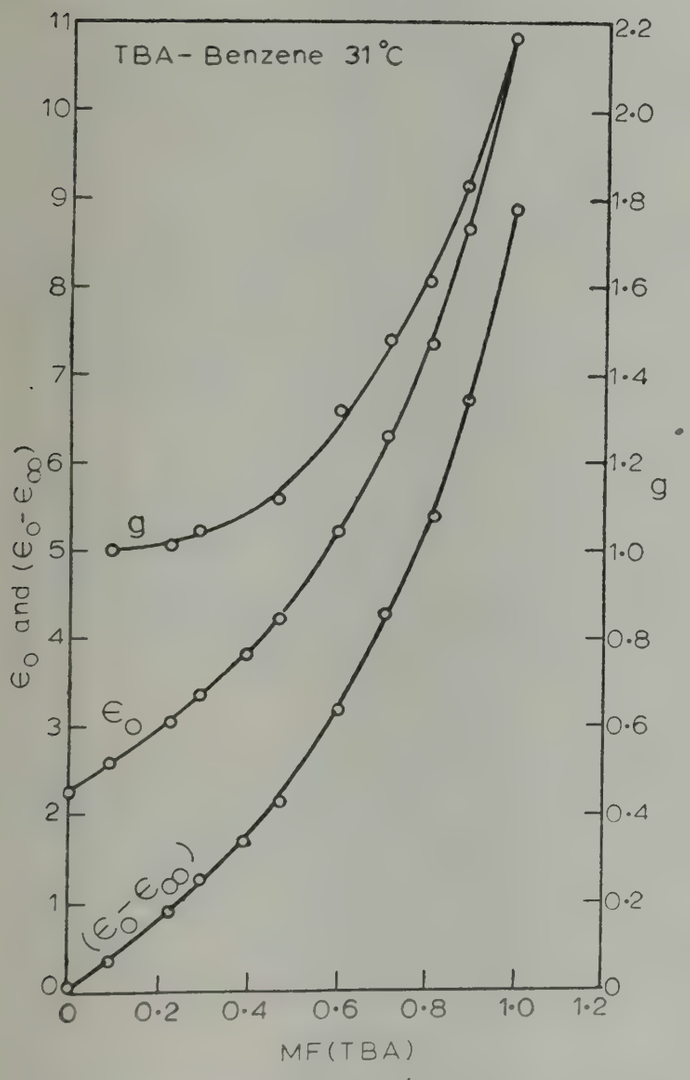

Fig. 1—Dependence of Kirkwood correlation parameter (g), static dielectric constant (ϵ_0) and the dielectric relaxation strength ($\epsilon_0 - \epsilon_\infty$) on MF of TBA for the system TBA-benzene

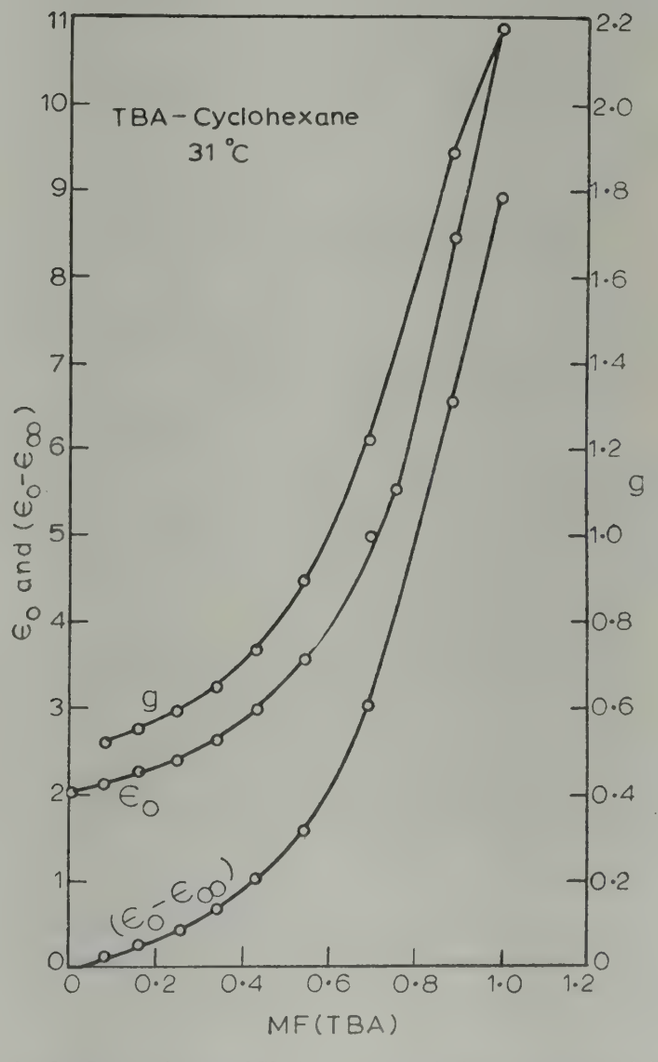

Fig. 2—Dependence of Kirkwood correlation parameter (g), static dielectric constant (ϵ_0) and the dielectric relaxation strength ($\epsilon_0 - \epsilon_\infty$) on MF of TBA for the system TBA-cyclohexane

where $\Delta=[(\epsilon_{012}-\epsilon_{\infty 12})-(\epsilon_{01}-\epsilon_{\infty 1})]$ and $c=(f_2/V_{12})$, V_{12} is the molar volume of the solution and is equal to $(M_1f_1+M_2f_2)/d_{12}$; d_{12} is the density of the solution and f_1, f_2 are the mole fractions of the solvent and the solute respectively. Suffixes 1, 2, and 12 correspond to the solvent, solute and the solution respectively. Using standard data from the literature[6,7] the value of μ of TBA comes out to 1·70 D and 1·21 D from the dilute solution data of the systems TBA-benzene and TBA-cyclohexane respectively.

3.1.2 *Modified Guggenheim equation* — The Guggenheim equation has been derived from the Debye equation assuming that,

$$(\epsilon_{012}+2)\,(\epsilon_{\infty 12}+2) = (\epsilon_{01}+2)\,(\epsilon_{\infty 1}+2)$$

but this assumption may not hold even at the low dilute solution limits where the measurements are usually carried out. For example, for the binary system TBA-benzene, $(\epsilon_{012}+2)\,(\epsilon_{\infty 12}+2)$ is 19·213 for $f_2 = 0{\cdot}0886$ and increases with the concentration, whereas for benzene $(\epsilon_{01}+2)\,(\epsilon_{\infty 1}+2)$ is 18·000. For the system TBA-cyclohexane also the above relation does not hold good. Hence, if we do not apply this assumption and in place of Δ substitute Δ' as given by

$$\Delta' = \frac{(\epsilon_{01}+2)\,(\epsilon_{\infty 1}+2)}{(\epsilon_{012}+2)\,(\epsilon_{\infty 12}+2)} \cdot (\epsilon_{012}-\epsilon_{\infty 12})-(\epsilon_{01}-\epsilon_{\infty 1})$$

the value of μ comes out to be 1·64 D instead of 1·70 D for TBA-benzene and 1·20 D instead of 1·21 D for TBA-cylohexane systems.

3.1.3 *Onsager equation*—The Onsager equation,[5] based on the semi-statistical calculations of the dipolar polarizabilities using the concept of reaction field to account for the local field correction, assuming the distribution of dipole moments according to Langevin's law, is given by:

$$\frac{4\pi N}{3kT} \cdot \frac{\mu^2}{3} = \frac{(\epsilon_{012}-\epsilon_{\infty 12})\,(2\,\epsilon_{012}+\epsilon_{\infty 12})}{\epsilon_{012}\,(\epsilon_{\infty 12}+2)^2} \cdot \frac{1}{c} \qquad \ldots(2)$$

Using Eq. (2), the dipole moments at different mole fractions (MF) of the solute for the two systems are listed in Table 2.

Taking the dipole moment of TBA as 1·67 D, for it is very near to the gas phase value, the value of Kirkwood correlation parameter[5] (g) may be calculated from the following equation:

$$\frac{4\pi N}{3kT} \cdot \frac{g\,\mu^2}{3} = \frac{(\epsilon_{012}-\epsilon_{\infty 12})\,(2\,\epsilon_{012}+\epsilon_{\infty 12})}{\epsilon_{012}\,(\epsilon_{\infty 12}+2)^2} \cdot \frac{1}{c} \qquad \ldots(3)$$

Table 2—Molecular Dipole Moment of TBA and Kirkwood Correlation Parameter g as a Function of Concentration

TBA-benzene system		
Conc. in MF	μ^*	g
Pure benzene	—	—
0·0886	1·67	1·00
0·2164	1·68	1·01
0·2948	1·71	1·05
0·3883	1·74	1·08
0·4736	1·77	1·12
0·5976	1·91	1·32
0·7104	2·03	1·48
0·8104	2·12	1·62
0·8920	2·26	1·83
1·0000	2·46	2·17
TBA-cyclohexane system		
Conc. in MF	μ^*	g
Pure cyclo-hexane	—	—
0·0778	1·21	0·52
0·1635	1·24	0·55
0·2470	1·28	0·59
0·3412	1·33	0·64
0·4328	1·43	0·73
0·5369	1·57	0·89
0·6907	1·85	1·22
0·7606	2·00	1·44
0·8831	2·29	1·89
1·0000	2·46	2·17
μ (Guggenheim Eq.)	1·70 D TBA-benzene system	
	1·21 D TBA-cyclohexane system	
μ (Mod. Guggenheim Eq.)	1·64 D TBA-benzene system	
	1·20 D TBA-cyclohexane system	

* The dipole moment according to the Onsager equation

Eq. (3) gives $g = 2{\cdot}17$ for pure TBA. Values of $g>1$ suggest parallel alignment of the dipoles of solute molecules, whereas $g<1$ suggest them to be antiparallel. Values of (g) for the two systems at different concentrations (in mole fraction of TBA) as calculated from Eq. (3) are listed in Table 2, and also shown in Figs. 1 and 2.

3.2 Significant Structure Theory

The significant structure theory has been applied to explain (i) the density of the systems, and (ii) the low and high limiting electric permittivities.

3.2.1 *Density of the systems*—According to significant structure theory any property in liquid state can be written as[2]:

$$X = \frac{V_s}{V} X_s + \frac{V-V_s}{V} X_g \qquad \ldots(4)$$

where X is the liquid property, and V is the molar volume of the liquid. The suffixes s and g stand for the solid and the gas phase respectively. On this

basis the equation for the density of the solution can be written as:

$$d_{12} = \frac{V_{s12}}{V_{12}} d_{s12} + \left(\frac{V_{12} - V_{s12}}{V_{12}}\right) d_{g12}$$

The second term on the right hand side can be neglected because the density in the gas phase is negligibly small compared to that in the solid phase; hence

$$d_{12} = \frac{V_{s12}}{V_{12}} d_{s12} \qquad ...(5)$$

where $d_{s12} = d_{s1} f_1 + d_{s2} f_2$, and

$$V_{s12} = V_{s1} f_1 + V_{s2} f_2 + A f_1 f_2 \sqrt{V_{s1} V_{s2}} \qquad ...(6)$$

The term $A f_1 f_2 \sqrt{V_{s1} V_{s2}}$ in the expression for V_{s12} is a correction term and signifies the nature of mixing in the solution. For an ideal mixing $A=0$, and for non-ideal mixing A is non-zero and < 1.

Calculated values of the density of solution, d_{12}, according to significant structure theory assuming the case of ideal mixing, i.e. $A = 0$, for the system TBA-benzene are given in Table 3. A considerable difference between the theoretical and the experimental values of d_{12} exists (Table 3). This shows that the solution has non-ideal behaviour in mixing and suggests some non-zero and negative values of A. Taking $A = -0{\cdot}024 \pm 0{\cdot}001$, the theoretical and the experimental values of the density are in agreement (Table 3). It may however be noted that the solid phase density and the volume (d_{s12} and V_{s12}) are inter-related parameters, and therefore, we may introduce the non-ideality parameter in the expression for d_{s12} instead of including it in the expression for V_{s12}. On doing so, Eq. (6) becomes:

$$d_{s12} = d_{s1} f_1 + d_{s2} f_2 + B f_1 f_2 \sqrt{d_{s1} d_{s2}}, \text{ and}$$

$$V_{s12} = V_{s1} f_1 + V_{s2} f_2 \qquad ...(7)$$

and the non-ideality parameter (B) again comes out to be $-0{\cdot}024 \pm 0{\cdot}001$ in order to explain the measured values of density at different MF of TBA. Similarly the density for the system TBA-cyclohexane has been calculated and listed in Table 3. Taking the non-ideality parameter A (or B) $= 0$, the results are in agreement with the experimental values. Thus TBA in cyclohexane is an ideal mixing case while the system TBA-benzene is an example of non-ideal mixing.

The excess volumes (V_E) for the two systems have been calculated from the equation:

$$V_E = \left(\frac{M_1 f_1 + M_2 f_2}{d_{12}}\right) - \left(\frac{M_1}{d_1} f_1 + \frac{M_2}{d_2} f_2\right) \qquad ...(8)$$

V_E (theoretical) corresponds to the density of the solution (d_{12}) as determined from the significant structure theory, and V_E (experimental) to the measured value of d_{12}. Fig. 3 shows the variation of V_E versus MF of the solute for the two systems. For the system TBA-cyclohexane, which is the case of ideal mixing, the excess volume is negative, showing its maximum value at MF = 0·5369. TBA-benzene is the case of non-ideal mixing and has V_E positive, with the maximum value at 0·4736 MF. The excess volume as a measure of the non-ideality in mixing may be misleading. We therefore suggest that the non-ideality of the solution be tested by the non-ideal parameter A (or B) of Eqs. (6) and (7).

3.2.2 *Low and high limiting frequency electric permittivity*—Eyring and coworkers extended the Onsager equation by applying the significant structure theory, and gave the following general relation for the solution of two liquids[2]:

$$\frac{(\epsilon_{012} - \epsilon_{\infty 12})(2\epsilon_{012} + \epsilon_{\infty 12})}{3\epsilon_{012}} = \frac{4\pi N}{V_{12}} \left(\frac{\epsilon_{\infty 12} + 2}{3}\right)^2 \left[\frac{V_{s12}}{V_{12}} P_{s12} + \frac{V_{12} - V_{s12}}{V_{12}} P_{g12}\right] \qquad ...(9)$$

Table 3—Experimental and Theoretical Density of the Solution (g/ml) for an Ideal and Non-ideal Mixing for the Systems TBA-Benzene and TBA-Cyclohexane at 31°C

TBA-Benzene system					TBA-Cyclohexane system		
Conc. in MF	d_{12}(exptl)	d_{12}(theor.)			Conc. in MF	d_{12}(exptl)	d_{12}(theor.)
		$A=B=0$	$A=-0{\cdot}024$	$B=-0{\cdot}024$			$A=B=0$
Pure benzene	0·8657	0·8657	0·8657	0·8657	Pure cyclo.	0·7679	0·7679
0·0886	0·8547	0·8563	0·8546	0·8548	0·0778	0·7663	0·7663
0·2164	0·8404	0·8438	0·8402	0·8405	0·1635	0·7657	0·7656
0·2948	0·8329	0·8370	0·8327	0·8330	0·2470	0·7654	0·7653
0·3883	0·8241	0·8287	0·8240	0·8242	0·3412	0·7653	0·7652
0·4736	0·8159	0·8207	0·8158	0·8158	0·4328	0·7652	0·7650
0·5976	0·8051	0·8097	0·8051	0·8050	0·5369	0·7658	0·7656
0·7104	0·7959	0·7999	0·7960	0·7958	0·6908	0·7673	0·7672
0·8104	0·7879	0·7908	0·7880	0·7878	0·7606	0·7687	0·7686
0·8920	0·7827	0·7845	0·7828	0·7826	0·8831	0·7716	0·7716
1·0000	0·7756	0·7756	0·7756	0·7756	1·0000	0·7759	0·7759

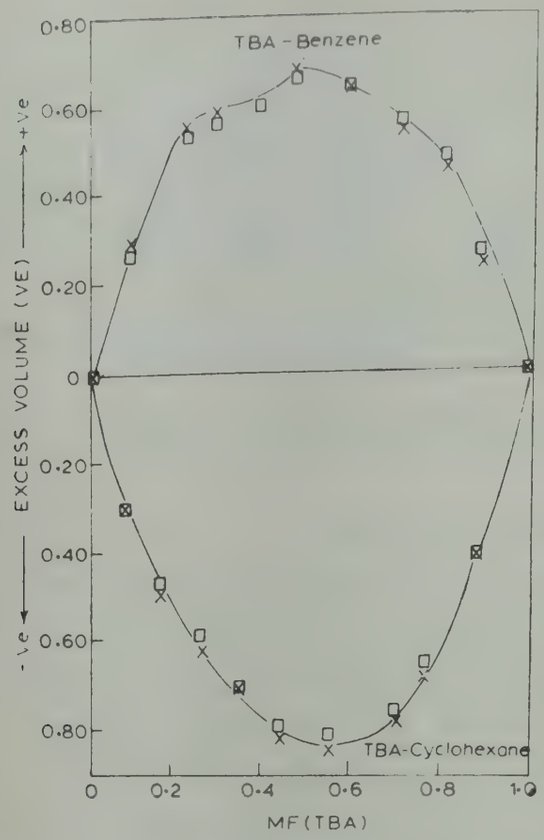

Fig. 3—Dependence of excess volume (V_E) on MF of TBA for the systems TBA-benzene and TBA-cyclohexane (Theoretical points are shown by '×', and the experimental points by '□'.)

where, $P_{s12} = f_1^2 P_{s1} + f_2^2 P_{s2}$

$$+ 2 f_1 f_2 \left(\frac{P_{s1} + P_{s2}}{2} \right) \quad ...(10)$$

and $P_{g12} = f_1 P_{g1} + f_2 P_{g2}$ ...(11)

$P_{g1} = (\mu_1^2/3kT)$ and $P_{g2} = (\mu_2^2/3kT)$ and the terms on the right hand side of Eq. (10) correspond to the solvent-solvent interactions, solute-solute interactions and the solute-solvent interactions respectively. In the systems presently studied, the solvents are non-polar and hence the above equations for P_{s12} and P_{g12} reduce to

$$P_{g12} = (\mu^2/3\ kT).\ f_2$$

$$P_{s12} = f_2^2 P_{s2} + f_1 f_2 P_{s2}$$

or $P_{s12} = f_2^2 (\mu^2/kT)\ G + f_1 f_2 (\mu^2/kT)\ G^*$ ...(12)

where G and G^* represent the adjustable solute-solute and solute-solvent parameters respectively. Thus finally we have,

$$\frac{(\epsilon_{012} - \epsilon_{\infty 12})\ (2\ \epsilon_{012} + \epsilon_{\infty 12})}{3\ \epsilon_{012}\ (\epsilon_{\infty 12} + 2)^2} = \left(\frac{4\pi N}{3\ kT} \right) \frac{\mu^2}{3V_{12}} f_2$$

$$\times \left[\frac{V_{s12}}{V_{12}} (f_2 G + f_1 G^*) + \frac{1}{3} \left(\frac{V_{12} - V_{s12}}{V_{12}} \right) \right]$$

.. (13)

3.2.3 *Calculation of G*—The solute-solute interaction parameter (G) may be calculated from the pure liquid data using the relation

$$\frac{(\epsilon_{02} - \epsilon_{\infty 2})\ (2\ \epsilon_{02} + \epsilon_{\infty 2})}{3\ \epsilon_{02}\ (\epsilon_{\infty 2} + 2)^2} = \left(\frac{4\pi N}{3\ kT} \right) \frac{\mu^2}{3V_2}$$

$$\times \left[\frac{V_{s2}}{V_2} G + \frac{1}{3} \left(1 - \frac{V_{s2}}{V_2} \right) \right] \quad ...(14)$$

Taking $\mu = 1{\cdot}67$ D, the value of G comes out to be $0{\cdot}727 \pm 0{\cdot}003$.

We can also inter-relate G, G^* and the Kirkwood correlation term (g). Thus from Eqs. (3) and (13) we get

$$g = 3 \left[\frac{V_{s12}}{V_{12}} (f_2\ G + f_1\ G^*) + \frac{1}{3} \left(1 - \frac{V_{s12}}{V_{12}} \right) \right]$$

...(15)

3.2.4 *Calculation of G**—G^* represents the solute-solvent interaction behaviour and, therefore, its value may be calculated from the solution data. Table 4 presents the values of G^* at different mole-fractions for the two systems. G^* has been calculated taking $G = 0{\cdot}73$ and $\mu = 1{\cdot}67$ D. From these derived constants (g) as given in Table 2 have also been reproduced.

3.2.5 *Explanation of the electric permittivity*—Although from Table 4 it is clear that no single value of G^* can be fitted to the data to explain the observed electric permittivities, the static dielectric constants have been calculated by taking large limiting values of G^*, viz. $G^* = 0{\cdot}256$ for TBA-benzene and $0{\cdot}200$ for TBA-cyclohexane systems.

Table 4—Solute-Solvent Interaction Parameter as a Function of Mole Fraction of TBA for the Systems TBA-Benzene and TBA-Cyclohexane

TBA-Benzene system			TBA-Cyclohexane system	
Conc. in MF	G^*		Conc. in MF	G^*
	Ideal mixing	Non-ideal mixing		Ideal mixing
Pure benzene	—	—	Pure cyclo.	—
0·0886	+0·2950	+0·2950	0·0778	+0·1215
0·2164	+0·2302	+0·2304	0·1635	+0·0719
0·2948	+0·1916	+0·1917	0·2470	+0·0149
0·3883	+0·1316	+0·1319	0·3412	−0·0630
0·4736	+0·0610	+0·0615	0·4328	−0·1335
0·5976	+0·0225	+0·0240	0·5369	−0·2102
0·7104	−0·0620	−0·0593	0·6907	−0·3085
0·8104	−0·2223	−0·2181	0·7606	−0·3042
0·8920	−0·2863	−0·2804	0·8831	−0·1006
1·0000	—	—	1·0000	—

Table 5—Comparison of Measured and Calculated (according to significant structure theory) Values of ϵ_0 for the Systems TBA-Benzene and TBA-Cyclohexane

TBA-benzene system			TBA-cyclohexane system		
Conc. in MF	ϵ_0		Conc. in MF	ϵ_0	
	Exptl	Theor.		Exptl	Theor.
Pure benzene	2·262	—	Pure cyclo.	2·005	—
0·0886	2·575	2·499	0·0778	2·109	1·938
0·2164	3·034	3·039	0·1635	2·241	1·950
0·2948	3·360	3·419	0·2470	2·398	2·067
0·3883	3·790	4·106	0·3412	2·620	2·350
0·4736	4·202	4·761	0·4328	2·947	2·800
0·5976	5·210	5·872	0·5369	3·522	3·564
0·7104	6·267	7·052	0·6907	4·953	5·236
0·8104	7·341	8·233	0·7606	5·991	6·207
0·8920	8·660	9·282	0·8831	8·464	8·495
1·0000	10·832	10·778	1·0000	10·832	10·831

Table 5 compares the experimental and theoretical values of ϵ_0 in the entire concentration range for both the systems.

4. Results and Discussion

The Guggenheim or the modified Guggenheim equation may not yield the values of dipole moment (see Table 2) near the gas phase value, because these obey the simple Debye equation which does not take into account of either the long-range solute-solute interactions, which are effective even in the dilute solution limit, or the short range (complex) solute-solute interactions responsible for the hydrogen bonding. These two equations also do not take care of the solute-solvent interaction which may be the most frequent phenomenon at higher concentrations. In the Onsager equation long-range solute-solute interactions have been accounted for, and hence it may give a satisfactory value of the dipole moment, although not exactly the same as the gas phase value, because the solute-solvent interactions and the short range solute-solute interactions remain still to be accounted for. The dipole moment of TBA in its gas phase is not reported, but we do not consider it to be very much different from the gas phase dipole moments of iso- and normal-butyl alcohols which are reported as[8] 1·63 D and 1·65 D respectively. Hence for the purpose of calculations, the dipole moment as calculated from the Onsager equation ($\mu = 1{\cdot}67$ D) has been used. On applying this value of the dipole moment to the molecular structure of TBA [$(CH_3)_3$ COH], the angle between the C—O and O—H bond comes out as 106°, which seems to be reasonable. Contributions of the solute-solvent and the solute-solute interactions are manifested from the variation of the static dielectric constants ϵ_0 and $(\epsilon_0 - \epsilon_\infty)$ (Figs. 1 and 2) and the evaluated molecular dipole moments (Table 2) at different MFs of TBA. The parameter (g) also does not vary linearly with concentration. A similar behaviour between ϵ_0 and concentration has also been reported by Higasi[9] for the system nitrobenzene-hexane.

From Table 2 we find that even in the dilute solution limit, the dipole moment of TBA is solvent dependent. Dipole moment in cyclohexane is less than that in benzene. Such a solvent dependence of μ of TBA has been reported by Crossley[10] with the sequence n-heptane $<$ p-xylene $<$ benzene $<$ p-dioxane in the value of the dipole moment. The dipole moment of TBA in p-xylene solution as reported by Crossley[10] is $1{\cdot}29 \pm 0{\cdot}04$ D.

Probably the large value of μ from the Onsager equation in pure liquid state suggests some kind of association of the parallel aligned molecular dipoles of TBA which leads to the formation of multimers. The parallel alignment is obvious because the value of $(g) > 1$. The association breaks partially or completely in the solution state with different extents of breaking at different concentrations of the same solvent as shown in Figs. 1 and 2. TBA in cyclohexane shows $g < 1$ in the concentration range 0-0·54, suggesting the antiparallel alignment of the solute dipoles. But at larger concentrations of TBA it flips over to parallel alignment.

From Table 3 we notice that for the system TBA-benzene, the non-ideality parameter A (or B) equals $-0{\cdot}024$, while this term is zero for TBA-cyclohexane. However, the density data do not seem to be as sensitive as the dielectric data are, for a measure of solute-solvent interactions, because the value of the interaction parameter G^* is finite for TBA-cyclohexane whereas A (or B) equals to zero. So it may not be correct to conclude from the density data alone that the solute-solvent interactions vanish in TBA-cyclohexane system.

In both the above systems G^* is appearing as concentration dependent with the values changing from positive to negative as the concentration increases (see Table 4). If we look into the environment between solute and the solvent molecules, we find that at low concentrations the solute molecule is surrounded by the solvent molecules, while at higher concentrations the solute molecules surround the solvent molecule. Probably this change of environment is responsible for the change of sign in the values of G^*. It is also clear from Table 4 that for the system TBA-benzene,

G^* becomes zero at about 0·6 MF while for the system TBA-cyclohexane G^* is zero at about 0·4 MF. However, excess volume (V_E) is maximum at about 0·5 MF for both the systems.

Thus we may conclude that the quantity (V_{s12}/V_{12}) is the factor responsible for the solid-like behaviour and ($1-V_{s12}/V_{12}$) is the factor representing the gas-like behaviour of the liquid structure. Solid-like contribution in the density and the dielectric data of the two systems consisting of TBA-benzene and TBA-cyclohexane from the present study therefore comes out to be as follows:

TBA 98·7%, benzene 91·8%, TBA-benzene varies from 91·0% at MF 0·0886 to 95·2% at MF 0·8920 of TBA. Cyclohexane 97·0% and TBA-cyclohexane varies from 96·9% at MF 0·0778 to 98·1% at MF 0·8831 of TBA.

Acknowledgement

We are grateful to Prof. Krishnaji for many suggestions and advice and to Dr Pradip Kumar and Dr S C Srivastava for their help in taking the measurements. One of us (DCD) thanks the University Grants Commission, New Delhi, for the award of a teacher fellowship.

References

1. Eyring H, Ree T & Hirai N, *Proc. nat. Acad. Sci. (USA)*, 44 (1958), 683.
2. Eyring H & Jhon M S, *Significant liquid structures* (John Wiley, New York), 1969.
3. Walter J & Eyring H, *J. chem. Phys.*, 9 (1941), 393.
4. Krishnaji & Mansingh A, *J. chem. Phys.*, 41 (1964), 827.
5. Hill N E, Vaughan W E, Price A H & Davies M, *Dielectric properties and molecular behaviour* (Van Nostrand-Reinhold, London), 1969.
6. Weast R C *et al.*, *Hand book of chemistry and physics* (The Chemical Rubber Co., Ohio), 1964.
7. *International critical tables*, Vol. 111, (National Research Council, USA), (McGraw-Hill, New York), 1928, p. 27.
8. Smyth C P, *Dielectric behaviour and structure* (McGraw-Hill, New York), 1955.
9. Higasi K & Kiyoshi U, *Bull. Res. Inst. Appl. Electricity*, 17 (1965), 164.
10. Crossley J, *Can. J. Chem.*, 49 (1971), 712.

Indian Journal of Pure & Applied Physics
Vol. 18, January 1980, pp. 47-50

Application of a Wall-stabilized dc Arc for Spectral Analysis of Solutions

M A Eid, K M El Behery & F A El Anany
Physics Department, National Research Centre, Cairo, Egypt

Received 26 *December* 1978

A wall-stabilized dc arc with a closed analytical gap is described. Optimal working conditions and detection limits for the elements Ca, Mg, Fe and Mn are determined. The device is applied for the determination of trace elements in a sample of human blood serum.

1. Introduction

A variety of plasma sources have been investigated by a number of workers, with the aim of finding a direct replacement for chemical combustion flames. Most of the work has been devoted to the inductively coupled plasma sources, while the dc arc has received little attention. Stabilized dc arcs have been constructed by a few researchers.[1-3] It has been shown that the introduction of elements of low ionization potential into the arc has a marked effect on the arc shape and its spectrum. Moreover, it facilitates the entry of the aerosol into the discharge and hence improves its analytical utility.

The present work was undertaken to investigate the possibility of application of a wall-stabilized dc arc for the analysis of some elements which are of importance in biological fluids.

2. Experimental Details and Results

2.1 The Arc and Its Characteristics

Fig. 1 shows a schematic diagram of the arc device. The arc burns between a tungsten cathode and a graphite anode through an axial channel which consists of openings in water cooled brass segments. A slight stream of argon is allowed to circulate around the electrodes. Solutions are sprayed in an argon stream using a pneumatic atomizer. The light from the closed analytical gap is focused on the slit of a Q24 spectrograph (Carl-Zeiss Jena). With this construction, CN bands disappeared completely from the spectrum of the arc. The spectra are recorded on Kodak spectral analysis plates type 103a. The plate emulsion was calibrated at each 100 Å interval using the two-step filter method.[4]

Introducing potassium chloride into the argon arc alters its shape and spectrum. The intense column of the argon arc is changed into a diffuse flame-like discharge. The spectrum of the arc consists of K-lines and OH-bands only.

The excitation temperature of the arc was measured as a function of the arc current using the relative intensity of ten Fe-lines in the spectral region between 3719·9 and 3763·5 Å.[4,5] The measurements were carried out while aspirating a 25 μg/ml Fe-solution added to an equal volume of 2*M* potassium chloride solution. The results of these measurements are shown in Fig. 2.

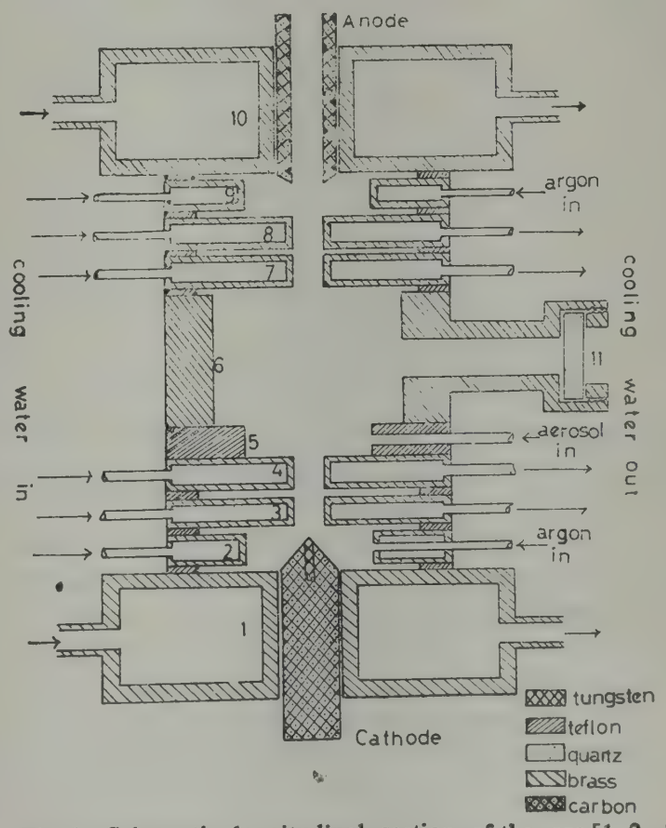

Fig. 1—Schematic longitudinal section of the arc [1, 2, 3, 4, 7, 8, 9 and 10, water-cooled brass segments, electrically insulated from one another; 5, teflon ring for introduction of aerosol; 6, analytical gap; 11 quartz window]

The electron density in the arc plasma was estimated using the relative intensity ratio of the magnesium ion-atom line pair 2795·5Å/2852·1Å.[6] The measurements were made while aspirating a 30 μg/ml Mg-solution mixed with an equal volume of 2*M*

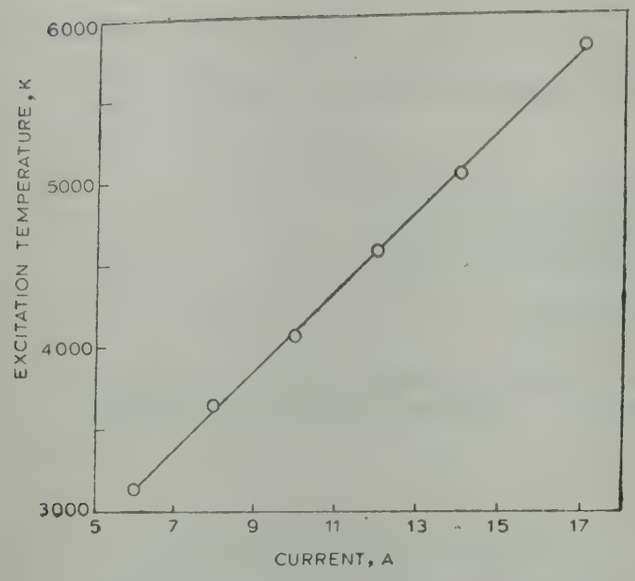

Fig. 2—Effect of arc current on excitation temperature

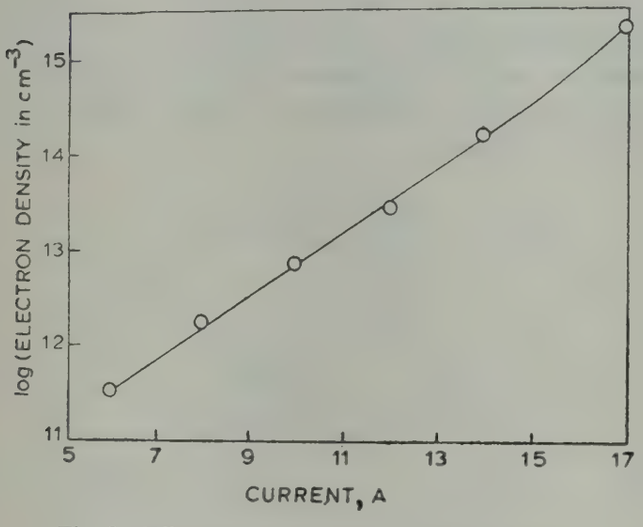

Fig. 3—Effect of arc current on electron density

potassium chloride solution. The variation of the electron density with arc current is represented in Fig. 3.

The foregoing results (Figs. 2 and 3) indicate that the excitation conditions in the arc can be varied remarkably with the arc current.

2.2 Factors Affecting the Intensities of Spectral Lines

For analytical purposes, the experimental variables of the source which affect the intensity of the analytical lines were studied. These variables are: arc current, concentration of potassium chloride and rate of introduction of aerosol into the discharge. The aim of this investigation is to get the optimal working conditions for the elements under investigation at which the working curves are to be plotted.

Effect of arc current—In this study, the concentration of potassium chloride was taken as 1*M* and the flow rate of the nebulizing gas was kept constant

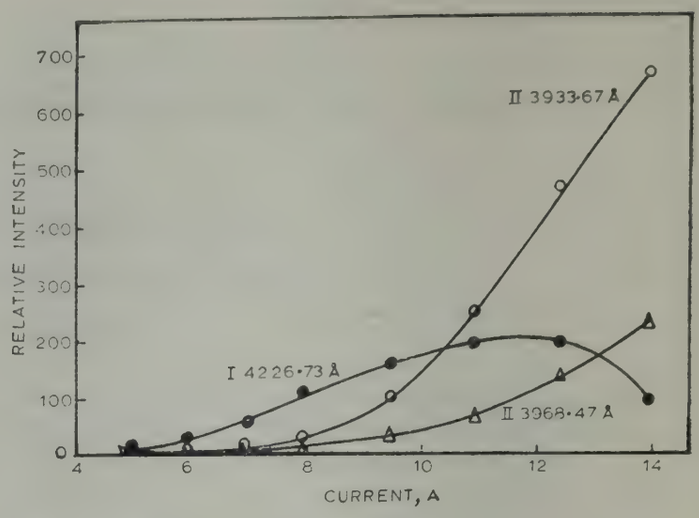

Fig. 4—Effect of arc current on intensities of Ca lines

at 8 l/min. This represents a solution uptake of 10 ml/min. The results for calcium are shown in Fig. 4. Similar results have been obtained for Mg, Mn, and Fe. It is seen that there is a remarkable difference between the behaviour of atom lines and that of ion lines. The intensity of an atom line increases with the arc current and reaches a maximum at a certain value of arc current. On the other hand, the intensity of an ion line increases first at a relatively low rate, then its rate of increase with the arc current becomes more pronounced. These observations may be explained if we take into consideration the measured increase in temperature and electron density with arc current. At a high temperature, effective ionization takes place which results in increasing the ion density. Accordingly the intensity of the ion lines increases, whereas that of the atom lines decreases.

Effect of buffer concentration—The influence of the buffer concentration on the intensity of the spectral lines of the elements under investigation was studied. Here the arc current was 10 A and the flow rate of the nebulizing gas was 8 l/min. The results are represented in Fig. 5 for calcium. For Mg, Mn, and Fe similar results have been obtained. It is seen that the maximum emission occurs at a concentration range between 0·5 *M* and 1·0 *M*. In fact, this is the concentration range at which the diffuse flame-like discharge is well established and fills the analytical gap.

Effect of aerosol flow rate—The intensities of spectral lines were measured as a function of the flow rate of the nebulizing gas (argon), at constant arc current of 10 A and a buffer concentration of 1 *M*. As before, the calcium results are shown in Fig. 6; similar results were observed for Mg, Mn, and Fe. One can see that by increasing the aerosol flow rate, the relative intensity of the spectral lines

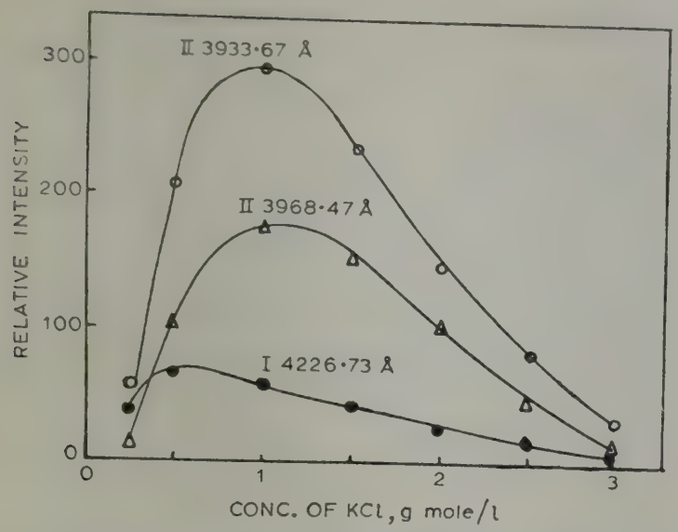

Fig. 5—Effect of buffer concentration on intensities of Ca lines

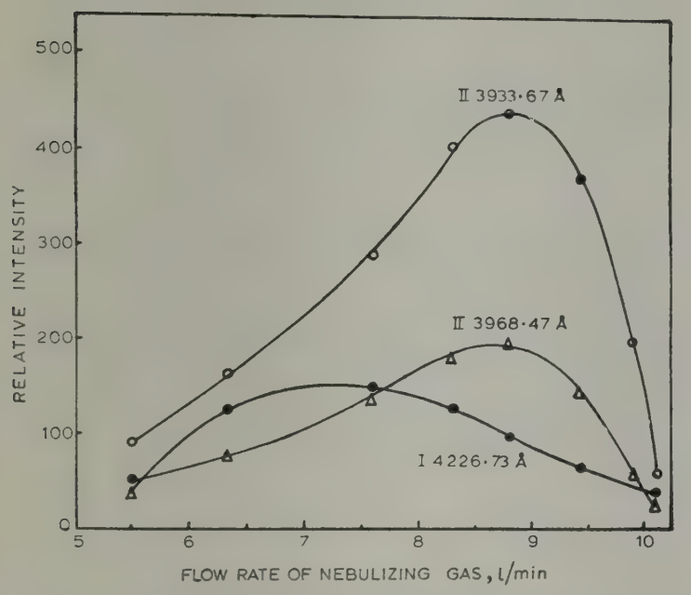

Fig. 6—Effect of flow rate of nebulizing gas on intensities of Ca lines

increases to a certain maximum after which more increase in the flow rate results in decreasing the residence time of the aerosol particles in the discharge. The latter leads to incomplete evaporation and consequently to a decrease in the intensities of the spectral lines.

It is to be mentioned here that the working conditions which give the maximum intensity of spectral lines are achieved when the diffuse flame-like discharge is well established and fills the analytical gap. Deviation from these conditions results in the appearance of the intense argon arc column with emission of argon lines and a corresponding increase of the spectral background.

2.3 Working Curves and Limits of Detection

For constructing the working curves standard, solutions of the elements with increasing concentration were prepared. The solutions were then added to equal volumes of 2*M* potassium chloride solution and sprayed into the discharge. For each element, the optimal arcing conditions, achieved in the previous section were considered. These conditions together with the spectral lines chosen for the working curves are given in Table 1. It was observed that when spraying a blank solution, prepared by dissolving spec-pure potassium chloride in bidistilled water, only faint Ca-lines are emitted (together with the K-lines and the OH-bands). The intensity of these lines had to be considered in constructing the working curve for calcium. The working curves obtained for the elements Ca, Mg, Fe and Mn are shown in Fig. 7. It is seen that the working curves are straight lines over a wide range of concentration. The limits of detection obtained for the four elements are also given in Table 1. Here the limit of detection is considered to be the concentration required to produce a spectral line intensity twice that of the background in the vicinity of the spectral line.

Table 1—Optimal Working Conditions and Limits of Detection

Element		Wavelength, Å	Arc current, A	Buffer concentration, *M*	Aerosol flow rate, l/min	Limit of detection, µg/ml
Ca	II	3933·67	10	1	8·8	0·00032
	II	3968·47	10	1	8·8	0·00160
	I	4226·73	10	0·5	7·0	—
Mg	II	2795·53	17	1	8·5	0·052
	I	2779·83	17	0·5	7·5	—
	I	2852·13	17	0·5	7·5	0 0104
Fe	I	3719·94	17	1	8·8	0·0052
	I	3737·13	17	1	8·8	0·0250
Mn	I	4030·75	17	1	8·8	0·0038
	I	4037·03	17	1	8·8	0·0038
	I	4034·49	17	1	8·8	—

3. Application of the Source for Analysis of Blood Serum

To test the application possibilities of the source, its suitability for the determination of trace elements in a sample of normal human blood serum was investigated. Trichloroacetic acid 10% was added to the serum (V/V) to precipitate the protein. After centrifugation at 3000 rpm for 10 min, the supernatant was added to an equal volume of 2*M* solution of spec-pure potassium chloride in bidistilled water. The mixture was excited at two values of arc current,

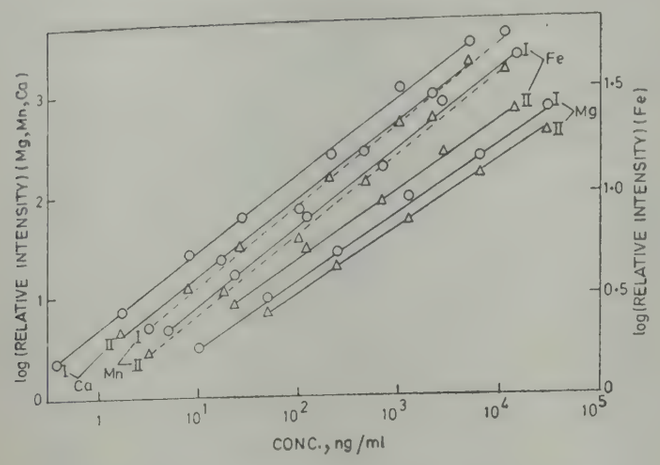

Fig. 7—Working curves for Ca, Mg, Fe and Mn

Table 2—Analysis of Blood Serum for Ca, Mg and Fe

Element	Concentration, μg/ml	
	Present work	Normal value
Ca	90·2	90-115
Mg	18·5	10-30
Fe	1·0	0·7-1·05

namely 10 and 17 A. The flow rate of the nebulizing gas was kept constant at 8·8 l/min.

At an arc current of 10 A, only lines of Ca, Fe together with those of K, Na appeared. At a value of 17 A, Mg-lines were also observed. Using the previously constructed working curves, the concentration of Ca, Fe and Mg in the sample was determined. The results are shown in Table 2 together with the normal[7] values of these elements.

4. Conclusion

From the present study one can see that the wall-stabilized arc, described in this work, can be used as an excitation source for the spectral analysis of solution samples in emission. The excitation conditions of the source can be varied widely by changing the arc current. At the optimal working conditions, the working curves are linear over a wide range of concentration and yield low detection limits. The results obtained for Ca, Mg and Fe in human blood serum indicate the capability of the source for trace analysis.

References

1. Kliska M & Marinkovic M, *Spectrochim. Acta*, **15** (1970), 138.
2. Murdik D A & Piepmier E M, *Anal. Chem.*, 46 (1974), 678.
3. Rippetoe W E, Johnson E R & Vickers T J. *Anal. Chem.*, 47 (1975), 431.
4. ASTM methods for emission analysis, 4th Edn, 1964.
5. De Galan L & Winefordner, *J. quant. Spectrosc. radiat. Transfer*, 7 (1967), 703.
6. Boumans P W J M, *Theory of spectrochemical excitation* (Hilger and Watts, London), 1966, 171.
7. Oser R L, *Hawk's physiological chemistry* (Tata McGraw-Hill, Bombay), 14th Edn, 1965.

Communications

Excess Thermodynamic Properties & Interactions in Benzene + Tetrahydrofuran & Methyl Ethyl Ketone + Butanol Solutions

(Miss) V Tiwari & J D Pandey

Department of Chemistry, University of Allahabad
Allahabad 211 002

Received 13 *June* 1979

Ultrasonic velocity and density of liquid mixtures of benzene + tetrahydrofuran and methyl ethyl ketone + butanol have been measured at 25° and 30°C and for the entire range of composition. The presence of interaction has been studied in the light of excess volume, excess adiabatic compressibility, excess free-length and excess available volume.

Ultrasonic velocity performs an important role[1-10] in the investigation of intermolecular interactions in binary liquid mixtures. When negative excess functions are observed experimentally, more often complex formation is suspected. This suggests the occurrence of discrete groups of molecules arranged into specific geometric structures. Therefore, these structural arrangements are influenced not only by the shape of molecules, but also by their mutual interaction. The ultrasonic velocity and adiabatic compressibility can be measured with great accuracy and consequently provide a powerful means for the prediction of intermolecular interactions and deviation from ideality in binary liquid mixtures. A number of attempts[11-13] have been made to study complex formation, using ultrasonic methods. Valuable studies have also been performed by Fort and Moore,[3] Mikhailov,[14] Nomoto,[15] Bhimsenachar *et al.*,[7] Seshadri *et al.*[16] Naidu and Krishnan,[17] Prakash *et al.*,[18] Piotrowska[19] and Mishra and Pandey[20] to evaluate ultrasonic velocity, adiabatic compressibility, free-volume, free-length and other acoustical parameters. Recently, Desnoyers and coworkers[21,22] made precise measurements on some thermodynamic properties and with the help of these properties, studied the interactions. Jain *et al.*[5] made an important advancement in this field and ultrasonic measurements have been used to relate even weak intermolecular interactions with excess thermodynamic and acoustical parameters. In the present work, a detailed study of the interaction has been made in the light of excess properties (excess volume, excess adiabatic compressibility, excess free-length and excess available volume) for the systems benzene + tetrahydrofuran and methylethyl ketone + butanol.

The compounds used were of BDH, AR grades and redistilled before use. Ultrasonic velocities were determined by using the fixed-path interferometer. The velocities measured by the interferometer had an accuracy better than ± 0·5 %.

The densities were determined using a pyknometer with an accuracy of ± 1 part in 10^5 and the adiabatic compressibility (β_s) was calculated using the relation, $\beta_s = 1/U^2\rho$.

Intermolecular free-length(L) in pure liquids and their mixtures was calculated using the Jacobson's relation.[6]

To calculate available volume, the formula suggested by Schaaffs[10] was used

$$V_a = V(1 - U/U^\infty) \qquad ...(1)$$

where U stands for ultrasonic velocity and $U_\infty = 1600$ m/sec. The advantage of this relation over the thermodynamic relation used by Kaulgud[9] is that it utilizes experimental ultrasonic velocity which can be measured with greater accuracy. The excess functions of mixtures were obtained from the following relations:

$$V^E = V_{mix} - (X_1V_1 + X_2V_2) \qquad ...(2)$$

$$\beta_s^E = (\beta_s)_{mix} - (X_1\beta_{s1} + X_2\beta_{s2}) \qquad ...(3)$$

$$L^E = L_{mix} - (X_1L_1 + X_2L_2) \qquad ...(4)$$

$$V_a^E = (V_a)_{mix} - (X_1V_{a1} + X_2V_{a2}) \qquad ...(5)$$

where the indices 1 and 2 stand for the components 1 and 2 respectively.

The variations of ultrasonic velocity and adiabatic compressibility of benzene + tetrahydrofuran and methyl ethyl ketone + butanol mixtures with composition, are shown in Fig. 1. Here X_1 represents the weight fraction of the first component of the liquid mixtures. An inspection of Fig. 1 shows that the ultrasonic velocity and compressibility curves show a nonlinear variation with the composition. Both the mixtures studied show a maximum velocity and a minimum compressibility around the same region of concentration. In this region, observations were made at a closer variation of concentration,

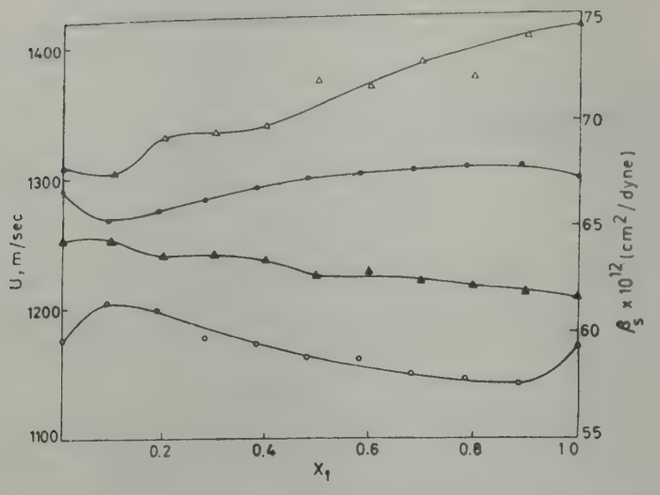

Fig. 1—Sound velocity (U) and adiabatic compressibility (β_s) versus mole fraction (x_1) curves for the systems: (1) benzene-tetrahydrofuran (25°C), ● sound velocity and ○ adiabatic compressibility; (2) methyl ethyl ketone-butanol (30°C), ▲ bound velocity and △ adiabatic compressibility

with a view to locating the positions of maxima and minima of the velocity and compressibility curves more accurately. In the mixture methyl ethyl ketone + butanol, the curves become linear at higher concentrations of component one. This shows that a small amount of component one is more effective to create intermolecular interaction than a large one. The systems under present investigation can be grouped into two categories : (a) nonpolar-nonpolar; and (b) weakly polar-weakly polar.

The system benzene-tetrahydrofuran belongs to category (a). The excess molar volume, excess compressibility, excess free-length and excess available volume for the experimental liquid mixtures were obtained from relations (2)-(5) and are listed in Table 1. An inspection of Table 1 reveals that positive as well as negative values of excess functions are observed. The magnitude of the excess functions varies with composition of the mixture showing minimum at higher benzene concentrations. Moreover, a perusal of Table 1 shows that the compressibility of the mixture at higher benzene concentration is lower than that of the average of its components considered separately. This confirms the presence of specific interaction which leads to the formation of a transient complex between the pairs of component molecules. Probably donor-acceptor interaction is present in this system due to presence of a lone pair of electrons on the oxygen atom in tetrahydrofuran. The system methyl ethyl ketone-butanol belongs to the category (b). The values of excess volume are all negative at all compositions whereas the rest of the excess functions show negative as well as positive values. This definitely indicates the presence of weak intermolecular interaction in the system. Probably weak hydrogen bond interactions are present which are more dominant in the higher concentration region of butanol in the mixture.

Table 1—Excess Acoustical & Thermodynamic Parameters Obtained from Liquids & Liquid Mixtures as a Function of Temperature & Composition

X_1	V^E	β_s^E	L^E	V_a^E
	Benzene-tetrahydrofuran (Temp.=25°C)			
0·0000	0·00	0·00	0·0000	0·00
0·0929	−0·63	−1·68	0·0082	0·93
0·1872	−0·33	1·45	0·0070	0·77
0·2831	−0·86	0·23	0·0018	0·29
0·3805	−0·38	−0·11	0·0001	0·03
0·4795	−0·47	−0·76	−0·0029	−0·28
0·5802	−0·26	−0·75	−0·0033	−0·32
0·6826	−0·93	−1·49	−0·0067	−0·57
0·7866	−1·10	−1·71	−0·0801	−0·66
0·8924	−1·24	−1·91	−0·0092	−0·74
1·0000	0·00	0.00	0·0000	0·00
	Methyl ethyl ketone-butanol (Temp. = 30°C)			
0·0000	0·00	0·00	0·0000	0·00
0·1012	−0·51	−0·01	0·0035	0·34
0·2021	−0·43	−0·02	0·0003	0·09
0·3028	−0·45	−0·59	−0·0018	−0·14
0·4032	−0·46	−0·74	−0·0023	−0·20
0·5034	−0·07	0·59	−0·0026	0·31
0·6033	−0·08	−0·34	−0·0008	−0·08
0·7028	−0·04	0·15	0·0424	0·11
0·8012	−0·51	0·04	0·0005	0·06
0·9012	−0·03	0·06	0·0005	0·05
1·0000	0·00	0·00	0·0000	0·00

The fact that the excess compressibilities of both the systems are negative, indicates that the difference between the ideal and the observed behaviour may be attributed to the existence of an increased correlation of molecular sites in these mixtures. The excess functions studied above do not predict exactly the nature of intermolecular interaction present in the system. They only give a qualitative but valuable idea of interactions present.

The financial support by CSIR, New Delhi, is gratefully acknowledged by one of the authors (VT).

References

1. Eyring H & Hirschfelder J O, *J. phys. Chem.*, **41** (1937), 249.
2. Rowlinson J S, *Liquids and liquid mixtures* (Butterworths, London), 1969.
3. Fort R J & Moore W R, *Trans. Faraday Soc.*, **61** (1965), 2102.
4. Zandler M E & Jhon M S, *Ann. Rev. Phys. Chem.*, **17** (1966), 387.
5. Jain D V S, Alstair M & Pethrick R A, *Trans. Faraday Soc.*, **70** (1974), 1292.
6. Jacobson B, *Acta chem. scand.*, **6** (1952), 1485.
7. Bhimsenachar J, Subrahmanyam S V & Reddy K C, *Trans. Faraday Soc.*, **58** (1962), 2352.
8. Tuomikoski P & Nurmi V, *Comment Phys. Math. Helsing.*, **10** (1940), 11.
9. Kaulgud M V, *Acustica*, **10** (1960), 316.
10. Schaffs W, *Acustica*, **33** (1975), 272.
11. Larionov N I, *Zh. Fiz. Khim.*, **27** (1953), 1050.
12. Sette D, *Ric. Sci.*, **25** (1955), 576.
13. Piercy J E & Lamb J, *Trans. Faraday Soc.*, **52** (1956), 930.
14. Mikhailov I G, *Dokl. Akad. Nauk SSSR*, **81** (1951), 779.
15. Nomoto O, *J. phys. Soc. Japan*, **3** (1958), 1528.
16. Seshadri K, Prabhakara Rao N & Reddy K C, *Z. phys. Chem. (Neue Folge)*, **89** (1974), 108.
17. Naidu P R & Krishnan V R, *J. phys. Soc. Japan*, **20** (1965), 1554.
18. Prakash S, Prasad N, Singh R & Prakash O, *Acustica*, **34** (1975), 121.
19. Piotrowska A, *Rocz. Chemii*, **39** (1965), 437.
20. Mishra R L & Pandey J D, *Acustica*, **40** (1978), 335.
21. Avedikian L, Perron G & Desnoyers J E, *J. Solution Chem.*, **4** (1975), 331.
22. Visser C D, Perron G & Desnoyers J E, *J. Can. Chim.*, **55** (1977), 856.

Notes

Flexibility of M—X Bond of Some Tetrahalides of Fourth Group Metals by Compliance Scheme

S L Gupta & R C Saxena

Molecular Spectroscopy Research Group, Physics Department
M M Postgraduate College, Modinagar 201 204
&
V K Rastogi

Physics Department, L R College, Sahibabad (Ghaziabad)
&
A N Pandey

Molecular Spectroscopy Research Laboratory
Physics Department, Meerut College, Meerut 250 001

Received 18 *December* 1978

An attempt has been made to evaluate the compliance constants of some tetrahalides of IV group metals by L matrix approximation method. The L-F approximation is used where the L matrix approximation is not suited. In order to arrive at a more reliable set of values, linear equation method has also been applied to those molecules for which sufficient experimental data are available. The flexibility of the chemical bonds is briefly discussed.

A number of studies made recently, have revealed the possible ambiguities in the unique determination of the force field of polyatomic molecules by the compliance scheme first introduced by Decius.[1] Hoy *et al.*[2] have stated the anomalies in the use of at least one quadratic equation in solving the eigenvalue problem and clearly mentioned that the force field may not be uniquely defined even if the data are more than the number of force constants to be determined. Therefore, the use of required number of linear equations and not the number of available parameters, guarantees unique determination of the force field. The compliance scheme has certain advantages over force constants, because firstly the compliance constants are more meaningful as they are directly connected to certain experimentally observable quantities such as mean square amplitudes of vibration, Coriolis coupling constants and the centrifugal distortion constants, and secondly these constants for a given coordinate or a pair of coordinates are uniquely defined and do not depend on the coordinate system used to describe the molecular configuration. Thus the compliance scheme is less ambiguous or more unique. Clark *et al.*[3,4] have reported the reliable vibrational frequencies of spherical top molecules MX_4 (M = Group IV element, X = F, Cl, Br or I) employing Raman technique. Therefore, in order to understand the force field for these molecules by compliance scheme and flexibility of the bonds, we have undertaken the present study.

Method of computation—The MX_4 molecules considered here belong to T_d point group. The A and E species belong to one-dimensional symmetry and hence the compliance constants C_{11} and C_{22} are unambiguously determined. To determine the compliance elements of F_2 species, approximate methods are used. In cases where the frequencies in the F_2 species are well separated, Müller's L matrix approximation method has been used, and in other cases the L-F approximation method[5] is applied. The compliance matrix elements obtained by these methods are reported in Table 1. In order to consider the more reliable values of the compliance constants of F_2 species, we require three equations. One equation is obtained from frequencies, which is of the form

$$G_{33}^{-1} C_{33} + 2 G_{34}^{-1} C_{34} + G_{44}^{-1} C_{44} = \phi_3 + \phi_4 \quad \ldots(1)$$

The vibrational frequencies are taken from Ref. 3. For some molecules, the Coriolis coupling constants[4] for F_2 species have been experimentally observed. The derived linear equation connecting the compliance constants and Coriolis constants is as follows :

$$-\frac{4}{3}\frac{m_X^2}{M} C_{33} + \left(\frac{m_M m_X}{M} + \frac{4 m_X^2}{3 M}\right) C_{34} + \left(\frac{m_M m_X}{4 M} - \frac{4}{3}\frac{m_X^2}{M}\right) C_{44} = \phi_3 \zeta_{33} + \phi_4 \zeta_{44} \quad \ldots(2)$$

The third linear equation is constructed with the help of mean amplitudes of vibration[6-11] for the M—X bond. The equation in usual notation is expressed as

$$\frac{4}{kT}\left\langle U_{M-X} \right\rangle^2 = C_{11} + 3 C_{33} + \left(\frac{h}{4\pi kT}\right)^2 \left(\frac{G_{11}}{4} + \frac{3 G_{33}}{4}\right) \quad \ldots(3)$$

Table 1—Compliance Matrix Elements of MX_4 Molecules (Å/mdyne)

Molecule	Method	C_{11}	C_{22}	C_{33}	C_{44}	C_{34}
CF_4	(b)	0·1083	1·4197	0·1703	1·2719	0·1956
	(c)	0·1083	1·4197	0·1863	1·0720	0·1417
SiF_4	(a)	0·1394	3·8427	0·1603	2·4495	0·1520
GeF_4	(a)	0·1655	6·5154	0·1884	3·6874	0·0974
CCl_4	(b)	0·2263	3·1304	0·3806	3·2013	0·5158
	(c)	0·2263	3·1304	0·3835	2·3564	0·2542
$SiCl_4$	(b)	0·2674	6·8125	0·3386	4·8827	0·3858
	(c)	0·2674	6·8125	0·3518	5·0915	0·3055
$GeCl_4$	(a)	0·3039	9·1927	0·3751	6·0909	0·2958
	(c)	0·3039	9·1927	0·4788	5·8626	0·3346
$SnCl_4$	(a)	0·3514	15·8490	0·4018	9·5806	0·2288
	(c)	0·3514	15·8490	0·4527	10·1033	0·8066
$TiCl_4$	(a)	0·3164	11·0525	0·3835	10·6975	0·3809
	(c)	0·3164	11·0525	0·3202	12·6846	0·6854
$ZrCl_4$	(a)	0·3369	14·9555	0·4160	12·8088	0·2839
$HfCl_4$	(a)	0·3281	13·9403	0·3981	10·9004	0·1667
$SiBr_4$	(b)	0·3490	8·8605	0·4178	7·0078	0·6030
$GeBr_4$	(b)	0·3824	11·4178	0·4759	8·1029	0·5215
	(c)	0·3824	11·4178	0·5129	8·0539	0·6594
$SnBr_4$	(a)	0·4306	18·0577	0·4997	11·6487	0·4728
	(c)	0·4306	18·0577	0·5019	13·2666	0·8764
$TiBr_4$	(b)	0·3964	13·5825	0·4435	13·8161	0·5820
$ZrBr_4$	(a)	0·4177	17·7001	0·4641	17·5576	0·5000
$HfBr_4$	(a)	0·3830	16·0573	0·4551	14·9850	0·3403
SiI_4	(b)	0·4859	12·1793	0·5764	10·6187	0·9055
GeI_4	(b)	0·5496	15·0669	0·6663	14·2471	1·7518
SnI_4	(b)	0·6131	22·4288	0·7364	15·5362	0·8128
ZrI_4	(b)	0·5358	21·7080	0·5919	21·2554	0·7366
HfI_4	(a)	0·5358	13·2659	0·5193	13·8110	0·5054

(a) *L*-approximation method; (b) *L-F* approximation method; (c) Linear equation method

The compliance constants so obtained are also included in Table 1 for comparison.

The symmetrized compliance constants are related to the bond stretching compliance constant C_r and bond-bond interaction compliance constant C_{rr}. The values of C_r and C_{rr} obtained by the two methods are reported in Table 2. The flexibility is directly related to the bond stretching compliance constant.

Discussion of results—From Table 1, it is observed that the compliance constants evaluated by the two methods are in close agreement in the case of most of the molecules except the off-diagonal element. From Table 2, it is noticed that the bond stretching compliance constant (C_r) has values in the range 0·1 to 1 Å/mdyne. It is also observed that the bond-bond interaction constant C_{rr} is very small and negative (except for HfI_4). Another important conclusion that we can draw from Table 2 is that the heavier the end atoms, the greater is the stretching compliance constant for the respective bonds, i.e. M—I > M—Br > M—Cl > M—F. As the bond stretching compliance constant is a measure of flexibility of a bond, the flexibility of the M—X bond increases from fluoride to iodide. This view is supported by the fact that the stability of the chemical bond of tetrahalides of IV group metals decreases[12] in the order M—F > M—Cl > M—Br > M—I. As to the effects of increasing the mass of the central atom keeping the halogen constant, it is observed that the bond stretching compliance constant increases for IV-A group metals in the order C—X < Si—X < Ge—X < Sn—X and for IV-B group metals in the order Zr—X > Hf—X > Ti—X. The latter trend is also supported by the values of total coordinate bond energies for the bonds Zr—Cl (83·1 eV) and Ti—Cl (94·5 eV).[13]

Table 2—Bond Stretching and Bond-Bond Interaction Compliance Constants of MX_4 Molecules

Molecule	C_r (Å/mdyne)		C_{rr} (Å/mdyne)	
	Method (a) or (b)	Method (c)	Method (a) or (b)	Method (c)
CF_4	0·1548	0·1668	−0·0155	−0·0195
SiF_4	0·1551	—	−0·0052	—
GeF_4	0·1826	—	−0·0057	—
CCl_4	0·3420	0·3442	−0·0386	−0·0393
$SiCl_4$	0·3208	0·3307	−0·0178	−0·0211
$GeCl_4$	0·3573	0·4351	−0·0178	−0·0437
$SnCl_4$	0·3892	0·4273	−0·0126	−0·0253
$TiCl_4$	0·3667	0·3192	−0·0166	−0·0009
$ZrCl_4$	0·3962	—	−0·0198	—
$HfCl_4$	0·3806	—	−0·0172	—
$SiBr_4$	0·4006	—	−0·0172	—
$GeBr_4$	0·4525	0·4802	−0·0234	−0·0326
$SnBr_4$	0·4825	0·4841	−0·0173	−0·0172
$TiBr_4$	0·4317	—	−0·0118	—
$ZrBr_4$	0·4525	—	−0·0116	—
$HfBr_4$	0·4370	—	−0·0180	—
SiI_4	0·5538	—	−0·0226	—
GeI_4	0·6372	—	−0·0292	—
SnI_4	0·7056	—	−0·0308	—
ZrI_4	0·5779	—	−0·0140	—
HfI_4	0·5234	—	−0·0041	—

(a), (b) and (c) same as in Table 1

Two of the authors (SLG & ANP) are thankful to the University Grants Commission, New Delhi, for providing the financial assistance.

References

1. Decius J C, *J. chem Phys.*, **38** (1963), 241.
2. Hoy A R, Stone J H R & Watson J K G, *J. molec. Spectrosc.*, **42** (1972), 393.
3. Clark R J H & Rippon D M, *J. molec. Spectrosc.*, **44** (1972), 479.
4. Clark R J H & Mitchell P D, *J. molec. Spectrosc.*, **51** (1974), 458.
5. Pandey A N, Sharma D K, Verma U P *et al.*, *Indian J. pure appl. Phys.*, **14** (1976), 815.
6. Cyvin S J, *Molecular vibrations and mean square amplitudes* (Universitetforlaget, Oslo), 1968.
7. Morino Y, Nakamura Y & Iijima T, *J. chem. Phys.*, **32** (1960), 643.
8. Morino Y & Murata Y, *Bull. chem. Soc. Japan*, **38** (1965), 104.
9. Fujii H & Kimura M, *Bull. chem. Soc. Japan*, **43** (1970), 1933.
10. Herranz J, Morcillo J & Gomez A, *J. molec. Spectrosc.*, **19** (1966), 266.
11. Shimanouchi T, Nakagawa I, Hiraishi J & Ishii M, *J. molec. Spectrosc.*, **19** (1966), 78.
12. Sutton L E, (Ed.), *Tables of interatomic distances and configuration in molecules and ions*, Special Pub. No 18, (The Chemical Society, London), 1965.
13. Jenkins H D B, private communication.

Thermal Expansion of V_3Si at Elevated Temperatures

B K Rao & D B Sirdeshmukh

Physics Department, Kakatiya University, Warangal 506 009

Received 2 *July* 1979

The linear coefficient of thermal expansion of V_3Si has been determined with the help of a differential push-rod dilatometer. At room temperature, the linear coefficient of thermal expansion (α in units of $10^{-6}/°C$) is 8·54 and over the range 20-300°C, it follows the equation $\alpha = 8{\cdot}15 + 1{\cdot}98 \times 10^{-2} t - 0{\cdot}23 \times 10^{-4} t^2$ where t is the temperature in °C. The Grüneisen constant calculated from thermal expansion data at room temperature is 1·46.

The intermetallic compound V_3Si crystallizes in the A-15 or β-tungsten structure. It is cubic at ordinary temperatures but undergoes a transformation at low temperatures to a tetragonal structure. There is great interest in the substance because it is a superconductor with a high superconducting transition temperature.

Fawcett[1] and Testardi[2] measured the thermal expansion of V_3Si at low temperatures. Measurement of thermal expansion at elevated temperatures does not seem to have been made so far.

The thermal expansion of V_3Si has been determined in this laboratory over the range 20-300°C using a differential push-rod dilatometer.[3] A single crystal of V_3Si about 6 mm long was used together with a copper standard supplied by the US National Bureau of Standards. Values of the linear coefficient of thermal expansion at different temperatures are presented in Table 1. These values are accurate to about 5%. The temperature variation is non-linear. By a least squares treatment, the values are found to follow the equation:

$$\alpha = 8{\cdot}15 + 1{\cdot}98 \times 10^{-2} t - 0{\cdot}234 \times 10^{-4} t^2 \quad \ldots(1)$$

where t is the temperature in °C and α is the linear coefficient of thermal expansion in units of $10^{-6}/°C$. The values calculated from Eq. (1) are also presented in Table 1.

Table 1—Values of the Linear Coefficient of Thermal Expansion

t °C	α, $10^{-6}/°C$	
	Exptl	Calc. from Eq. (1)
20	—	8·54
60	9·30	9·19
100	10·00	9·90
140	10·40	10·47
180	11·00	10·96
220	11·40	11·38
260	11·70	11·72
300	11·90	11·99

Testardi[2] fitted his data to the equation $\alpha = 4{\cdot}2 \log (T/50)$. From this equation, we obtain a value of 7·53 for α at room temperature. The value of α at room temperature obtained in the present work is 8·54.

The Grüneisen constant has been calculated from the thermal expansion value at room temperature. For this purpose, the compressibility was calculated from the elastic constants reported by Garcia and Barsch[4] and the specific heat was estimated from the Debye temperature from the same source. The value of the Grüneisen constant is 1·45. This is higher than the value 1·08 obtained by Garcia and Barsch from the pressure variation of elastic constants.

Thanks are due to Dr R K Kirby of the US National Bureau of Standards for the gift of the copper standard and to Dr L R Testardi of Bell Laboratories for the gift of the V_3Si sample.

References

1. Fawcett E, *Phys. Rev. Lett.*, 26 (1971), 829.
2. Testardi L R, *Phys. Rev.*, B5 (1972), 4342.
3. Sirdeshmukh D B & Rao B K, *Proc. Am. phys. Soc.*, **17** (1973), 56.
4. Garcia P F & Barsch G R, *Phys. Status Solidi* (*b*), **59** (1973), 595.

Evaluation of Grüneisen Constant of KCl-KBr Mixed System

BRINDA SUBRAMANIAM

School of Studies in Physics, Jiwaji University
Gwalior 474 002

Received 6 *December* 1978; *revised received* 4 *August* 1979

Grüneisen constant γ has been calculated for a KCl-KBr mixed system for the first time by plotting log θ vs log V, where θ is the Debye temperature and V the molar volume. The average value of γ for the system has been found to be 1·9, indicating more anharmonicity of the mixed system than that of the pure alkali halide crystals.

Grüneisen parameter is a dimensionless parameter, showing the effects of anharmonicity. The amplitude of thermal vibrations of atoms or molecules of which a solid is composed, increases with increasing temperature, giving rise to the phenomenon of thermal expansion on account of the anharmonicity of these vibrations. As little is known about the specific values of anharmonic terms, Grüneisen constant is studied within a quasiharmonic approximation. It neglects anharmonic terms but instead it assumes the ionic vibrational frequency to be volume dependent, thus accounting at least in part for the anharmonic effects. The measure of the volume dependence of frequency of vibration is defined as Grüneisen constant, γ, expressed by

$$\gamma = -d(\log \nu)/d(\log V) \qquad ...(1)$$

where ν is the frequency and V the molar volume.

Attempts[1-5] have been made to evaluate γ from the equation of state for solids but the agreement between the experimentally determined and calculated values is not satisfactory. An independent method to evaluate average γ value for a group of metals or alloys or compounds having the same crystal structure and bond type has been suggested by Bansigir.[6]

In this note, an attempt has been made to evaluate the average value of γ for a KCl-KBr mixed system using the method suggested by Bansigir.[6]

The Grüneisen constant is usually defined by the relation.[7]

$$\gamma = -d(\log \theta)/d(\log V) \qquad ...(1A)$$

which readily leads to the equation

$$\log \theta = -\gamma \log V + C \qquad ...(2)$$

where θ is the Debye temperature and C the constant of integration. Eq. (2) is valid for a given substance for which γ is a constant.

Table 1—Debye Temperature (θ) and Molar Volume (V) for Different Compositions of KCl-KBr at 300 K

Sample*	θ, K	V, cm^3
26% KBr	206·96	28·2628
49% KBr	192·72	39·6242
61% KBr	186·07	40·3469
75·5% KBr	178·99	41·2450

*Column 1 indicates the molar percentage of KBr in KCl solid solution.

The log θ vs log V plot is linear for a group of substances having the same structure and bond type. The Debye temperatures for the compositions have been calculated from known values of elastic constants[8] using the expression,

$$\theta = (h/k)\,(9/4\pi)^{1/3}\,(2N/M)^{1/2}\,(Va)^{1/6}\,[G(B+4G/3)]^{1/3}\,\{1/[G^{3/2}+2(B+4G/3)^{3/2}]\}^{1/3} \qquad ...(3)$$

$$\text{where } G = (G_V G_R)^{1/2} \qquad ...(4)$$

$$G_V = (C_{11} - C_{12} + 3C_{44})/5 \qquad ...(5)$$

$$G_R = [5C_{44}\,(C_{11} - C_{12})]/[3\,(C_{11} - C_{12}) + 4C_{44}] \qquad ...(6)$$

The terms in Eqs. (3)-(6) have their usual significance. The shear modulus G is obtained by using Hill's geometric mean method.[9] Molar volumes for different compositions have been calculated using X-ray diffraction data of Sengar (Sengar D S, private communication, 1978). The calculated values of θ and V are given in Table 1. A straight line graph is obtained when log θ is plotted against log V for the four compositions, giving an average value of γ equal to 1·9.

For all the sixteen alkali halides having fcc structure and ionic bonding, the average value of γ was found to be 1·67 (Ref. 6). The KCl-KBr mixed system having the same structure and bond type has an average value of γ (=1·9) greater than that for other halides. This shows that the dependence of ionic vibrational frequency on volume increases in the mixed systems, although they are having the same structure and bond type.

The Grüneisen parameter being a measure of the anharmonicity, the above result indicates that the mixed alkali halide crystals are more anharmonic in nature than the pure alkali halide crystals.

The author is deeply grateful to Prof. K G Bansigir for valuable discussions. She also wishes to thank Shri D S Sengar for permission to use his X-ray diffraction data prior to publication. She also acknowledges with thanks the grant of a research fellowship by the CSIR, New Delhi.

References

1. Slater J C, *Introduction to chemical physics* (McGraw-Hill, New York), 1939, 390.
2. Dugdale J S & MacDonald D K C, *Phys. Rev.*, **88** (1953), 832.
3. Druyvesteyn M I & Meyering L, *Physica*, 8 (1941), 851.
4. Gilvarry J J, *Phys. Rev.*, **102** (1956), 308, 317, 325, 331.
5. Kachhava C M & Saxena S C, *J. chem. Phys.*, **44** (1966), 986.
6. Bansigir K G, *J. appl. Phys.*, 39 (1968), 4024.
7. Kittel C, *Introduction to solid state physics* (John Wiley, New York), 1956, 154.
8. Sharko A V & Botaki A A, *Soviet J. Phys.*, **14** (1971), 1710.
9. Hill R, *Proc. phys. Soc.*, A65 (1952), 349.

Prediction of Dipole Moments of Polar Molecules from the Relation between τ_{Solute} & $\eta_{Solvent}$

SHEKHAR KUMAR DATTA*

Department of Physics, University College, Raiganj 733 134
Dist. West Dinajpur

Received 30 *December* 1978

A linear relationship has been found to exist between the relaxation times of six polar solutes at microwave frequencies (λ=3·17 cm) and viscosity of the nonpolar solvent (benzene) at different temperatures. Using the data, the dipole moments of three polar molecules, viz. *p*-phenitidine, 3-nitro-*o*-anisidine and 2-chloro-*p*-nitroaniline have been predicted for the first time.

In a recent paper,[1] the values of relaxation times (τ) of some polar solutes dissolved in a nonpolar solvent (benzene) at microwave frequencies and at different temperatures have been reported. In this note, it is shown that within a considerable range of viscosity (η), the relationship between τ and η is governed by the following formula propounded by Krishnaji and Mansingh[2]

$$\tau = \frac{B}{T}\ \eta^x \qquad \ldots(1)$$

where B is a constant for a given substance, T the temperature, and $x=\Delta H_\tau/\Delta H_\eta$ (ΔH_τ and ΔH_η being the heats of activation for the dielectric relaxation and viscosity processes).

Eq. (1). suggests that a plot of log (τT) versus log η should give a straight line.

Using the reported values of relaxation times of six polar substances at microwave frequencies (λ=3·17 cm) and the literature values of the viscosity of the solvent at different temperatures, the linearity has been found to hold approximately.

The values of x and B for the six substances are given in Table 1. It is seen that in all the cases $x<1$, which is actually the case. The constant value of ΔH_η has been evaluated using the literature values of η at different temperatures and using this value of ΔH_η, the value of ΔH_τ has been calculated for each substance.

Table 1—Computed Values of Heats of Activation and Dipole Moments

(For benzene, ΔH_η=2500 cal)

Sample	$B\times10^8$	x	ΔH_τ, cal.	μ, D
p-Anisidine	2·0198045	0·5667653	1416·9	1·87 (L)
o-Nitroaniline	0·8438317	0·2217672	554·4	4·25 (L)
3, 6-Dichloro-aniline	2·7974023	0·4049282	1012·3	1·68 (L)
p-Phenitidine	0·7667318	0·1694877	423·7	1·53 (P)
3-Nitro-*o*-anisidine	15·359019	0·7303554	1825·9	2·24 (P)
2-Chlro-*p*-nitroaniline	1·3679724	0·2944125	736·0	3·96 (P)

L, literature; P, predicted value.

It is evident that B depends upon the molecular structure, such as molecular diameter. Assuming that the parameter x is a function of the dipole moment μ of the molecule, the following empirical relation between x and μ has been found to exist:

$$x = -1{\cdot}3874502 + \frac{9{\cdot}3415099}{\mu} - \frac{10{\cdot}6349280}{\mu^2} \qquad \ldots(2)$$

where μ is in debyes.

Using Eq. (2), the dipole moments of the three substances *p*-phenitidine, 3-nitro-*o*-anisidine and 2-chloro-*p*-nitroaniline, have been predicted for the first time.

The author is grateful to all senior teachers in the Department of Physics for valuable discussions.

References

1. Somevanshi S K S, Misra S B L & Mehrotra N K, *Indian J. pure appl. Phys.*, 16 (1978), 57.
2. Krishnaji & Mansingh A, *Indian J. pure appl. Phys.*, **2** (1964), 176.

Diffraction Intensities from a Cluster of Curved Crystallites with Layer Shift

A K DE, B K RAY & S BHATTACHERJEE

Department of Physics, Indian Institute of Technology
Kharagpur 721 302

Received 7 *September* 1978; *revised received* 8 *June* 1979

Theoretical expressions for intensity of X-rays diffracted by an aggregate of cylindrically curved crystallites with stacking fault, have been derived. The model and the mathematical

*Present address: Department of Physics, Uluberia College, P.O. Uluberia, Dist. Howrah (West Bengal)

treatment are very much similar to that of G B Mitra and S Bhattacherjee [*Acta crystallogr.*, A27 (1971), 22]. The lattice disorder consists of a layer shift by an angular distance $\phi/3$. Results of numerical computations have been discussed and compared with those of layer shift by $\phi/2$ and ordered lattices.

In a recent publication,[1] the present authors derived an expression for the diffracted intensities of X-rays from an aggregate of cylindrically curved crystallites with different types of stacking faults. One of the faults considered consists of a cylindrical layer displaced parallel to itself about the common axis by an angular distance $\phi/2$ with respect to its adjacent layer. The starting model and mathematical treatment were based primarily on the work of Mitra and Bhattacherjee.[2] Following a similar approach, the intensity of X-rays diffracted by a conglomeration of disordered cylindrical crystallites with layer shift of the above type by an amount $\phi/3$ has been worked out. The model and symbols used in the present calculations are exactly the same as defined by the above authors.[1,2]

Let the disordered cylindrical fragment consist of three different types of layers A, B and C. The crystallite starts with A which is taken as the reference layer. B and C are shifted layers displaced by $\frac{1}{3}\phi$ and $\frac{2}{3}\phi$ respectively with respect to reference layer (Fig. 1). Let α_s denote the probability of a mistake occurring to each added layer such that the sequence changes from AAA.....to BBB or CCC.....as described by Wilson.[3] Assuming α_s to be the same for both the mistakes and following Wilson,[3] it may be written as

$$A_m + B_m + C_m = 1 \qquad \ldots(1)$$

where A_m, B_m and C_m are the probabilities of the mth layer being A, B or C respectively as defined by Wilson.[3]

Now, considering exactly the same model of disordered cylindrical lattice and applying similar arguments as that of Ray *et al.*,[1] the average angular position of any lattice point (r, m, t) is given by

$$(r + B_m)\,\phi \qquad (\text{since } B_m = C_m)$$

Other symbols used have the same meaning as defined by Mitra and Bhattacherjee.[2] In the present model, only the azimuthal coordinate $r\phi$ is to be replaced by $(r + B_m)\,\phi$ for intensity calculation. Introducing this modification and proceeding exactly in the same manner as in the previous case, the intensity $I(hkl_0)$ can be shown to be given by

$$I(h\,k\,l_0) = T^2 N \sum_{m=0}^{M-1}\sum_{n=0}^{M-1} J_0 \left\{ x_m^2 + y_n^2 - 2\,x_m\,y_n \right.$$

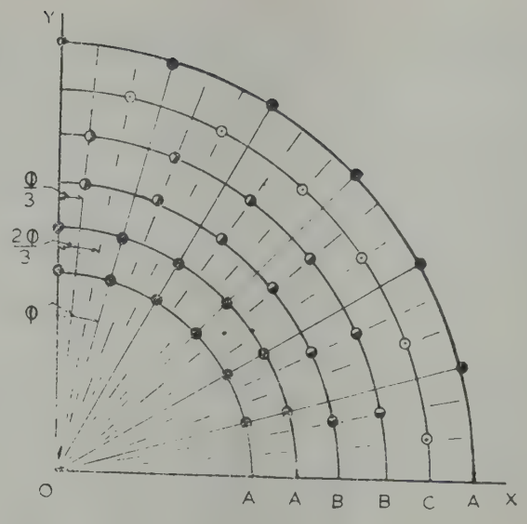

Fig. 1—Models of cylindrical lattice with stacking faults [A is a normal layer; B and C layers are shifted by $\phi/3$ and $2\phi/3$ respectively from their normal position.]

$$\left. \times \cos(B_m - B_n)\,\phi \right\}^{1/2} + T^2 \sum_{m=0}^{M-1}\sum_{n=0}^{M-1}\sum_{q=0}^{N-1} (N-q)$$

$$\times \left[J_0 \left\{ x_m^2 + y_n^2 - 2\,x_m\,y_n \cos(q + B_m - B_n)\,\phi \right\}^{1/2} \right.$$

$$+ J_0 \left\{ x_m^2 + y_n^2 - 2\,x_m \cdot y_n \cos \right.$$

$$\left. \left. (q - B_m + B_n)\,\phi \right\}^{1/2} \right] \qquad \ldots(2)$$

with

$$x_m = QN(h + mk\phi)\sqrt{1-(l_0/l)^2}$$

$$y_n = QN(h + nk\phi)\sqrt{1-(l_0/l)^2}$$

$$Q = \frac{2\pi}{N\phi};\ h = (2a\sin\theta)/\lambda$$

$$k = (2b\sin\theta)/\lambda$$

$$l\cos\gamma = l_0 \text{ (integer)};\ l = \frac{s \cdot c}{\lambda}$$

γ is the angle between the vector $\mathbf{S}$ ($|\mathbf{S}| = 2\sin\theta$) and the z-axis of the coordinate system (please refer to Fig. 2b of the paper by Mitra and Bhattacherjee[2]). Introducing $r_1 = c/a$ and $r_2 = b/a$, the above intensity expression can be written in a more simplified form as

$$I(h\,l_0) = T^2 N \sum_{m=0}^{M-1}\sum_{n=0}^{M-1} J_0 \left(\psi \left\{ u_m^2 + v_n^2 \right.\right.$$

$$\left. \left. - 2\,u_m.v_n \cos(B_m - B_n)\,\phi \right\}^{1/2} \right) + T^2 \sum_{m=0}^{M-1}\sum_{n=0}^{M-1}\sum_{q=1}^{N-1}$$

$$\times (N-q) \left[J_0 \left(\psi \left\{ u_m^2 + v_n^2 - 2\,u_m.v_n \right.\right.\right.$$

$$\left. \left. \times \cos(q + B_m - B_n)\,\phi \right\}^{1/2} \right) + J_0 \left(\psi \left\{ u_m^2 + v_n^2 \right.\right.$$

$$\left. \left. \left. - 2\,u_m\,v_n \cos(q - B_m + B_n)\,\phi \right\}^{1/2} \right) \right] \qquad \ldots(3)$$

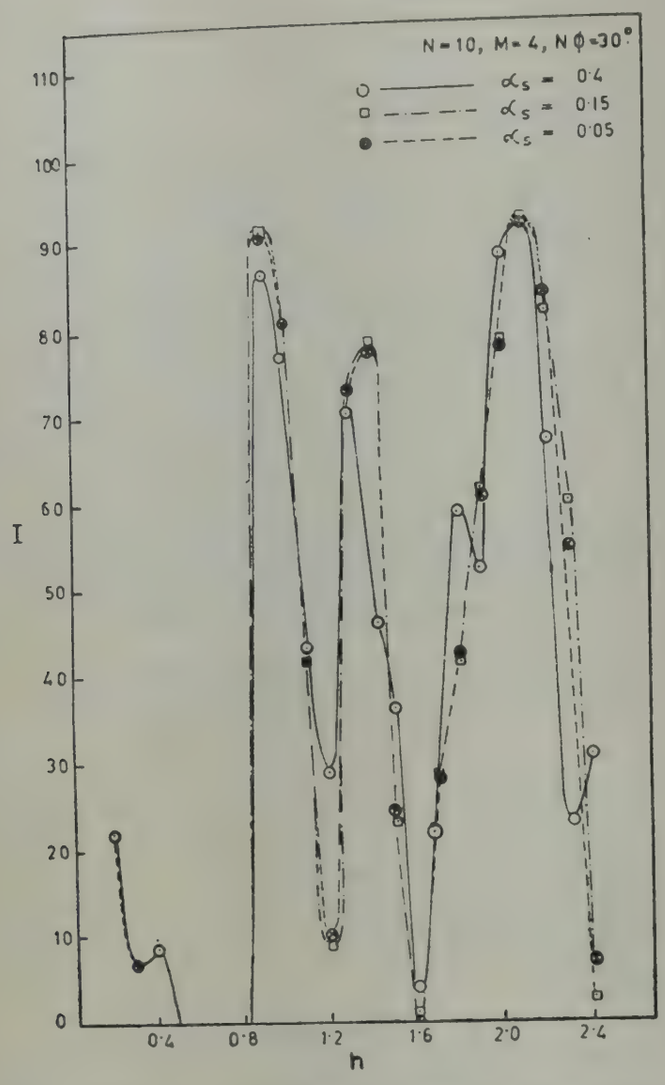

Fig. 2—Diffracted intensities from a cluster of faulted cylindrical crystallites for different values of α_s

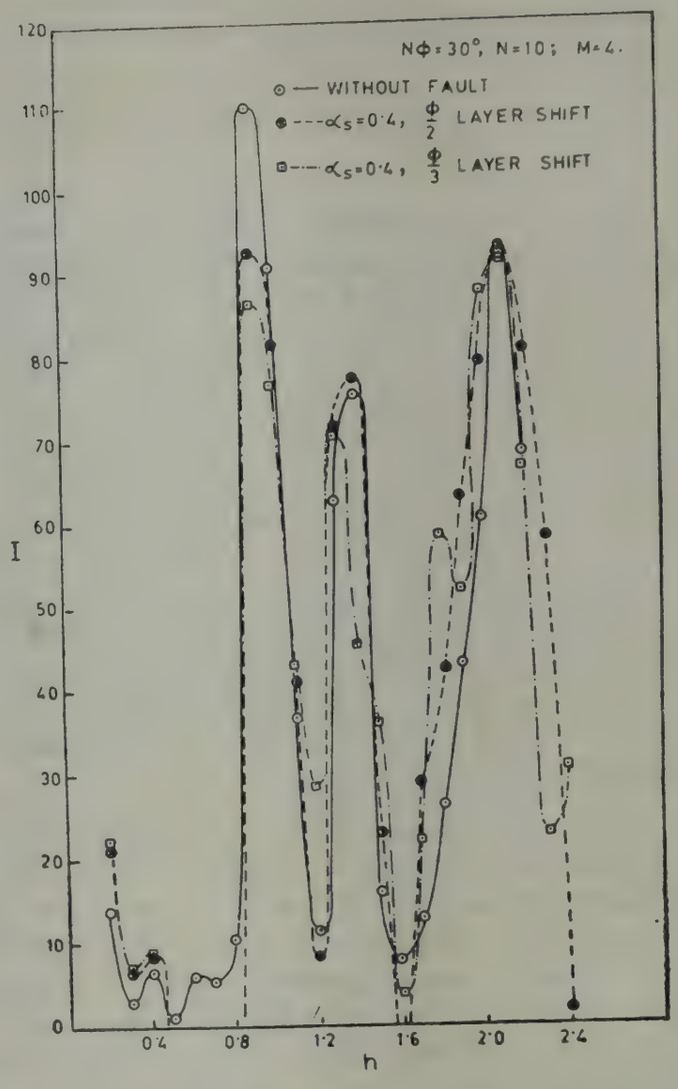

Fig. 3—Diffracted intensities from a cluster of cylindrical crystallites with faults ($\phi/3$) and ($\phi/2$) and without fault

where

$$\psi = QNh\sqrt{1-\frac{I_0^2}{r_1^2 h^2}}\ ;\ u_m = 1 + mr_2\,\phi$$

$$v_n = 1 + nr_2\,\phi$$

For, $B_m = B_n = 0$, the above equation transforms into Eq. (16) of Mitra and Bhattacherjee,[2] as expected.

Numerical computations for several cases have been carried out in a Ryad 1030 computer. Results of some typical cases have been illustrated in Figs. 2 and 3. Fig. 2 shows the intensity distributions for three different values of α_s, viz. 0·05, 0·15 and 0·40. It is observed that the general pattern is very much similar in all the cases. However, the first two peaks appear to decrease in height with increase in α_s while the heights of the peak around $h = 2{\cdot}2$ are same for all cases. However, there appears to be a tendency of peak shift and formation of a secondary maximum before the primary maximum on the high angle side with increase in the value of α_s.

Fig. 3 shows clearly that although the broad features of the pattern remain unchanged, the peak heights and positions change very slightly but progressively as the shift increases. Also some more peaks appear in case of shift by $\phi/3$. However, to arrive at definite conclusions more detailed numerical analysis is necessary.

The authors wish to express their grateful thanks to Prof. G B Mitra for his continuous encouragement and interest in the work.

References

1. Ray B K, De A K & Bhattacherjee S, *Acta crystallogr.*, A34 (1978), 637.
2. Mitra G B & Bhattacherjee S, *Acta crystallogr.*, **A27** (1971), 22.
3. Wilson A J C, *X-ray optics* (Methuen, London), 1962.

Crystal Growth from Binary Immiscible Liquid Systems

K Ravindran Nair

Department of Inorganic & Physical Chemistry
Indian Institute of Science, Bangalore 560 012

Received 2 *November* 1978; *revised received* 21 *February* 1979

Growth of single crystals from binary immiscible or partially miscible liquid systems has been tried. The interface of the

two liquids has been found to behave as a useful barrier which prevents uncontrolled solute transport from the lower layer when growth is taking place in the upper layer under the influence of a temperature gradient. Crystals of benzoic acid have been grown from the water layer in nitrobenzene-water system and 8-hydroxy quinoline and *p*-anisidine from the cyclohexane layer of cyclohexane-water system. These crystals were found to be better than those grown from a single-phase system.

When a solute is dissolved in two phases of a binary immiscible liquid system, at steady state, its concentration in both phases bears a constant ratio at a given temperature. This constant is known as distribution coefficient. In such a system if crystallization takes place in one phase the resultant depletion in concentration of the solute causes the transport of a corresponding amount from the other phase through the interface. Since it is governed by an equilibrium this transport will have to be continuous and smooth. Therefore, the interface between the two liquids could serve as a barrier that controls the transport of solute required for crystal growth. The effect of such systems on crystal growth was studied and the results are reported here.

Consider a system of two immiscible liquids A and B in which A is the heavier (and therefore lower) layer. The system is saturated with a solute C and an excess of undissolved C is allowed to remain at the bottom. A seed crystal of C is kept at the upper region and the temperature is reduced at this part by a few degrees when crystallization occurs. The solute required for crystal growth is transported from A through the interface and B to the crystal growing region. A baffle with a limited opening is kept in B midway between crystal growing region and A-B interface to control convection currents.

Nitrobenzene-water-benzoic acid system happens to be a convenient system for this study. The experiments are carried out in a simple apparatus. Saturated solutions of benzoic acid in nitrobenzene and water are prepared at 55°C in a water thermostat. Twenty millilitres of the solution in nitrobenzene and 40 ml of that in water are mixed and shaken well in a flask. The mixture is transferred into a cylindrical glass vessel of 100 ml capacity (2·5 cm diam.) in which 5 g of nutrient benzoic acid has been placed. An aluminium baffle with 5 holes of 2 mm diam is placed in the aqueous layer at half its height. A few seed crystals are kept suspended at the upper part of the solution by means of a thread. The thread is tied to a hook in a stopper which closes the glass vessel tightly. The glass vessel is kept dipped in the water thermostat (temperature 55°C) up to the level of the baffle. The aqueous layer above the baffle is exposed to atmosphere and the temperature in this region is 45 ± 1°C at steady state. The whole set-up was kept in this manner for seven days. During this period crystals grow and it could be visually observed that the excess of solute remaining at the bottom disappears slowly.

Crystals obtained were long flakes of 1 cm length and 2 mm width. They are quite different from crystals obtained from a single-phase aqueous solution under the influence of the same temperature gradient. Fig. 1 shows photographs of crystals obtained from aqueous solution and binary systems. The surfaces of the crystals obtained by the present procedure are smooth with minimum number of steps or layers whereas those obtained from the monophase system were needle shaped with a multitude of defective features. The better quality of crystals in the present case is probably due to the controlled transport of solute species through the binary liquid interface.

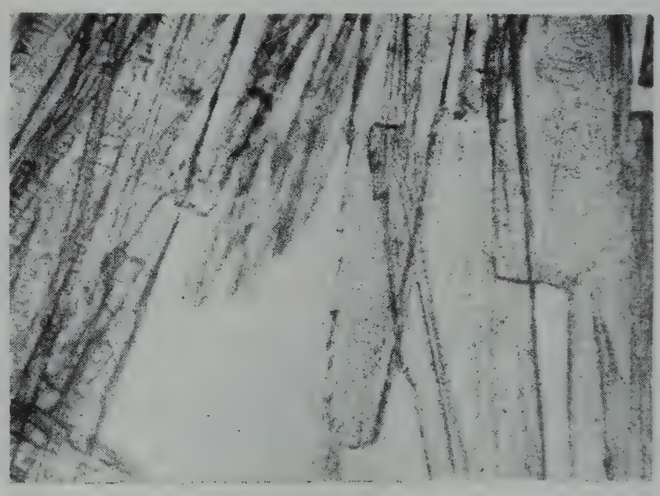

a

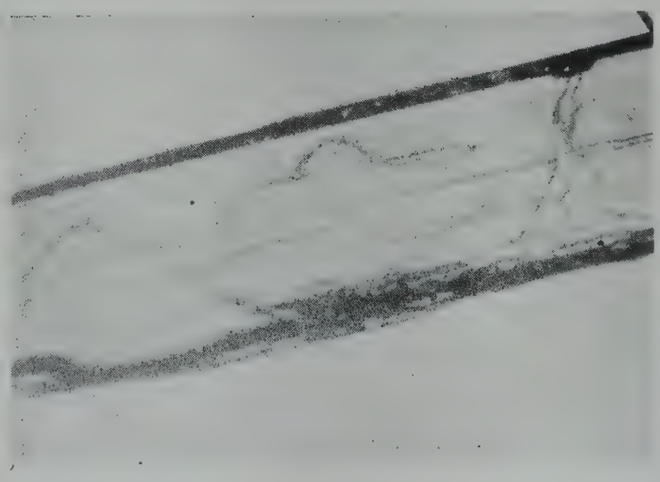

b

Fig. 1—Photomicrographs (× 20) of crystals of benzoic acid [a, crystals from aqueous solution; and b, crystals from water-nitrobenzene system]

Cyclohexane-water system is another one which could be used for such studies. Crystals of oxine (8-hydroxy quinoline) and *p*-anisidine (*p*-methoxy aniline) have been grown from this liquid system. Cyclohexane forms the top layer in these cases and good crystals are grown in this layer using the same experimental set-up outlined earlier.

In all the cases the growth of crystals is very slow, viz. 1-2 mm per day. This is probably because the free supply of solute to the growing crystal is hampered by the interface between the two liquid layers. The single phase aqueous solution of benzoic acid gives faster crystal growth under the same conditions.

Preliminary Single Crystal X-ray Study of N-Methyl Crotananinium Iodide

K N Goswami, S D Sharma & O P Suri*

Department of Physics, University of Jammu
Jammu 180 001

Received 20 *December* 1978; *revised received* 26 *March* 1979

The space group and unit cell dimensions of N-methyl crotananinium iodide have been determined by the X-ray diffraction method. The compound has been found to be orthorhombic with space group $P2_12_12_1-D_2^4$ having four molecules per unit cell.

Crotananine (m.p. 174-175°C), an alkaloid, is isolated from the seeds of *Crotalaria nana* Burm.[1] It has been established to be a pyrrolizidine macrocyclic diester (12-hydroxy-13, 14, 15-trimethyl senec-l-enine) on the basis of spectral and chemical evidences. The compound has been found to be strongly hepatotoxic.

To study the crystal structure of the compound by X-ray diffraction method, crotananine methiodide, a heavy atom derivative, was prepared from the parent alkaloid by heating it with purified methyl iodide (1 mole) on a steam bath for 2 hr. Initial crystallization was carried out from methanol and acetone mixture. The crystals were obtained from slow evaporation of saturated methanol solution of the compound by allowing it to stand at room temperature for 3 days. The crystals are colourless with rectangular to plate-like shape. They are insoluble in carbon tetrachloride, chloroform, benzene and ether.

The chemical structure of the compound (4-methyl, 12-hydroxy-13, 14, 15-trimethyl-senec-l-eninium iodide) is as follows :

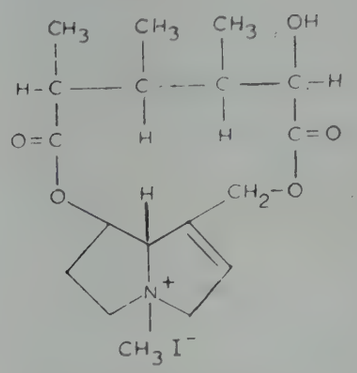

A single crystal of dimensions $2{\cdot}5\times1{\cdot}5\times1{\cdot}0$ mm was mounted along its longer dimension, *c*-axis. After proper centring, it was subjected to X-ray diffraction studies using Cu-radiation filtered through nickel foil of suitable thickness. Oscillation and rotation photographs along the *a*- and *c*-axes have shown the presence of mirror plane perpendicular to the axis of rotation. The complete symmetry, however, can be derived by examining the zero-level Weissenberg photograph. The zero-level Weissenberg picture displayed mirror lines along the r.l. axes (90° apart) dividing the festoons into distorted images. This indicates the *mmm* symmetry. Rotation and zero layer Weissenberg pictures along *c*- and *a*-axes gave the cell parameters: $a = 13{\cdot}38 \pm 0{\cdot}02$ Å; $b = 19{\cdot}37 \pm 0{\cdot}02$ Å; $c = 7{\cdot}70 \pm 0{\cdot}02$ Å; and $\alpha=\beta=\gamma=90°$. A higher degree of accuracy, however, is not claimed as no allowance has been made for the film shrinkage etc.

Sets of data *h*00, 0*k*0, 00*l*, *hk*0, 0*kl* and *hkl* were recorded on the Weissenberg photographs using equi-inclination Weissenberg method. The spectra found absent were (*h*00) for *h* odd, (0*k*0) for *k* odd, and (00*l*) for *l* odd. These extinctions uniquely indicated the space group $P2_12_12_1-D_2^4$, with four molecules per unit cell.

The calculated density, d_c, assuming four molecules per unit cell was found to be 1·547 g cm^{-3}. This agrees well with the observed density d_0 (1·548) g cm^{-3}). determined by the floatation method, using the mixture of carbon tetrachloride and benzene at room temperature (180°C).

The crystal system and the physical data can be summarized as :

Molecular formula	:	$C_{17}H_{25}O_5N—CH_3I$
Molecular weight	:	465 g
Crystal system	:	Orthornombic
Space group	:	$P2_12_12_1-D_2^4$
Lattice parameters	:	$a = 13{\cdot}38 \pm 0{\cdot}02$ Å
		$b = 19{\cdot}37 \pm 0{\cdot}02$ Å
		$c = 7{\cdot}70 \pm 0{\cdot}02$ Å
		$\alpha = \beta = \gamma = 90°$

*Present address : Chemistry Division, Regional Research Laboratory, Jammu

No. of molecules per unit cell = 4

Calculated density (d_c) = 1·547 g cm^{-3}

Observed density (d_o) = 1·548 g cm^{-3}

The 3-dimensional intensity data have been collected and calculations for the structural analysis are in progress.

References

1. Siddiqi M A, Suri K A, Suri O P & Attal C K, *Phytochemistry*, 17 (1978), 2143.

A Heuristic Formula for the Dielectric Loading Factor of a Helix Supported by Dielectric Circular Rods

B N Basu

Department of Physics, Regional Institute of Technology
Jamshedpur 831 014

&

S N Joshi

Central Electronics Engineering Research Institute
Pilani 333 031

Received 20 *November* 1978; *revised received* 30 *July* 1979

An approximate formula is derived for the dielectric loading factor of a practical slow-wave structure for a travelling wave tube that consists of a helix supported by circular dielectric rods. Results of experimental verification of the formula are discussed.

Loshakov and Ol'derogge[1] field-analyzed a slow-wave structure for travelling wave tubes (TWTs) that consists of a helix supported by a number of longitudinal dielectric wedge bars symmetrically arranged around the helix. They assumed the support to be radially extended up to infinity and ignored the effect of the envelope of the structure, considering it to be usually much less than that of the supports. In this note, we have studied a helix supported by a number of circular dielectric rods—a structure that is non-symmetrical azimuthally—unlike what has been studied by Loshakov and Ol'derogge.[1] Consequently, much complexity is involved in analyzing such a structure. In the present note, we have, however, proposed a simple heuristic formula for such a structure.

Loshakov and Ol'derogge[1] have shown that the dielectric loading factor D for a helix supported by a number of dielectric wedge bars of relative permittivity ϵ_r is the same as that for a helix surrounded by a continuous dielectric of relative permittivity ϵ'_r, touching the helix and extending up to infinity, and arrived at an expression for D, as

$$D = 1 + (\epsilon_r' - 1)\gamma a\, I_0(\gamma a)\, K_1(\gamma a) \qquad \ldots(1)$$

where γ is the radial propagation constant, a the helix radius, I_0 and K_1 are the modified Bessel functions, and ϵ_r' is given by[1]

$$\epsilon_r' = 1 + \frac{\phi N}{2\pi}\ (\epsilon_r - 1) \qquad \ldots(2)$$

where N is the number of supports and ϕ the angle of wedge of each support. It is interesting to interpret ϵ_r' as

$$\epsilon_r' = \frac{(\epsilon_r)\,(V_s) + (1)\,(V - V_s)}{(\epsilon_r)\,(V)} \qquad \ldots(3)$$

where V_s is the volume occupied by the support-dielectric wedges up to a given large radial extent, and V the total volume outside the helix up to the same radial extent, $(V - V_s)$ being the volume occupied by the free space of relative permittivity 1. Now, Eq. (3) may be simplified as:

$$\epsilon_r' = 1 + \frac{V_s}{V}\ (\epsilon_r - 1) \qquad \ldots(4)$$

which reduces to Eq. (2), using the following relation that is easy to obtain:

$$V_s/V = \phi N/2\pi$$

Let us now take a helix that is supported by a number of large diameter dielectric circular rods symmetrically arranged around the helix. Eq. (4), in this case, with

$$V_s = N\pi(d^2/4)\, l \text{ and } V = \pi[(d+a)^2 - a^2]\, l$$

takes the following form:

$$\epsilon_r' = 1 + (\epsilon_r - 1)\left(\frac{N}{4}\right)\left(\frac{d}{d+2a}\right) \qquad \ldots(5)$$

where d is the diameter of each rod and l represents the axial dimension of the structure. Using Eqs. (1) and (5), one obtains an approximate formula for the D of a helix supported by dielectric rods as

$$D \cong [1 + (\epsilon_r - 1)\left(\frac{N}{4}\right)\left(\frac{d}{d+2a}\right)\gamma a I_0(\gamma a)\, K_1(\gamma a)]^{-1/2} \qquad \ldots(6)$$

It is of interest to examine the above formula experimentally. For this purpose, two helices are constructed: one supported by dielectric rods (helix I) and the other without supports (helix II) (see Table 1). The two helices have the same radius but different pitches. Helix II is wound to have the pitch p' given by

$$p' = Dp \qquad \ldots(7)$$

where p and D are the pitch and the dielectric loading factor of helix I. D is calculated using Eq. (6). In Eq. (6), γ is approximately taken as β, the axial propagation constant of helix I which is found experimentally, following the usual method[2] of cold

Table 1—Dimensional Description and Experimental/ Calculated Values of the Propagation Constant of the Two Helices

Dimension/experimental or calculated value	Helix I (with supports)	Helix II (in free space)
Helix radius ($=a$)	1·6 mm	1·6 mm
Number of supports ($=N$)	3	0
Rod diameter ($=d$)	3·9 mm	0
Relative permittivity of the support	5·1	1
Axial propagation constant ($=\beta$) at 3 GHz (experimental)	8·5 radian/ cm	9·2 radian/ cm
Dielectric loading factor ($=D$) [calculated using Eq. (6)]	0·67	1
Pitch	0·9 mm ($=p$)	0·6 mm ($=p'=Dp$)

measurements on helices to find the guide wavelength λ_g. The method is to signal-feed one end of the helix structure through an assembly of a slotted line together with a probe, a detector and a VSWR meter, and terminate the other end in a movable short. The VSWR reading indicates a series of alternate maxima and minima as the short is moved inside the helix along the axis of the structure. The separation between two positions of the short that corresponds to two consecutive minima in the reading of the VSWR meter equals $\lambda_g/2$; the axial propagation constant is then found from the relation $\beta=2\pi/\lambda_g$. The detailed description of the method may be found elsewhere (Swift-Hook[2]).

Helices I and II which have been wound so as to satisfy the relation (7) are expected to result in the same experimental value for the axial propagation constant β. But the values of the propagation constant of these two helices, as can be seen from Table 1, though they are near, are not equal. This discrepancy can be partly accounted for by the failure of the experimental condition to realize the actual "helix in free space" condition for helix II. It is likely that any dielectric surrounding, say the close proximity of the working table, loads helix II, and increases the apparent β of helix II. Finally, the formula for the D of a practical helix has been deduced here on a heuristic basis; one should use Eq. (6) considering its importance from preliminary design considerations only.

The problem was suggested by, and carried out under the guidance of, Dr S S S Agarwala. The authors are indebted to Dr Amarjit Singh for helpful discussions.

References

1. Loshakov L N & Ol'derogge E B, *Radio Engng electron. Phys.*, 13 (1968), 45.
2. Swift-Hook D T, *Proc. IRE*, 105 (1958), 747.

Field Analysis of a Practical Helical Slow-wave Structure for TWTs*

B N Basu
Department of Physics, Regional Institute of Technology Jamshedpur 831 014

Received 27 *November* 1978; *accepted* 18 *October* 1979

A field analysis has been developed for a sheath helix supported by a number of longitudinal, wedge-shaped dielectric bars in a metal shell. The present analysis is potentially more accurate than the equivalent circuit analysis developed by several earlier workers. The results of these two analytical approaches are compared for the dielectric loading factor of the structure, and are found to be in good agreement for shields not too close to the helix. For smaller shield radii, the present field analysis approach gives more accurate results than the equivalent circuit approach.

Several workers[1-3] have developed a field analysis for a sheath helix in free space and also for the same surrounded by a continuous dielectric or supported by dielectric wedges. The effect of a metal enclosure around the helix has not, however, been considered by them, though this effect has been studied by others using the equivalent circuit approach.[4-6]

In the present note, the field analysis approach has been used to study a helical slow-wave structure (SWS) consisting of a sheath helix supported by a number of wedge-shaped longitudinal dielectric bars and the whole enclosed in a cylindrical metal shield. This structure closely approximates that used in practical high-power, octave-bandwidth TWTs. The equivalent circuit analysis of this configuration[5,6] is based on combining the results of two simple configurations [Fig. 1] : one the shielded sheath helix without any dielectric support/surrounding, and the other the sheath helix enclosed in a uniform dielectric extending to infinity. This approach is not valid for shields close to the helix. The present analysis, however, does not have this limitation.

Field expressions— The electric (E) and the magnetic (H) fields inside and outside the helix, in the cylindrical co-ordinates (r, θ, z), are:[2]

$$E_{zn} = A_n I_0(\gamma_n r) + B_n K_0(\gamma_n r) \quad \ldots(1)$$

$$H_{zn} = C_n I_0(\gamma_n r) + D_n K_0(\gamma_n r) \quad \ldots(2)$$

$$E_{\theta n} = \frac{-j\omega\mu_n}{\gamma_n}\left[C_n I_0'(\gamma_n r) + D_n K_0'(\gamma_n r)\right] \quad \ldots(3)$$

and

$$H_{\theta n} = \frac{j\omega\epsilon_n}{\gamma_n}\left[A_n I_0'(\gamma_n r) + B_n K_0'(\gamma_n r)\right] \quad \ldots(4)$$

*Presented at the Symposium on Electron Devices held at the Central Electronics Engineering Research Institute, Pilani, in September 1978.

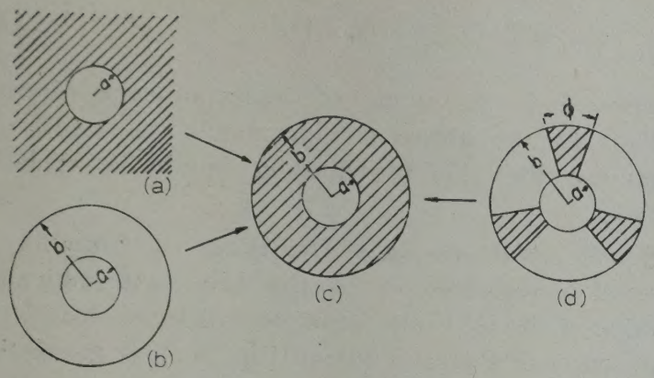

Fig. 1—The method of combining together the results for simpler helix configurations

where A_ns and B_ns are the constants; $n = 1$ and 2 represent the quantities inside and outside the helix respectively; I_0 and K_0 are the zeroth order modified Bessel functions.
Here

$$\gamma_n = (\beta^2 - \omega^2 \mu_n \epsilon_n)^{1/2} \quad \ldots (5)$$

is the radial propagation constant, where β is the longitudinal propagation constant. The factor $\exp\{j(\omega t - \beta z)\}$ has been omitted from Eqs. (1)-(4), for the sake of convenience.

Since the fields E_{z1} and H_{z1} inside the helix are to be finite at its axis, one shoud have:[1]

$$B_1 = D_1 = 0 \quad \ldots (6)$$

Boundary conditions— Considering the sheath helix radius to be a, we have the following boundary conditions to be satisfied at $r = a$:[1]

$$E_{z1}(a) \sin\psi + E_{\theta 1}(a) \cos\psi = 0 \quad \ldots (7)$$

$$E_{z2}(a) \sin\psi + E_{\theta 2}(a) \cos\psi = 0 \quad \ldots (8)$$

$$H_{z1}(a) \sin\psi + H_{\theta 1}(a) \cos\psi = H_{z2}(a) \sin\psi + H_{\theta 2}(a) \cos\psi \quad \ldots (9)$$

and

$$E_{z1}(a) = E_{z2}(a) \quad \ldots (10)$$

where ψ is the pitch angle.

Considering the external metal shield of radius b to be perfectly conducting, we have, in addition to the above, the following boundary conditions satisfied at $r = b$:

$$E_{z2}(b) = 0 \quad \ldots (11)$$

and

$$E_{\theta 2}(b) = 0 \quad \ldots (12)$$

Dispersion relation— Substituting Eqs. (1)-(4) through (6) into the boundary conditions (7)-(12), one obtains a set of six equations with six unknown coefficients A_1, A_2, B_2, C_1, C_2, and D_2. The condition that this set of equations shall have a nontrivial solution is that the following determinantal relation should hold good:

$$\Delta = 0 \quad \ldots (13)$$

where the determinant Δ has been spelt out in Table 1.

In the present case, since the inside of the helix is free space and the space between the helix and the metal enclosure is filled up with a continuous dielectric of relative permittivity ϵ_r, say, we have

$$\mu_1 = \mu_2 = \mu_0;\ \epsilon_1 = \epsilon_0;\ \epsilon_2 = \epsilon_0 \epsilon_r \quad \ldots (14)$$

One can also take

$$\gamma_1 = \gamma_2 = \gamma \cong \beta \quad \ldots (15)$$

which is a fairly good "slow-wave" approximation.[2]

Substituting Eqs. (14) and (15) into (13), one obtains the following dispersion relation after some lengthy manipulations:[7]

$$\left(\frac{k \cot\psi}{\gamma}\right)^2 = \frac{I_0(\gamma a)\, K_0(\gamma a)}{I_1(\gamma a)\, K_1(\gamma a)}\, D^2 \quad \ldots (16)$$

Table 1—The Determinant Occurring in Eq. (13)

$\Delta =$

$I_0(\gamma_1 a)\sin\psi$	$-\left(\frac{j\omega\mu_1}{\gamma_1}\right) I_1(\gamma_1 a) \cos\psi$	0	0	0	0
0	0	$I_0(\gamma a)\sin\psi$	$K_0(\gamma_2 a)\sin\psi$	$-\left(\frac{j\omega\mu_2}{\gamma_2}\right) I_1(\gamma_2 a) \cos\psi$	$\left(\frac{j\omega\mu_2}{\gamma_2}\right) K_1(\gamma_2 a) \cos\psi$
$\left(\frac{j\omega\epsilon_1}{\gamma_1}\right) I_1(\gamma_1 a) \cos\psi$	$I_0(\gamma_1 a)\sin\psi$	$-\left(\frac{j\omega\epsilon_2}{\gamma_2}\right) I_1(\gamma_2 a) \cos\psi$	$\left(\frac{j\omega\epsilon_2}{\gamma_2}\right) K_1(\gamma_2 a) \cos\psi$	$-I_0(\gamma_2 a)\sin\psi$	$-K_0(\gamma_2 a)\sin\psi$
$I_0(\gamma_1 a)$	0	$-I_0(\gamma_2 a)$	$-K_0(\gamma_2 a)$	0	0
0	0	$I_0(\gamma_2 b)$	$K_0(\gamma_2 b)$	0	0
0	0	0	0	$I_1(\gamma_2 b)$	$-K_1(\gamma_2 b)$

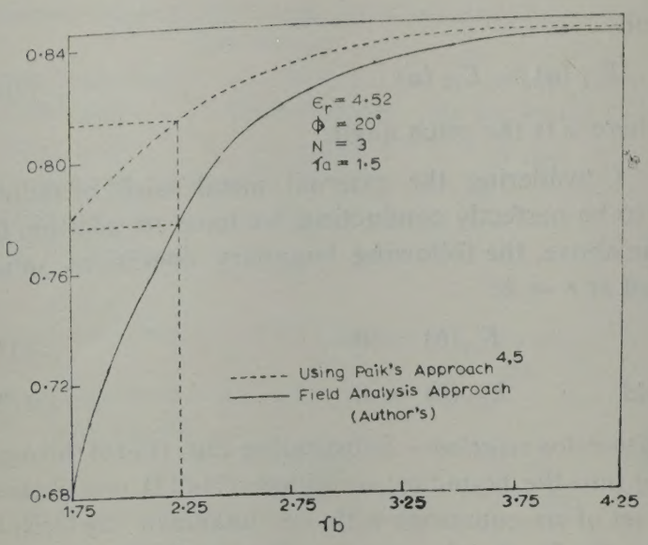

Fig. 2—Comparison of the variation of D with the normalized shield radius γb by Paik's approach[4,5] and the present method

where

$$D = \left[\left\{ 1 + (\epsilon_r - 1)\,\gamma a\, I_0(\gamma a)\, K_1(\gamma a) \left(1 + \frac{I_1(\gamma a)\, K_0(\gamma b)}{K_1(\gamma a)\, I_0(\gamma b)}\right)\right\} \times \left\{1 - \frac{I_0(\gamma a)\, K_0(\gamma b)}{K_0(\gamma a)\, I_0(\gamma b)}\right\}^{-1} \left\{1 - \frac{I_1(\gamma a)\, K_1(\gamma b)}{K_1(\gamma a)\, I_1(\gamma b)}\right\}\right]^{-1/2} \quad ...(17)$$

is the dielectric loading factor (DLF) of the configuration, k $[=(\omega^2\, \mu_0\, \epsilon_0)^{1/2}]$ is the free-space propagation constant, and I_1 and K_1 are the first order modified Bessel functions.

Practical example— Let us now consider a helix supported by longitudinal, wedge-shaped dielectric bars and enclosed in a metal shield. Loshakov and Ol'derogge[3] have shown that a number of such dielectric wedges each of permittivity ϵ_r placed symmetrically around a helix can be looked upon as equivalent to a helix supported by a continuous dielectric tube of an effective permittivity ϵ_r' given by

$$\epsilon_r' = 1 + \frac{\phi N}{2\pi}\,(\epsilon_r - 1) \quad ...(18)$$

where ϕ is the angle of wedge of each support. Thus, for the above configuration [Fig. 1 (d)], one can use Eq. (17) in which ϵ_r should be replaced by ϵ_r'.

Results and discussion — The effect of bringing the metal enclosure closer to the helix is to reduce the value of the DLF and hence to "dielectric-load" the structure to a greater extent [Fig. 2]. It is interesting to compare the DLF obtained by the present method of field analysis with that obtained by the method of combining together the results for simpler helix configurations as suggested by Paik[5] and subsequently adopted by us[6] [Fig. 1]. These two methods are found to be in good agreement for shields not too close to the helix; for smaller shield radii they differ [Fig. 2], and the present method gives more accurate results, since it does not require to combine the results for simpler configurations as in Paik.[5]

The problem was suggested by, and carried out under the guidance of, Dr S S S Agarwala. The author wishes to thank Dr Amarjit Singh for his kind interest and many fruitful suggestions. Thanks are also due to Mr S N Joshi for many helpful discussions.

References

1. Pierce J R, *Proc. IRE*, 35 (1947), 111.
2. Swift-Hook D T, *Proc. IRE*, **105** (1958), 747.
3. Loshakov L N & Ol'derogge E B, *Radio engineering and electronic physics*, 13 (1968), 45.
4. Kino G S & Paik S F, *J. appl. Phys.*, **33** (1962), 3002.
5. Paik S F, *IEEE Trans.*, ED16 (1969), 1010.
6. Basu B N & Joshi S N, *CEERI Internal Rep.* No. IR-Ol-VT/78 (Central Electronics Engineering Research Institute, Pilani), March 1978.
7. Basu B N, *CEERI Internal Rep.* No. IR-02-VT/78 (Central Electronics Engineering Research Institute, Pilani), March 1978.

ARE YOU AWARE OF ... ...

ANNALS OF PHYSICS publishes original work of broad significance in all areas of physics with an emphasis on clarity and intelligibility which makes it accessible to the widest possible audience. The papers contain sufficient background and detail to enable a reader who has worked in the field within the last few years to follow the arguments and understand their significance.

Published by Academic Press Inc., New York

Annual Subscription : 1979, Vol. 117-123 (13 iss.) $ 439.25

JOURNAL OF COMPUTATIONAL PHYSICS is devoted to papers on the computational aspects of physical problems; it emphasizes the techniques involved in the numerical solution of mathematical equations and in automated data reduction over the physical significancc of the solutions of these problems; an invaluable journal for all who must work with the numerical solution of problems in the physical sciences and must make effective use of computers.

Published by Academic Press Inc., New York

Annual Subscription : 1979, Vol. 30-33 (12 iss.) $ 248.00

Please direct your enquiries to :

India Book House Subscription Agency

Post Bag No. 6301, Bombay-400 013

INDIAN TECHNOLOGIES

Developed by
CSIR LABORATORIES

Compiled by

TECHNOLOGY UTILIZATION, COUNCIL OF SCIENTIFIC & INDUSTRIAL RESEARCH, NEW DELHI

- A useful compendium of technologies developed in CSIR Laboratories and Cooperative Research Associations of Industries.
- Contains basic non-technical information regarding more than 460 processes/patents which have either been commercialized or developed on pilot plant/prototype scale.
- Covers processes relating to different sectors of industries—metals and alloys; machinery; chemicals and allied products; paper; foods and beverages; vegetable oils and waxes; leather and auxiliaries, glass, ceramics and refractories; roads and buildings; instruments and equipment and textiles.

Price: Rs. 32.00 in India $ 11.00 overseas

Kindly contact

THE SALES & DISTRIBUTION OFFICER
PUBLICATIONS & INFORMATION DIRECTORATE, CSIR
HILLSIDE ROAD, NEW DELHI 110 012

CSIR PUBLICATIONS

WEALTH OF INDIA

An encyclopaedia of the economic products and industrial resources of India issued in two series

RAW MATERIALS SERIES—contains articles on plant, animal and mineral resources

	Rs	$	£
Vol. I (A-B)	25.00	7.50	2.50
Vol. II (C)	37.50	11.50	3.75
Vol. III (D-E)	40.00	12.00	4.00
Vol. IV (F-G)	25.00	7.50	2.50
Supplement (Fish & Fisheries)	10.50	3.00	1.05
Vol. V (H-K)	30.00	9.00	3.00
Vol. VI (L-M)	40.00	12.00	4.00
Supplement (Livestock)	60.00	18.00	6.00
Vol. VII (N-Pe)	30.00	9.00	3.00
Vol. VIII (Ph-Re)	70.00	21.00	7.00
Vol. IX (Rh-So)	83.00	24.00	8.30
Vol. X (Sp-W)	152.00	65.00	23.00
Vol. XI (X-Z)	102.00	42.00	20.00

INDUSTRIAL PRODUCTS SERIES—deals with major,small-scale and cottage industries

Part I (A-B)	20.00	6.00	2.00
Part II (C)	25.00	7.50	2.50
Part III (D-E)	25.00	7.50	2.50
Part IV (F-H)	25.00	7.50	2.50
Part V (I-L)	30.00	9.00	3.00
Part VI (M-Pl)	28.00	8.00	2.80
Part VII (Pl-Sh)	60.00	18.00	6.00
Part VIII (Si-Ti)	66.00	27.00	10.00
Part IX (To-Z)	80.00	34.00	12.00
BHARAT KI SAMPADA (Hindi Edition of Wealth of India), Raw Materials : Vol. I	38.00	16.00	6.50
Vol. II	36.00	15.00	6.00
Vol. III	36.00	15.00	6.00
Vol. IV	83.00	34.00	16.00
Livestock (Kukkut Palan)	34.00	15.00	6.00
Fish & Fisheries (Matsya aur Matsyaki)	49.00	21.00	8.00

OTHER PUBLICATIONS

Flora of Delhi by J. K. Maheshwari	28.00	8.00	2.80
Indian Fossil Pteridophytes by K. R. Surange	23.00	8.00	2.30
Cedrus by P. Maheshwari & Chhaya Biswas	24.00	8.00	2.40
Indian Thysanoptera by T.N. Ananthakrishnan	26.00	8.00	2.60
The Millipede Thyropygus by C. Krishnan	12.00	3.50	1.20
Drug Addiction with special reference to India by R. N. Chopra & I. C. Chopra	12.00	3.50	1.20
Glossary of Indian Medicinal Plants by R. N. Chopra & I. C. Chopra	8.00	2.50	0.80
Fluidization & Related Processes	24.00	8.00	2.40
Evolution of Life by M. S. Randhawa, A. K. Dey, Jagjit Singh & Vishnu Mittre	45.00	14.00	4.50
Corrosion Map of India	18.00	5.00	1.80
Collected Scientific Papers of Meghnad Saha	60.00	18.00	6.00
Proteaceae by C. Venkata Rao	34.00	11.00	3.40
Pinus by P. Maheshwari & R. M. Konar	27.00	8.50	2.70
Antibiotics	7.50	2.25	0.75
Cellulose Research I	3.00	0.90	0.30
Cellulose Research II	6.00	1.75	0.60
Chemical Process Design	9.00	2.50	0.90
Low Temperature Carbonization of Non-caking Coals & Lignites & Briquetting of Coal Fines: Vol. I	17.50	5.50	1.75
" " " Vol. II	17.50	5.50	1.75
Nucleic Acids	10.00	3.00	1.00
IGY Symposium: Vol.I	9.00	2.50	0.90
IGY Symposium: Vol.II	9.00	2.50	0.90
CNS Drugs	16.50	5.00	1.65
Kinetics of Eletrode Processes & Null Points of Metals	2.50	0.75	0.25
Utilization of Indian Vegetable Oils as Lubricants in Internal Combustion Engines	2.00	0.60	0.70
Indian Sardines by R. V. Nair	22.00	7.00	2.20
Termite Problems in India	9.00	3.00	0.90
Loranthaceae by B. M. Johri & S. P. Bhatnagar	32.00	11.00	3.20
Abies and Picea by K. A. Chowdhury	14.00	6.00	2.10
A Dictionary of Flowering Plants in India by H. Santapau & A. N. Henry	22.00	9.00	3.50
Gnetum by P. Maheshwari & Vimla Vasil	20.00	6.00	2.00
Aquatic Angiosperms by K. Subramanyan	20.00	6.00	2.00
Supplement to Glossary of Indian Medicinal Plants by R. N. Chopra, I. C Chopra & B. S. Varma	14.00	4.50	1.40
Cottonseed Chemistry and Technology in Its setting in India by K. S. Murti & K. T. Achaya	77.00	32.00	13.00
Herbaceous Flora of Dehra Dun by C. R. Babu	144.00	60.00	22.00

Packing and Postage extra, *Please contact*

THE SALES & DISTRIBUTION OFFICER, PUBLICATIONS & INFORMATION DIRECTORATE, CSIR, HILLSIDE ROAD, NEW DELHI 110012

Printed and Published by Shri D. S. Sastry, Publications & Information Directorate, Council of Scientific & Industrial Research, New Delhi, at the Leipzig Press, D-52 South Extension Part I, New Delhi-110 049, India

Regd. D-(C)-540